3-DIMENSIONAL CARBON MICRO-ELECTRO-MECHANICAL SYSTEM (MEMS) ELECTRODE FOR POTENTIAL DIELECTROPHORETIC HEPATIC CELL PATTERNING APPLICATION

WAN NURLINA BINTI WAN YAHYA

FACULTY OF ENGINEERING
UNIVERSITY OF MALAYA
KUALA LUMPUR

2019

University of Malaya

3-DIMENSIONAL CARBON MICRO-ELECTRO-MECHANICAL SYSTEM (MEMS) ELECTRODE FOR POTENTIAL DIELECTROPHORETIC HEPATIC CELL PATTERNING APPLICATION

WAN NURLINA BINTI WAN YAHYA

THESIS SUBMITTED IN FULFILMENT OF THE REQUIREMENTS FOR THE DEGREE OF DOCTOR OF PHILOSOPHY

FACULTY OF ENGINEERING
UNIVERSITY OF MALAYA
KUALA LUMPUR

2019

University of Malaya

UNIVERSITY OF MALAYA
ORIGINAL LITERARY WORK DECLARATION

Name of Candidate: Wan Nurlina binti Wan Yahya

Matric No: KHA120097

Name of Degree: Doctor of Philosophy

Title of Thesis (“this Work”): 3-Dimensional Carbon Micro-Electro-Mechanical System (MEMS) Electrode For Potential Dielectrophoretic Hepatic Cell Patterning Application

Field of Study: BioMEMS

I do solemnly and sincerely declare that:

(1) I am the sole author/writer of this Work;
(2) This Work is original;
(3) Any use of any work in which copyright exists was done by way of fair dealing and for permitted purposes and any excerpt or extract from, or reference to or reproduction of any copyright work has been disclosed expressly and sufficiently and the title of the Work and its authorship have been acknowledged in this Work;
(4) I do not have any actual knowledge nor do I ought reasonably to know that the making of this work constitutes an infringement of any copyright work;
(5) I hereby assign all and every rights in the copyright to this Work to the University of Malaya (“UM”), who henceforth shall be owner of the copyright in this Work and that any reproduction or use in any form or by any means whatsoever is prohibited without the written consent of UM having been first had and obtained;
(6) I am fully aware that if in the course of making this Work I have infringed any copyright whether intentionally or otherwise, I may be subject to legal action or any other action as may be determined by UM.

Candidate’s Signature Date:

Subscribed and solemnly declared before,

Witness’s Signature Date:

Name:

Designation:

University of Malaya

[3-DIMENSIONAL CARBON MICRO-ELECTRO-MECHANICAL SYSTEM (MEMS) ELECTRODE FOR POTENTIAL DIELECTROPHORETIC HEPATIC CELL PATTERNING APPLICATION]

ABSTRACT

The maintenance of liver tissue unique pattern remains a great challenge in the generation of functional engineered liver tissue *in vitro*. This thesis presents a carbon-dielectrophoresis (DEP) based cell patterning for generating hepatic cell constructs, mimicking biological hepatic lobule. A new design of electrode named interdigitated radiating-strips electrode (IRSE) was simulated and optimized using COMSOL Multiphysics 4.2a. The simulation result proved that IRSE is capable to provide uniform distribution of electric field for generating three-dimensional (3D) DEP force. The use of carbon electrodes has been an alternative to traditional metal electrodes and insulator structures for DEP applications since more advantages offered. The proposed lab-on-a-chip (LOC) device composed of three layers and feature 3D carbon IRSE which was fabricated using a carbon micro-electro-mechanical system (CMEMS) technique. The electrical characterization result of the fabricated carbon electrode shows that the average electrode resistivity is $10.36 \pm 1.19 \times 10^{-4}$ Ω·m, which low enough to generate an electric field for DEP application using 10 of volts. A proof-of-concept experiment using an interdigitated circular post electrode was conducted to confirm the functionality of the fabricated LOC device. Results show that with the presence of a 15 V voltage input, this carbon structure was capable of manipulating polystyrene microbeads through negative-DEP and positive-DEP in a range of frequency. In the guise of IRSE, both two-dimensional (2D) and 3D structures were fabricated and 10 µm polystyrene microbeads were used as a model to demonstrate dielectrophoretic cell patterning. Under 15 V of AC signal and 50 MHz of frequency in 1 minute, 3D IRSE shows a 67% increase in trapping efficiency of pDEP microbeads as compared to the 2D IRSE. This result suggests that the

University of Malaya

3D carbon electrode has the capacity to generate strong electric field gradients over the microchannel which is in line with the simulation result. Certainly, this CMEMS technique can be utilized to engineer a 3D carbon electrode for DEP application and has a great potential to be applied for 3D hepatic cell patterning. Future applications of the fabricated LOC device include artificial organs for integration in the human-on-a-chip system, drug development, and toxicity screening, as well as the modeling of patient specific liver illness.

Keywords: Dielectrophoresis, cell patterning, carbon electrode, carbon MEMS, liver.

University of Malaya

[KARBON MIKRO-ELEKTRI-MEKANICAL SISTEM (MEMS) ELEKTROD 3-DIMENSI YANG BERPONTENSI UNTUK APLIKASI MENCORAKKAN SEL HEPATIK SECARA DIELEKTROPORASI]

ABSTRAK

Penyelenggaraan pola tisu hati yang unik kekal sebagai satu cabaran besar dalam penjanaan kejuruteraan tisu hati secara *in vitro*. Dalam kajian ini, corak sel berasaskan karbon-dielektroporesis (DEP) untuk menghasilkan sel-sel hepatic, menyerupai lobular hati biologi. Reka bentuk elektrod baru yang dipanggil elektrode jalur-jalur terpencar (IRSE) telah disimulasikan dan dioptimumkan menggunakan aplikasi COMSOL Multiphysics 4.2a. Hasil simulasi membuktikan IRSE mampu memberikan pengagihan seragam medan elektrik untuk menghasilkan daya DEP secara tiga-dimensi (3D). Penggunaan elektrod karbon telah menjadi alternatif kepada elektrod logam tradisional dan struktur penebat untuk aplikasi DEP kerana lebih banyak kelebihan yang ditawarkan. Alat yang dicadangkan pada peranti canggih (LOC) terdiri daripada tiga lapisan dan mempunyai IRSE karbon yang dihasilkan dengan menggunakan teknik sistem mekanik elektro-mekanik karbon (CMEMS). Keputusan pencirian elektrik elektrod karbon dibuat memberikan purata ketahanan elektrod sebanyak $10.36 \pm 1.19 \times 10^{-4}\ \Omega\cdot\text{m}$ di mana masih rendah nilainya untuk menghasilkan medan elektrikuntuk aplikasi DEP menggunakan 10 volt. Percubaan konsep eksperimen telah dijalankan untuk mengesahkan fungsi peranti LOC yang dihasilkan dengan menggunakan elektrod silinder. Keputusan menunjukkan bahawa dengan kehadiran input voltan 15 V, struktur karbon ini mampu memanipulasi manik mikro polistirena melalui negatif-DEP dan positif-DEP dalam pelbagai kekerapan. Dengan menggunakan IRSE, kedua-dua struktur dua-dimensi (2D) dan 3D digunakan sebagai model untuk menunjukkan corak sel dielektroporatik oleh manik mikro polistirena sebesar 10 μm. Di bawah isyarat AC 15 V dan frekuensi 50 MHz dalam 1 minit, 3D IRSE menunjukkan peningkatan sebanyak 67% bagi kecekapan penangkapan

University of Malaya

manik mikro oleh positif-DEP berbanding 2D IRSE. Hasil ini menunjukkan bahawa elektrod mempunyai keupayaan untuk menghasilkan kecerunan medan elektrik yang kuat ke atas saluran mikro yang sejajar dengan hasil simulasi. Oleh itu, teknik CMEMS ini boleh digunakan untuk menghasilkan 3D elektrod karbon untuk aplikasi DEP dan mempuntai potensi besar untuk digunakan mencorak sel hepatik secara 3D. Antara aplikasi masa hadapan bagi peranti LOC yang dihasilkan adalah organ buatan untuk integrasi sistem *human-on-a-chip*, pembangunan dadah dan pemeriksaan toksik serta permodelan penyakit hati tertentu pesakit.

Kata Kunci: Dielektroporasi, pencorakan sel, elektrod karbon, karbon MEMS, hati

University of Malaya

ACKNOWLEDGEMENTS

In the Name of Allah, the Most Beneficent and the Most Merciful

Alhamdulillah, all praise to Allah for His blessing in completing this Ph.D. thesis. I thank Allah for all the chances, trials, and strengths that have been showered on me throughout this Ph.D. journey. I had so much experience during this process, not only the academic aspect but also life in general.

First and foremost, I would like to sincerely express gratitude to my supervisors Assoc. Prof. Dr. Nahrizul Adib and Prof. Ir. Dr. Fatimah for continuous support and supervision. Their invaluable knowledge and ideas have guided me to the success of this research. It has been a great pleasure and honor to have them as supervisors. Special thanks go to my advisor, Prof. Marc Madou, and the BioMEMS team at the University of California, Irvine for allowing me the research attachment opportunities in their team and leading me working on this exciting research.

Sincere thanks to the Dean, Faculty of Engineering, Deputy Dean, and all the staff of the Postgraduate Office for their administrative support and help towards my postgraduate affair. My acknowledgment also goes to all the engineer assistance, especially Mr. Yuslialif for their co-operations in laboratory works.

I also want to extend my thanks to the CIME team especially those who work together in carbon MEMS. During my early year until now, Dr. Bashar has always shared his knowledge and ideas especially in the Dielectrophoresis subject, we were also working together in the IEEE committee and he also one of the key people who set up the CMEMS laboratory. I thanks my fellow labmate, Adam, we were always helping each other in this carbon MEMS research especially during our attachment in the University of California, most importantly he also the backbone of the CMEMS laboratory. Not forgotten, I would

University of Malaya

like to thank the rest of my former and current colleagues: Mr. Karunan, Mrs. ‘Asykikin, Dr. Swe Jyen, and other team members.

Nobody has been more important to me in pursuit of this Ph.D. than my family. I would like to thank my beloved parents, Wan Yahya (Ayah) and Sharifah Normaziah (Ende), and also my sibling for their unconditional love, pray and support along this journey. Most importantly, I wish to thank my loving and supportive husband, Muhammad Syazally, and my two wonderful sons, M. Ammar Mukhlis and M. Addin Mukhlis, who provide eternal inspiration. To those who indirectly contributed to this Ph.D. journey, my dear in-law family and beloved friends, I thank them wholeheartedly.

Last but not least, this research would not have been possible without the financial support from the Ministry of Higher Education (MyBrain 15) and MARA. Other research grants that contributed to this research are University Malaya High Impact Research Grant UM-MOHE (UM.C/625/1/HIR/MOHE/05) and Prototype Research Grant Scheme (PRGS: PR003/2012A).

May Allah shower His blessing to all of them. Aaminn.

Wan Nurlina Wan Yahya, Ogos 2019

University of Malaya

TABLE OF CONTENTS

University of Malaya

University of Malaya

University of Malaya

University of Malaya

LIST OF FIGURES

University of Malaya

University of Malaya

University of Malaya

University of Malaya

LIST OF TABLES

University of Malaya

LIST OF SYMBOLS AND ABBREVIATIONS

DEP : Dielectrophoresis
2D : Two-dimensional
3D : Three-dimensional
CMEMS : Carbon micro-electro-mechanical system
LOC : Lab-on-a-chip
ECM : Extracellular matrix
LCST Lower critical solution temperature
IRSE : Interdigitated radiating-strips electrode
CAD : Computer-aided design
AC : Alternating current
pDEP : Positive DEP
nDEP : Negative DEP
UV : Ultraviolet
GC : Glassy carbon
XRD : X-ray diffraction
DI : Deionized
ITO : Indium tin oxide
SEM : Scanning electron microscopy
SiO_2 : Silicon dioxide
IPA : Isopropanol alcohol
PEB : Post exposure bake
PMMA : Polymethyl methacrylate
FESEM : Field emission scanning electron microscopy
ε* : Complex permittivity

University of Malaya

σ_p : Conductivity of particle

σ_m : Conductivity of surrounding medium

ω : Angular frequency

r : Radius of particle

V : Volt

F_{DEP} : Dielectrophoretic force

μm : Micrometer

University of Malaya

CHAPTER 1: INTRODUCTION

1.1 Overview

Engineering biological tissue from the living cells is an emerging field known as tissue engineering with the aim to repair and enhance the function of damaged or defected tissue. Looking forward to bigger and better desires, more complex with microstructural features of tissue such as liver tissue engineering have been developed. The liver is one of the complex inner organs that control over 500 of the body functions mainly metabolism, synthesis of plasma protein, and detoxification to keeping the body alive. Although the liver has a high degree of regenerative competency, liver damages caused by a viral infection, toxin, or chronic liver diseases may eventually lead to permanent liver failure. Clinical studies have shown that liver transplantation can support long term therapeutic, however, the quality and amount of compatible donors are severely limiting (Palakkan, Hay, & Ross, 2013). Therefore, these limitations have urged the research in liver tissue engineering to construct functional engineered liver tissue (K.-H. Lee, Lee, & Lee, 2015; J. Zhang et al., 2018).

Conventionally, engineered tissue required a porous, biocompatible, and biodegradable scaffold where cells are seeded and patterned. Both natural and synthetic scaffolds offer physical and chemical stimuli to guide tissue development and then cultured in a bioreactor with a controlled microenvironment system. However, although advanced biodegradable scaffolds have been developed to morphologically mimic native tissue, it is still not enough to reconstruct more complex organs such as the liver which compose of heterogeneous cells mainly hepatocyte and endothelial cells which organized in a specific hexagonal lobule pattern. Therefore, precise manipulation of cells through cell patterning techniques have been developed and demonstrated the excellent promising on engineering tissues. Cell patterning falls into two categories that are passive and active, which both can guide cells into desired patterns mimicking the native tissue by applying

University of Malaya

external manipulation. The effectiveness of passive cell patterning techniques including micro-contact printing and microfluidic patterning have been reported but are limited by the spontaneous cell adhesion process which is slow and uncontrollable. Compared to those techniques, active patterning methods use external forces such as magnetic, optical, electrokinetic, and fluidic to actively direct the cells to the desired patterns.

Among the available electrokinetic forces, dielectrophoresis (DEP) has been recently widely used for cell patterning because it offers more selective, controllable, and accurate manipulation as well as simple equipment requirement (Abd Rahman, Ibrahim, & Yafouz, 2017). Besides, a large number of cells could be patterned simultaneously without any need for cell pre-modification or labeling signifying its benefits for tissue engineering. Hence, DEP is highly appropriate for *in vitro* liver cell patterning in order to mimic the complicated microstructural of native liver tissue to preserve the optimum liver functions. For instance, to maintain viability and specific functions of human liver cell, HepG2, C. T. Ho, R. Z. Lin, W. Y. Chang, H. Y. Chang, and C. H. Liu (2006) had designed an array of a planar concentric-stellate-tip electrode to yield radial-pattern of electric fields for dieletrophoretically manipulate viable liver cells in a hexagonal manner. However, the planar or two-dimensional (2D) DEP system shows low trapping and patterning efficiency because the DEP force will rapidly decrease as the distance from the planar electrodes increase. As an alternative, three-dimensional (3D) electrode structures are introduced to create a larger volume of DEP forces.

Increasing demand in liver tissue engineering has emerged microscale technologies as the powerful tools to complement the cellular microenvironment *in vitro*. Carbon micro-electro-mechanical system (CMEMS) is one of the recent microscale approach incorporating advanced microfabrication of polymer-derived carbon structures for the used in various fields such as electrochemical sensors, batteries, DEP, and cell culture substrates (Beidaghi, Chen, & Wang, 2011; Hassan, 2018; Martinez-Duarte, Renaud, &

University of Malaya

Madou, 2011; Min et al., 2008; G Turon Teixidor et al., 2008; Thiha, Ibrahim, Muniandy, & Madou, 2019). The polymer-derived carbon structure produced from CMEMS is the glass-like carbon which has good thermal conductivity, wide electrochemical stability window, good mechanical stability, and most essentially biocompatible for the tissue engineering application since the carbon structure is working directly with the living cells.

The innovation in DEP research couple with advanced microfabrication technique primarily CMEMS has introduced a better microfluidic system, lab-on-a-chip (LOC) to develop more complex artificial organs such as the liver. In this study, a unique design of the 3D electrode has been designed and optimized to mimic the microstructure of the hexagonal hepatic lobule. Numerical simulation was done to determine better DEP configuration and optimized geometry of the 3D electrode to obtain optimum DEP effect on hepatic cells. By employing the CMEMS process, a 3D patterned carbon electrode was fabricated and has been microstructural and electrically characterized. To complete the LOC device, a microfluidic platform has been incorporated. The use of a carbon electrode for dielectrophoretic manipulation was demonstrated by polystyrene microbeads as a proof-of-concept. Furthermore, DEP patterning experiments were conducted using the new design electrode, which is expected to mimic the native hepatic lobule pattern and potentially applied for hepatic cell patterning application.

1.2 Research Objectives

The objective of this study is to develop a LOC device featuring a 3D carbon MEMS electrode. This carbon-based device has the potential for dielectrophoretic hepatic cell patterning application. The following are the sub-objectives:

i. To design and optimize electrode to generate electric field intensity up to 10^5 V/m for dielectrophoretic cell patterning based on simulation analysis.

University of Malaya

ii. To fabricate and characterize 3D carbon electrode (micro-scale height with the resistivity of 1×10^{-4} Ω·m) and design a microfluidic platform to develop a LOC device.

iii. To conduct DEP experiments on trapping efficiency of polystyrene microbeads for device proof-of-concept and patterning application.

1.3 Problem Statement

Complex liver tissue morphology is to compensate and control the numerous body functions. However, it is a challenging task to provide adequate position and maintain liver cells to reconstruct complex liver tissue according to its native morphology, *in vitro*. Conventional tissue engineering used a biodegradable scaffold for cell seeding and tissue development, but it is still not enough to reconstruct complex organs such as the liver. Therefore, cell-based patterning techniques are shown to be promising for precise cell manipulation. One of the versatile manipulation mechanisms is DEP where it requires no complicated pretreatments, more selective, controllable, and accurate manipulation.

University of Malaya

1.4 Scope of Work

This study focus on the design and development of a LOC device specifically used to pattern hepatic cells using DEP force in 3D. The electrode used to generate the DEP force is a glass-like carbon electrode derived from an organic polymer (SU-8). The advantage of the use of carbon electrode in dielectrophoretic patterning is from the relatively easy fabrication process of 3D structure using the CMEMS technique involving photolithography and pyrolysis. Due to the dynamic behavior of polystyrene microbeads, it has been used for device proof-of-concept and patterning characterization.

1.5 Thesis Organization

The rest of the thesis is organized as follows:

Chapter 2 includes a brief literature review on the topics of liver structure and functions and its relative to liver tissue engineering particularly DEP, DEP theory, and types of electrode used, followed by a description on CMEMS microfabrication of carbon electrode.

Chapter 3 describes the design and development of the LOC device, including electrode design and simulation by COMSOL, electrode preparation, fabrication, and characterization. A proof-of-concept experiment was performed to test the fabricated LOC device for the DEP application. Lastly, DEP patterning experiments were conducted to demonstrate the potential application of dielectrophoretic hepatic cell patterning.

Chapter 4 discusses the results obtained from this study. Specifically, discussion on simulation results of the newly designed electrode. Following that is the outcome of CMEMS fabrication and electrode characterization. Finally, the DEP experiment results in a proof-of-concept of the LOC device and cell patterning demonstration using polystyrene microbeads.

To end with, Chapter 5 presents a general conclusion of this study and the declaration of contributions. Besides, several suggestions for future works and potential applications have been presented.

University of Malaya

CHAPTER 2: LITERATURE REVIEW

2.1 Introduction

This chapter provides background information related to this study. Along with the progress in the field of liver tissue engineering, various aspects of liver structure and functions, the current state of liver disease, and failure will be discussed. Following that is focusing on one of the engineering approaches that is DEP theory, the DEP system for liver cell patterning, and types of electrode commonly used for DEP. Finally, details on the glass-like carbon electrode will be presented including the microfabrication process of the carbon electrode using the CMEMS technique.

2.2 Overview of Liver Tissue Engineering

The importance of development in liver tissue engineering is thoroughly illustrated by the increasing number of deaths because of liver failure (Hernaez, Solà, Moreau, & Ginès, 2017; Mazza, Al-Akkad, Rombouts, & Pinzani, 2018). Liver transplantation is the most current treatment but limited by the number of available donors and the need for endless immunosuppressive treatment. Hence, a variety of progress in the field of liver tissue engineering has shown great promises to supplement the transplant shortage while opening up spaces for cellular study for other biomedical applications.

In vivo, liver cells live in a comfortable microenvironment in which adequate nutrients, growth factors, and oxygen are supplied by the circulatory system and provide biochemical and mechanical interactions with the neighboring environment. Cells regularly receive numerous cues through communications between cells and the extracellular matrix (ECM) promoting differentiation, proliferation, growth, and assembly to form functional tissue. ECM components include collagen, laminin, and fibronectin, which have proven to be favorable in hepatic development and regeneration in a variety of ways, such as networking with cell surface receptors and delivering

University of Malaya

cytokines (Bonnans, Chou, & Werb, 2014; Maher, 1998; Martinez-Hernandez & Amenta, 1995). Furthermore, control interactions between parenchymal and non-parenchymal cells are significant to preserve hepatocyte morphology and a variety of functions such as metabolism, detoxification (Kadota et al., 2014; Lerche et al., 1997), and protein synthesis (S. N. Bhatia, Yarmush, & Toner, 1997b; Weiskirchen & Tacke, 2014).

Due to those resourceful surroundings, when enzymatically isolated hepatocytes are cultured in static and monolayer systems, they rapidly lose their morphology and many phenotypic functions. As discussed before, research has shown that liver cells have a high capacity to repair themselves. However, this remarkable ability is difficult to implement *in vitro*, but it is possible with the support of a suitable microenvironment prior to implantation. In consequence, by utilizing the principles of biology and engineering, functional engineered liver tissue could be developed to resemble the biological tissue by *in vitro* culture. This interdisciplinary field, called tissue engineering, offers a great opportunity to overcome the health issues regarding loss or damage of the liver, drug toxicity and can be used to investigate deep within the liver's biological system.

2.3 Liver

2.3.1 Liver Architecture and Functions

The liver is one of the vital organs in the human body, located in the upper right-hand of the abdominal cavity, inferior to the diaphragm as shown in Figure 2.1. The liver is encapsulated by a connective tissue capsule that is supported by the peritoneum of the abdominal cavity. The peritoneum connects the liver by four ligaments: left triangular ligament, right triangular ligament, coronary ligament, and membranous falciform ligament. The liver anatomy consists of four separate lobes which are right (largest), left, caudate, and quadrate lobes. This detail of structures shown in Figure 2.2. The lobes divide the parenchyma of the liver into approximately 100,000 small functional units

University of Malaya

called lobules. Each lobule shaped as hexagonal-like pattern plates of hepatocytes cell radiating outward from a central vein. At the pinnacles of the lobule is consists of portal triads, including a hepatic portal vein, hepatic artery, and a bile duct.

The unique yet complex architecture of the liver is indeed designed to carry out a broad range of liver functions. This extraordinary organ is responsible for controlling body metabolism by chemically converting nutrients into energy; it also synthesizes substances needed by the cells, such as proteins, carbohydrates, and fats (Ge, Du, & Mao, 2014; Wright, Anderson, & Bridges, 1990). To continuously sustain the living state of the body tissue, the liver also acts as a filter, detoxifying the undesired elements found in the blood and lymph circulatory systems such as toxins and excess hormones (Liska, 1998). Thus, research has found that significant changes in liver function, such as immune dysfunction and chronic diseases such as cancer and fibromyalgia, can cause liver damage (Campana & Iredale, 2017; Kozanoglu, Canataroglu, Abayli, Colakoglu, & Goncu, 2003; Than & Newsome, 2015).

University of Malaya

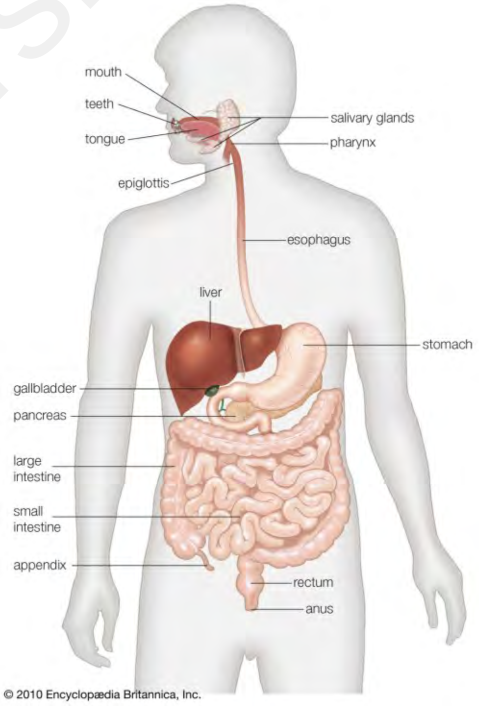

© 2010 Encyclopædia Britannica, Inc.

Figure 2.1: Human digestive system. Adapted from http://www.britannica.com.

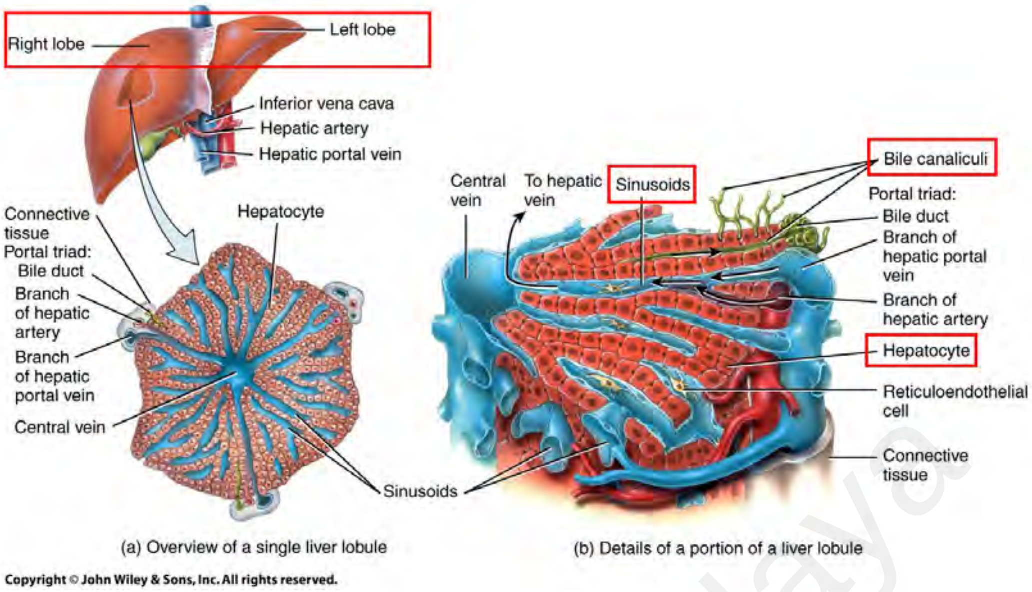

Copyright © John Wiley & Sons, Inc. All rights reserved.

Figure 2.2: Structure of liver lobule. Adapted from http://anotomychartpad.com.

2.3.2 Liver Regenerative Mechanism

The normally functioning liver has a unique feature whereby the hepatocytes rarely proliferate in normal conditions but are able to regenerate upon the loss of hepatic tissue mass. Nearly a century ago, Higgins (1931) showed the ability of the liver of the white rat to self-regenerate after performing a 70% partial hepatectomy, and the restoration was completed within just 3 weeks. This finding has encouraged scientists to deepen the understanding of this remarkable event. Rhim, Sandgren, Palmiter, and Brinster (1995) developed a transgenic mouse system to evaluate the regenerative capacity of hepatocytes. In their study, they showed that the transplantation of xenogeneic liver cells into albumin-urokinase (Alb-uPA) transgenic mice completely regenerated in several weeks with a liver mass similar to that of the control. Moreover, adequate liver function was identified in the transplanted rat hepatocytes by secretion of proteins as well as drug metabolism and detoxification (Rhim et al., 1995). On the other hand, decreases in liver mass occurred when the functional capacity of the liver went beyond the body’s ideal requirements.

University of Malaya

Extensive studies have been conducted to analyze the mechanisms that regulate regenerative development using animal models, commonly mice, subjected to partial hepatectomy. Hepatocytes regenerate in response to a series of various gene activations, growth factor production, and morphologic arrangement throughout several phases, as shown by the general flow in Figure 2.3 (Fausto, 2001). Every growth factor plays a definite role during the regenerative process, including hepatocyte growth factor (HGF), epidermal growth factor (EGF), transforming growth factor-α (TGF-α), tumor necrosis factor-α (TNF-α), interleukin-6 (IL-6), insulin, and norepinephrine. However, dysregulation of these growth factors may lead to hepatocarcinogenesis (Kiss, Wang, Xie, & Thorgeirsson, 1997). Studies suggest that overexpression or imbalance of either growth stimulatory or inhibitory factors is fundamental in tumor development (Kawaguchi & Kataoka, 2014; Michalopoulos, 2017). Therefore, it is essential to deliberate these biological circumstances during tissue construction.

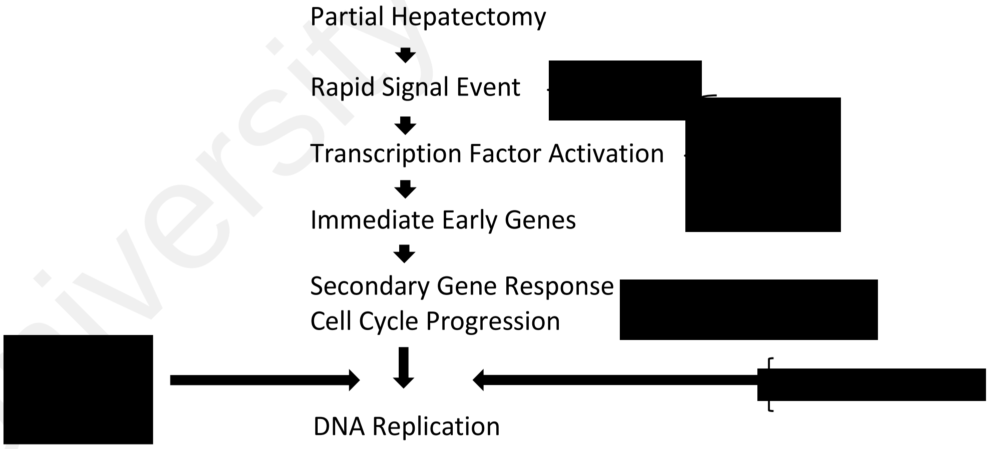

Figure 2.3: A broad outline of important events in liver regeneration. Reproduced with permission (Fausto, 2001).

2.4 Engineering Approaches

Continued advancements in tissue engineering have provided appropriate environments on the microscale to suit the micro dimensions of cells. Emerging microelectromechanical system (MEMS) technologies allow new opportunities to

University of Malaya

understand the electrochemical and mechanical processes responsible for changes in cell culture performance (James, Mannoor, & Ivanov, 2008; Pan, Wang, Ru, Sun, & Liu, 2017). Unlike conventional apparatus, with the aim of liver-on-a-chip, many recent tools have been developed with the ability to operate small volumes of fluid, are portable and easy to integrate with other systems, and are low-cost products for the purpose of commercialization. Figure 2.4 shows some techniques available for liver tissue engineering.

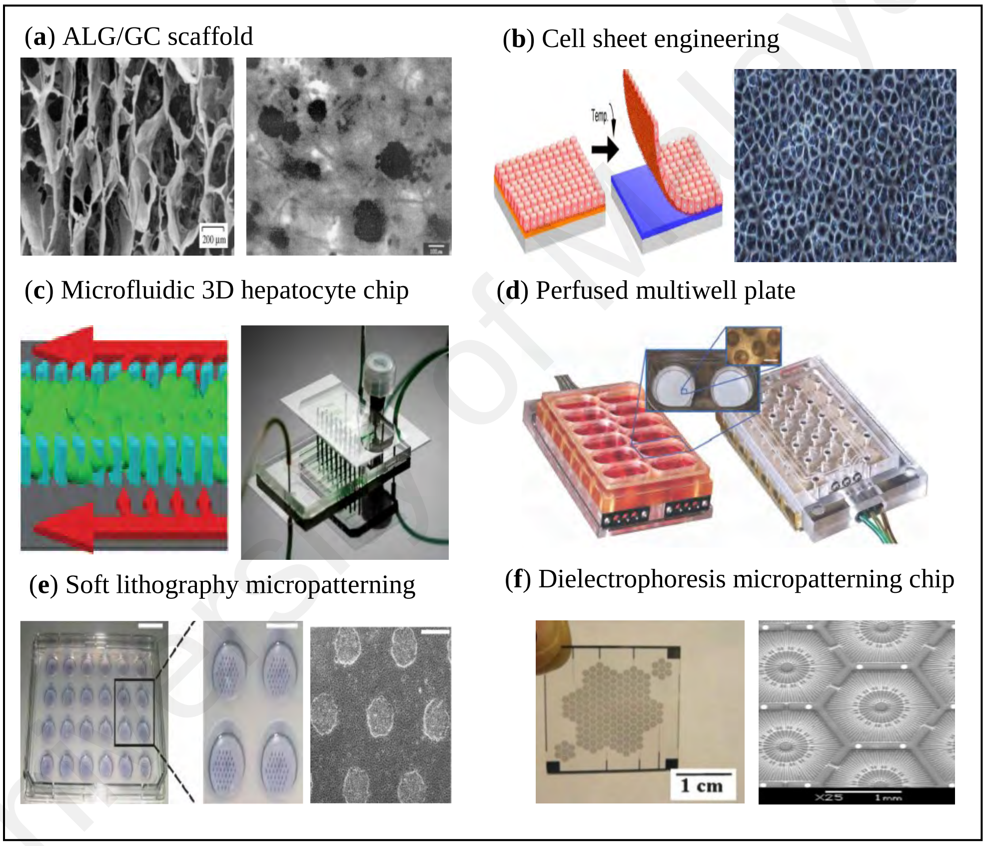

Figure 2.4: (a) SEM image of ALG/GC scaffold for hepatocytes attachment (T. W. Chung et al., 2002). (b) Cell sheet technology for passive cell patterning using PIPAAm-grafted surface (Kikuchi & Okano, 2005). (c) Microfluidic 3D hepatocyte chip utilizing micro-pillars for cell culture (Toh et al., 2009). (d) Perfused multi-well plate with an array of 12 scaffold-based bioreactors (Domansky et al., 2010). (e) Soft lithography to fabricate hepatocytes micropatterning in a multiwell format (Khetani & Bhatia, 2008). (f) Microelectrode for active liver cell patterning via DEP mechanism (Ho et al., 2013). Reproduced with permissions.

However, the major attraction of those tools for cell culture applications is the competency to imitate the *in vivo* microenvironment of cells with good cell-cell and cell-ECM interactions, optimum oxygen and nutrient supplies, precisely controlled

University of Malaya

temperature and pH, biochemical and mechanical stress, and many other factors. In this section, we briefly review some engineering approaches that address some desirable parameters for generating liver tissue cultured *in vitro*. Moreover, a summary of representative literature of comparison between available engineering approaches specifically for liver tissue engineering is included in Table 2.1.

2.4.1 Scaffold-based

Scaffolds are designed to function as *in vitro* ECM for cell culture to promote cell differentiation, proliferation, and migration, and they gradually degrade upon implantation in the patient and are substituted by neo-tissue. Generally, scaffold structure should have a highly interconnected porous network to allow perfusion of gases, nutrients, and growth factors to the cells; 3D; be biodegradable, for easy elimination out of the body; be biocompatible with the host tissue; and possess good mechanical properties to support and sustain the preferred shape (Dhandayuthapani, Yoshida, Maekawa, & Kumar, 2011; Eltom, Zhong, & Muhammad, 2019; Hutmacher et al., 2001). These structures can be fabricated from a wide variety of materials, either natural biomaterials or synthetic polymers.

One of the most widely used natural biomaterials for liver tissue engineering is alginate. In addition to its biocompatibility and low toxicity, the hydrophilic nature of the alginate scaffold facilitates the efficient seeding of hepatocytes onto the sponge-like scaffold. Glicklis, Shapiro, Agbaria, Merchuk, and Cohen (2000) observed the aggregation behavior of freshly isolated adult rat hepatocytes seeded within a 3D alginate-based scaffold. This work showed that within 24 hours after cell seeding, small groups of hepatocytes begin to appear, and by day 4, they become as large as the pore size of the scaffold and form spheroids with the presence of fibronectin. Within a week, the cells performed typical hepatocyte functions, such as secreting albumin and urea at the

University of Malaya

maximal rate, indicating that the alginate scaffold facilitated their functional expression. Unfortunately, poor mechanical properties due to unstable ion exchange and a deficiency of cell-adhesive signals prevent the maintenance of these good conditions for hepatocytes for a long period (Shoichet, Li, White, & Winn, 1996). Thus, a hybrid alginate/galactosylated chitosan (ALG/GC) porous scaffold was fabricated by lyophilization, and the mechanical strength was enhanced by changing the ALG to GC ratio and controlling the freezing temperature (T. W. Chung et al., 2002; J. Yang et al., 2001). Primary hepatocytes isolated from mouse seeded onto ALG/GC showed a 30% increase of hepatocyte attachment compared to the alginate scaffold alone. These results were due to good interactions between the ligands and receptors available in the appropriate combination of ALG and GC. Besides, hepatocyte functions such as albumin secretion and ammonia removal were significantly higher and were maintained for a longer time than on alginate scaffolds without chitosan.

Advances in polymer chemistry have aided the engineering of synthetic biomaterials to overcome the disadvantages of natural polymers. Poly(L-lactic acid) (PLLA), poly(lactic-co-glycolic acid) (PLGA) and poly(ε-caprolactone) (PCL) are among the wide variety of synthetic polymers available with the benefits of good mechanical properties, controllable degradation rates, and easy accessibility. For example, collagen-coated PLGA scaffolds were to be useful for culturing rat hepatocytes, which exhibited urea synthesis after two weeks of culturing (Hasirci et al., 2001). The culturing efficacy of PLLA 3D scaffolds was investigated by culturing porcine hepatocytes in the presence of hepatocyte growth factor. Liver specific functions were reported to be enhanced, with increased levels of albumin secretion, cytochrome P450, ammonia removal, and urea synthesis compared to those of the control (Huang, Hanada, Kojima, & Sakai, 2006).

University of Malaya

Table 2.1: Comparison between available engineering approaches.

Engineering Approaches	Features/Tools	Fabrication Technique	Cell Viability	Advantages	Limitations
Scaffold-based	• Natural biomaterials • Synthetic polymer • Hydrogels	• Needs an expert to handle	• 1-3 days	• 3-D environment • No external forces	• Not applicable for complicated structure tissue • Need highly-control over microscale histoarchitecture • Poor mass transport properties • Inflammatory response • Weak real-time imaging system
Microfluidic Platforms	• Scaffold-based microbioreactor • Microchannels perfusion • Micropillars perfusion • Microwell/microplate arrays	• Low cost • Easy to handle	• 4-7 days	• 3-D environment • Multicellular culture system • Sophisticated control of a dynamic environment • Integrated microdevices • Real-time imaging system • Point-of-care device	• Needs special attention to surface chemistry of substrate
Micropatterning	• Photolithography • Switchable surface - Cell sheets engineering • Magnetism • Optics – optoelectronic DEP • Electrokinetics – Dielectrophoresis (DEP)	• Low cost • Easy to handle	• 3-7 days	• 2-D and 3-D environment • 3-D patterned cell culture system • Multicellular culture system • Integrated microdevices • Real-time imaging system • Point-of-care device	• Needs special attention to surface chemistry of substrate

University of Malaya

However, due to several issues, scaffold-based engineering of highly structured liver replacements is not applicable. In some cases, the scaffold does not fully degrade and affecting the amount of ECM deposited by cells, thus delaying the regeneration of neo tissue resembling natural liver and possibly causing fibrosis (Y. Wang, Ameer, Sheppard, & Langer, 2002). The inflammatory response also occurred with the biodegradation process in certain cases, even with non-toxic material (Babensee, Anderson, McIntire, & Mikos, 1998; Sung, Meredith, Johnson, & Galis, 2004). Another significant drawback is a poor perfusion rate, which disturbs the smooth flow of nutrients and waste products and hence affects the cell viability.

2.4.2 Microfluidic Platform

The ability to work with small volumes of fluids flowing through a microchannel with high analytical precision are the main advantages offered by microfluidic platforms for biomedical applications including tissue engineering (S. Chung, Sudo, Vickerman, Zervantonakis, & Kamm, 2010; Das & Chakraborty, 2009; Liu et al., 2010; Materne et al., 2015). A wide variety of microfluidic platforms have been developed for liver tissue engineering, and each addresses certain factors such as cell seeding method, cell density needed, gradient and flow rate of fluids and oxygen concentration, as well as differing in design and fabrication techniques (Goral & Yuen, 2012).

Early work had fabricated a scaffold-based microbioreactor that allowed continuous perfusion of nutrients to the hepatocytes (Powers et al., 2002). The scaffolds were designed to provide a 3D culture environment as well as mechanical support, while the microbioreactor consisted of chambers with individual channels to permit the flow of culture medium controlled by the low permeability of the filter system. More recently, with some improvements, Domansky et al. (2010) developed perfused multiwell plates where each well contained a scaffold-based bioreactor. Hepatocytes were seeded onto

University of Malaya

each ECM-coated scaffold to deliver the optimum concentration of oxygen and biochemical force. Additionally, an external pneumatic diaphragm micropump was integrated to maintain constant perfusion of the culture medium, as well as model oxygen sensors to assess the oxygen tension received by hepatocytes. Another key feature of this multiple microbioreactor was that its design resembled conventional multiwell plates for tissue culture to enable ease of handling.

On the other hand, Goral et al. (2010) cultured hepatocytes in 3D perfused microfluidic devices without the presence of biological or synthetic matrices. The 3D microenvironment was maintained by a line of micropillars surrounding the cell culture chamber, and unlike other microfluidic devices, the base of the cell culture chamber also featured patterned micropillars to enhance the cellular organization. The micropillars were designed to allow the continuous flow of culture media from two side microchannels and the bottom of the microstructure. The formation of gap junctions and extended bile canaliculi during *in vitro* hepatocyte culturing indicated that a 3D microenvironment could be induced in the absence of ECM provided with dense cell-cell interactions on a perfused microfluidic platform. More recently, another hepatocyte culturing technique utilizing gel-free microfluidic platforms was presented (Shih, Tseng, Weng, Chu, & Liu, 2013). The authors proposed a multi-row square-pillar microstructure as the perfusion mechanism with a larger cell culture area. Up to 90% of the cultivated hepatocytes showed viability at day 5, supporting the hypothesis that the proposed design enables a balance between the low shear stress and high mass-transfer rate experienced during cell seeding.

In general, many parameters have been considered in each development of microfluidic platforms for the use of liver tissue engineering; high cell density to favor cell-cell and cell-ECM interactions, proper cell seeding to reduce cell damage, a good

University of Malaya

perfusion rate to provide adequate nutrients as well as sufficient oxygen supply to promote angiogenesis. However, because the liver comprises a microstructure of heterogeneously arranged cells, cell patterning technology for liver reconstruction could be compulsory. Thus, the high function and long term viability of engineered liver might be achieved with micropatterning technologies that can precisely position cells to closely mimic the natural pattern of the liver.

2.4.3 Micropatterning

Early work in the micropatterning of heterogeneous liver cells employed photolithography techniques requiring which cell-adhesive materials such as collagen, fibronectin, and polylysine. Using photolithography, S. N. Bhatia, Yarmush, and Toner (1997a) coated collagen on a substrate in specific regions to promote hepatocyte attachment. A second cell type, fibroblasts, were then seeded, these cells attached and occupied the remaining untreated areas with the favor of serum-mediated attachment, thus forming a well-ordered pattern (S. Bhatia, Balis, Yarmush, & Toner, 1998). Regardless of the well-known photolithography technique, this approach of micropatterning is restricted when it is subjected to the efficiency of cell-cell and cell-substrate adhesiveness. For instance, the first cell type must strongly adhere to the patterned area and weakly adhere to the unpattern area, and the opposite should be the case for the second cell type. Furthermore, the ordinary cell adhesion process is slow and uncontrollable, thereby decreasing the effectiveness of this technique for further application in liver tissue engineering.

Progress in surface engineering has introduced a controllable surface to dynamically regulate the interactions between cells and substrate for the successive patterning of heterogeneous cells. Cell sheets are a tissue engineering method utilizing a temperature-responsive cell culture dish. This special dish is prepared by covalently grafting a thin

University of Malaya

layer of polymer, poly(N-isopropylacrylamide) (PIPAAm), onto typical polystyrene cell culture dishes by electron beam radiation, which is sensitive to the culture temperature (Hirose, Kwon, Yamato, Kikuchi, & Okano, 2000). At a standard culture temperature of 37 °C, the PIPAAm-grafted surfaces behave as polystyrene dishes that enable cell adhesion, proliferation, and culture. By decreasing the culture temperature to 32 °C, the polymer's lower critical solution temperature (LCST), the PIPAAm-grafted surfaces rapidly become hydrophilic, facilitating cultured cell detachment and forming cell sheets without any need of chemical or mechanical forces.

Hirose, Yamato, et al. (2000) have developed two cell co-culture arrangements of patterned primary hepatocytes and endothelial cells. In the first arrangement, patterned co-culture was performed by utilizing an electron beam with a patterned mask to treat the PIPAAm-grafted surface. Hepatocytes were cultured under standard culture temperature and spontaneously detached below the LCST. Endothelial cells were then cultured on the same surfaces at 37 °C and occupied the exposed PIPAAm-grafted area to form heterogeneous cell patterns. In contrast, another arrangement included a double-layered co-culture achieved by covering the hepatocyte monolayers with endothelial cell sheets. Both arrangements appeared to maintain their differentiated state and functions for approximately one week and could be transferred with the desired shape. Maintaining the cell shape along with the ECM adhered onto the basal of cells sheet was another positive feature of this method. Compared to the conventional method using trypsin, this temperature-responsive cell culture dish offers a non-invasive harvesting method, as the cultured cells spontaneously detach in response to temperature change. Through examination by surface analysis and characterization, a group of proteins indicating the presence of ECM and good cell adhesion was found when endothelial cells were detached by simply reducing the temperature (Canavan, Cheng, Graham, Ratner, & Castner, 2005a, 2005b).

University of Malaya

However, although cell sheet engineering is very efficient in cell detachment, this method is highly dependent on the surface chemistry of the thermo-responsive dish to preserve good cell adhesion in a micropatterned manner (Kikuchi & Okano, 2005; Kumashiro, Yamato, & Okano, 2010). Numerous types of thermo-responsive dishes were developed to counteract several effects such as rapid dehydration due to poor grafting techniques of PIPAAm on the surface. Furthermore, additional steps are required, such as microcontact printing of collagens to enhance the production of ECM because they are essential for stacking multiple types of cell sheets to form 3D heterogeneous tissue (Isenberg et al., 2008).

In contrast to the above-mentioned passive cell patterning, various approaches have been developed and are still under research to actively position cells in desired patterns. With the aid of external forces such as magnetism, optics, and electrokinetics, or by combining some of these, multiple cell types, such as hepatocytes and endothelial cells, can be precisely controlled and rapidly direct cell adhesion.

Ink-jet patterning, which uses a computer-aided design (CAD) system to position cells layer-by-layer for 3D organ building offers rapid and high-resolution patterning of single and multiple cell types (Mironov, Boland, Trusk, Forgacs, & Markwald, 2003). However, the sequential processes, including designing the organ using CAD, cell printing to form cell aggregates according to the CAD design, and lastly, organ conditioning to promote cell maturation, are quite laborious and costly. Moreover, high concentrations of cells cannot be used because they may cause nozzle clogging during cell printing and thereby influence the patterning accuracy (Saunders, Gough, & Derby, 2008). Advances in optical technology have led to laser-guided writing capable of simultaneously directing multiple types of cells via a laser beam (Odde & Renn, 1999). However, the energy loading used is still a major concern, as it may lead to cell damage. Meanwhile, owing to the unique

University of Malaya

dielectric properties of every cell type, electrical force may have the ability to position multiple types of cells with high selectivity and accuracy. The electrical forces used for cell patterning at the microscale involve electrophoresis and DEP (Gonzalez & Remcho, 2005; Hughes, 2002; Manz et al., 1994), which are useful for transporting cells in microfluidic systems (Voldman, 2006; C. Zhang, Khoshmanesh, Mitchell, & Kalantar-Zadeh, 2010). In addition, large numbers of cells can be patterned simultaneously without any need for cell pre-modification or labeling, signifying benefits for tissue engineering. In the next section, the fundamental principles of DEP will be briefly described along with a presentation of electrodes for liver cell patterning.

2.5 Dielectrophoresis (DEP)

2.5.1 Principle of DEP

DEP force is the movement of polarized particles within a medium when subjected to non-uniform alternating current (AC) electrical field as has been earliest described by Pohl (1951). Biological cells are good candidates of polarizable particles, besides of microbeads, DNA, protein, bacteria, and so on for particles manipulation by isolation, characterization, separation, and patterning (N. Green, Morgan, & Milner, 1997; Hashimoto, Kaji, & Nishizawa, 2009; Hughes, Morgan, Rixon, Burt, & Pethig, 1998; Jubery, Srivastava, & Dutta, 2014; Yantzi, Yeow, & Abdallah, 2007).

Biological cell when suspended in a non-uniform AC electrical field will become polarized and experienced DEP force, F_{DEP} which is given by Eq. (2.1):

$$F_{DEP} = 2\pi r^3 \varepsilon_0 \varepsilon_\mathrm{m} \mathrm{Re}[\mathrm{K}(\omega)] \nabla \mathrm{E}^2 \tag{2.1}$$

where r is the radius or cell, ε_0 and ε_m are the permittivity of free space and surrounding the cell respectively, $\mathrm{Re}[\mathrm{K}(\omega)]$ is the Clausius-Mossotti factor, ∇ is the Del

University of Malaya

gradient operator and E is the electrical field. The Clausius-Mossotti factor is further described by Eq. (2.2):

$$Re[K(\omega)] = \frac{\varepsilon_p^* - \varepsilon_m^*}{\varepsilon_p^* + 2\varepsilon_m^*} \tag{2.2}$$

where ω is the angular frequency and ε_p^* and ε_m^* are the complex permittivities of the cell and medium, respectively. Additionally,

$$\varepsilon^* = \varepsilon - \frac{j\sigma}{\omega} \tag{2.3}$$

where j is the imaginary unit, ε is the permittivity, σ is the conductivity and ω is the angular frequency of the given AC electric field. The direction of movement cell depends upon the relative polarizability of the cell in the suspending medium verify by the Clausius-Mossotti factor which further depends on the applied frequency, $f = \omega/2\pi,$ and properties of both the suspending medium and cell. As illustrated in Figure 2.5, in the case where the polarizability of cells is higher than the medium, the cells tend to move towards the smaller electrode where the electrical gradient is high. If the cells experienced less polarizable than the medium, the cells will then move towards a low electrical gradient near the larger electrode. The collection of cells to the high electric fields is identified as positive DEP (pDEP) and repulsion from the high electric fields is identified as negative DEP (nDEP).

This phenomenon was then believed to be beneficial for cell patterning. The fact that DEP is a frequency-dependent force enables cells to be precisely controlled and manipulate by a certain frequency and guided to the desired pattern relative to the non-uniform electric field generated by the electrode. In addition, the innovation in DEP research couple with advanced microfabrication of CMEMS and microfluidic technique

University of Malaya

has introduced another type of electrode to develop better tissue engineering tools primarily for the liver.

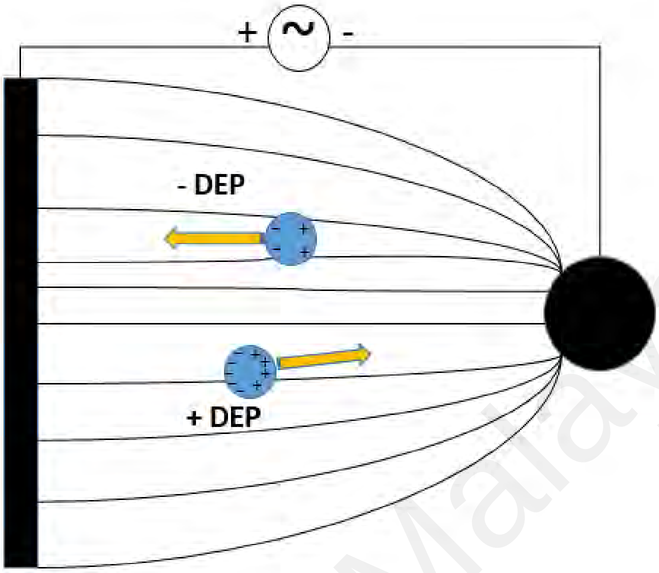

Figure 2.5: Schematic diagram of the DEP phenomenon.

2.5.2 Electrodes for DEP-Based Cell Patterning

Electrode devices designed specifically for cell patterning have particular requirements that differentiate them from other applications. Significant considerations in the development of electrode cell patterning include electrode geometry and dimensions for specific cell patterning and culture, as well as the patterning configuration used for DEP cell manipulation. Therefore, one must be aware of all the possible choices to ensure that the design is in line with the desired application. This section highlights the several types of geometry that exist, specific configurations to control the patterning of liver cells.

2.5.2.1 **Electrode Geometry**

In order to dielectrophoretically move the cells, a non-uniform electric field is necessary to generate an unbalanced force on the suspended cells in the field. The non-uniform field can be created by applying a voltage across geometrical electrodes (Bashar Yafouz, Kadri, & Ibrahim, 2013; Yao, Zhu, Zhao, & Takei, 2019), by placing an insulator

University of Malaya

between electrodes (Ozuna-Chacón, Lapizco-Encinas, Rito-Palomares, Martínez-Chapa, & Reyes-Betanzo, 2008; Saucedo-Espinosa & Lapizco-Encinas, 2015; Srivastava, Gencoglu, & Minerick, 2011) or even electrodeless (Chiou, Pan, Chien, Lin, & Lin Jr, 2013; Chou & Zenhausern, 2003; Pesch, Kiewidt, Du, Baune, & Thöming*, 2016).

A wide range of electrode geometries has been demonstrated for patterning multiple types of cells with different formations (Khoshmanesh, Nahavandi, Baratchi, Mitchell, & Kalantar-zadeh, 2011). The most common and cost-effective microfabrication technique, photolithography, can precisely form electrode gaps to create pearl-chain effects with the use of specific DEP configurations (Kretschmer & Fritzsche, 2004; Bashar Yafouz et al., 2013). This approach was proven to provide significant effects in the patterning of complex and interconnected heterogeneous liver cells. Ho and colleagues, with their proposed microfluidic chip, have designed an array of concentric-stellate-tip electrodes to yield radial-patterned electric fields for dielectrophoretically manipulating viable liver cells (C.-T. Ho, R.-Z. Lin, W.-Y. Chang, H.-Y. Chang, & C.-H. Liu, 2006). As illustrated in Figure 2.6, the concentric-ring array electrodes were designed to generate radial electric fields with random pearl-chain effects.

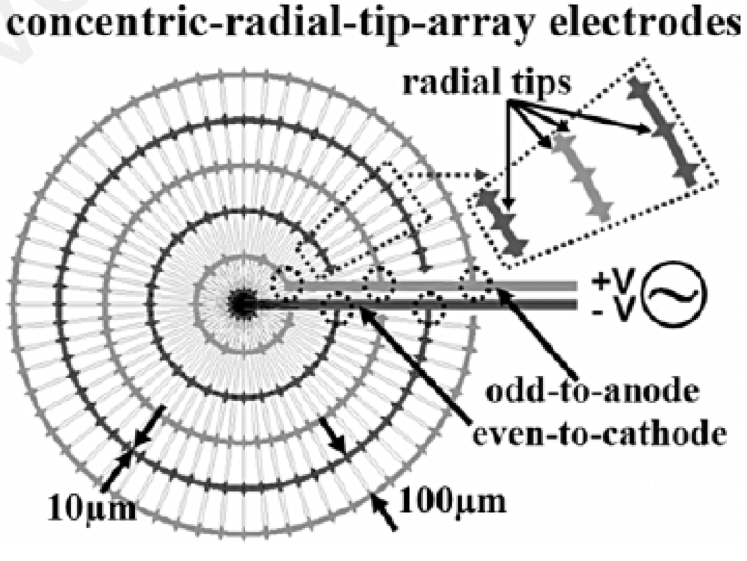

Figure 2.6: Concentric-stellate-tip electrode for 2D liver cell patterning. Reproduces with permission (C.-T. Ho et al., 2006).

University of Malaya

To further form and align the hepatocyte cell chains with radial orientation, each ring included stellate tips to enhance the electric field gradient, thereby attracting the cells. The gaps between the adjacent rings were fixed at 100 µm to trap approximately 8 cells in a line. Such 2D concentric-stellate-tip electrodes were designed to purposely mimic the lobular structure of biological liver tissue, in which vascular endothelial cells were then trapped in between hepatocyte cell chains radiating outward from the center by DEP manipulation.

However, recently, Ho and other researchers have made some modifications in the electrode arrangement to achieve 3D liver cell patterning by generating a vertical DEP force, as shown in Figure 2.7a (Ho et al., 2013). In addition, they also made some changes to the liver-mimetic electrode design, which consists of two independent electrodes as shown in Figure 2.7b. The first DEP patterning electrode functions to snare hepatocytes, while the second electrode is for snaring endothelial cells. Moreover, just as in the previous design, the outer part of both electrodes has a compact electrode design for denser cell patterning.

University of Malaya

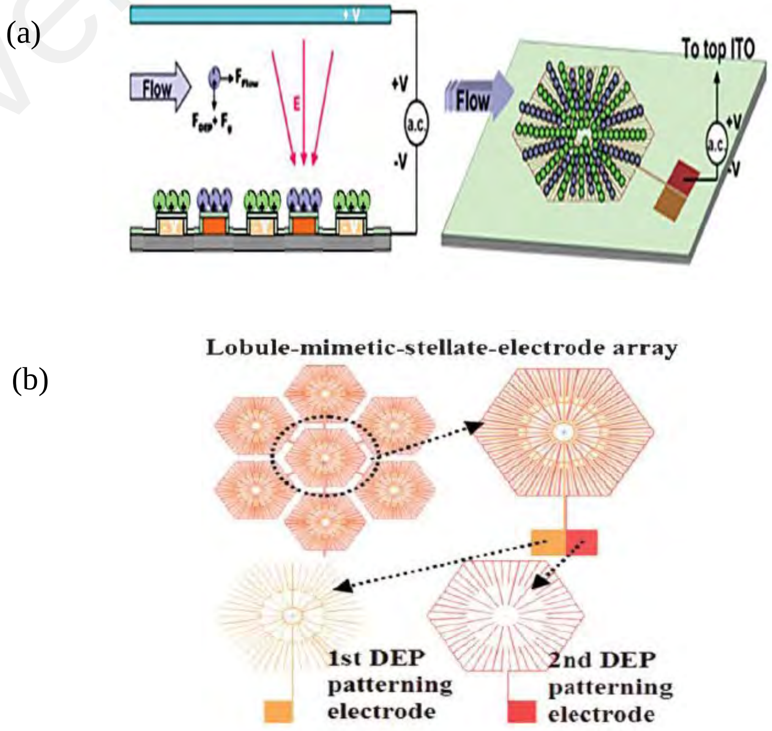

Figure 2.7: (a) Vertical setup for 3D heterogeneous cells patterning by DEP. (b) The lobule-mimetic-stellate-electrode arrays for 3D liver cell patterning. Reproduced with permission (Ho et al., 2013).

In another strategy, Schütte et al. (2011) utilized insulator-based DEP cell patterning to guide human primary hepatocytes and endothelial cells into a liver-sinusoid pattern. Moreover, their microfluidic chip also provided continuous perfusion of culture media and automated cell seeding. A set of electrodes in the sidewalls of the microchannels with cross-sections in between was used to generate non-uniform electric fields to produce DEP force to guide hepatocytes surrounded by endothelial cells towards the assembly gaps in the well-designed cell culture chambers. By increasing the height of the gaps to 100 µm and decreasing the inclination angle to 30°, the numerical simulation results showed that the cells could experience high DEP forces to further assemble into the gaps in a liver sinusoid-like pattern within 2 minutes. Furthermore, the micropillars placed at the front and back of the assembly gaps were also found to successfully control the flow velocity and shear stress during cell seeding and culture. However, ongoing research for long-term sinusoid cell culture on-chip is still in progress; more parameters still need to be investigated, such as electrical effects on the cells and the essential culture conditions.

2.5.2.2 Patterning Configuration

Live cells can maintain their viability under strong DEP force under many conditions. Applying high-voltage electric pulses may cause cell damage such as electropermeabilization due to the high permeability of the cell membrane. Nevertheless, short-term exposure to certain ranges of frequency showed few acute changes in cells under DEP force (Glasser & Fuhr, 1998). Furthermore, high-frequency electric fields can indirectly reduce electrochemical effects at the electrode, such as corrosion and bubble formation (Voldman, Gray, Toner, & Schmidt, 2002). In terms of DEP manipulating buffer, a high-conductivity buffer is required to keep cells alive and to maintain their adherence capability. Media containing high concentrations of Ca^{2+} and Mg^{2+} ions are

University of Malaya

favorable for activating cadherins and integrins, molecules needed for cell adhesion (Grzesiak & Pierschbacher, 1995). However, a low-conductivity buffer is required for effective DEP cell manipulation. In addition to significantly reducing the heating effect, reducing the medium conductivity can minimize the electropermeabilization effect (Pucihar, Kotnik, Kandušer, & Miklavčič, 2001).

As described earlier, cells can be configured either by pDEP or nDEP, depending on the working frequency. In the case of cell patterning, pDEP is more appropriate because it attracts and assembles cells exposed to a high electric gradient according to the electrode geometry. There were also some studies that utilized nDEP for cell patterning. After an AC voltage was applied, nDEP forces pushed the cells away from electrodes yet still reflected the electrode shape (Matsue, Matsumoto, & Uchida, 1997). Moreover, an inverted design can also be used under nDEP for patterning (Yu et al., 2004). However, aside from the smaller forces generated by nDEP, the main disadvantage for cell patterning is that the cells are unlikely to remain in the pattern design and rapidly move out of the design after removing the DEP force.

Both horizontal and vertical pDEP have been proven to successfully pattern hepatocytes and endothelial cells according to designed electrodes, closely mimicking the morphology of real liver tissue (C.-T. Ho et al., 2006; Ho et al., 2013). In early electrode designs, horizontal DEP forces were generated by two concentric electrodes placed on the same plane, identified as odd-ring and even-ring, which were subjected to an AC voltage. To achieve both robust DEP forces and high cell viability, the parameters were set to be below 5 V at 1 MHz with a low-conductivity medium of 10 $mS{\cdot}m^{-1}$. Upon voltage application, in parallel, pDEP forces guided the randomly distributed hepatocytes towards the high potential region provided by the stellate tips, and the cells aggregated to it. The optimum cell density achieved then resulted in strong interactions between the

University of Malaya

cells due to the dipole induced by DEP and eventually formed a radial pearl-chain pattern from tip to tip (Schwan & Sher, 1969). To ensure high hepatocyte viability, the DEP manipulating buffer was replaced by a standard cell culture medium without DEP presentation for some time. The pearl-chain formation allowed direct communication between cells, thus enhancing the adherent forces and preventing the well-patterned hepatocytes from falling apart. In addition, prior to the experiment, the substrate was coated with poly-D-lysine to facilitate the immobilization of the hepatocytes on the substrate and maintain the liver-like formation. Later, continuing the pDEP manipulation, endothelial cells were loaded and resided in the empty spaces between the hepatocyte chains, mimicking the sinusoid pattern of vascular endothelial tissue in the real liver. In another arrangement, Ho et al. (2013) utilized vertical pDEP across two lower electrodes for trapping cells, and upper electrodes acted as ground electrodes biased with an AC voltage. The first electrode, as depicted in Figure 2.7b, was supplied with vertical pDEP voltage to attract, trap, and pattern hepatocytes according to the electrode design. Then, pDEP forces were again used to move, snare and pattern endothelial cells according to the second electrode design, which sandwiched them between the first patterned hepatocytes to attain a heterogeneous cell pattern mimicking the morphology of biological tissue.

2.5.2.3 **Types of Electrode Commonly Used for DEP**

One of the essential parameters of the DEP system is the electric field gradient generated by electrodes or electrodeless/insulator structures. Herein, we focus on the types of the electrode and the structure itself (i.e. 2D and 3D) while the microfabrication of the electrode will be discussed in the next Section 2.6.

Traditionally, most of the DEP work use a metal electrode with a 2D planar structure confined in the microchannel to induce a non-uniform electric field in the sample since

University of Malaya

metal is a good conductor. However, the 2D planar electrode only affects the movement of particles that close to the surface of the electrode which usually patterned at the bottom of the microchannel. Alternatively, a variety of 3D electrode structures have been developed such as sidewall-patterned, top-bottom patterned, and extruded vertical electrode (M. Li, Li, Zhang, Alici, & Wen, 2014).

The use of a 3D structure can generate DEP force over a larger volume within the microchannel. Nevertheless, the fabrication involving the 3D metal electrode turns out to be a more complicated technique and costly relative to the 2D metal electrode. Besides, electrolysis regularly happens when the metal electrode is in direct contact with the sample caused by the excessive applied voltage. For example, Voldman et al. (2002) used electroplated extruded gold electrodes to induce DEP on cells for flow cytometry application. L. Wang, Flanagan, and Lee (2007) has also been used the electroplating technique to implement arrays of 3D electrodes on the sidewall of the microchannel and used DEP to align a stream of particles.

An alternative to metal electrodes is to use insulator structures placed in the microchannel to distort the electric field applied to electrodes placing at the inlet and outlet of the microchannel. This insulator-based dielectrophoresis or iDEP was first introduced by Masuda, Itagaki, and Kosakada (1988). iDEP usually fabricated from glass or polymers, hence the chance of sample electrolysis is decreased (Davalos et al., 2008; Lapizco-Encinas, Davalos, Simmons, Cummings, & Fintschenko, 2005). However, iDEP involves very high voltages to produce an appropriate electric field for DEP due to large separation between metal electrodes which increase the threat of electrical shock during operation (Braff, Pignier, & Buie, 2012).

In 2005, C. Wang, Jia, Taherabadi, and Madou (2005) introduced a novel method of fabrication 3D glass-like carbon electrode using CMEMS. Over the years, carbon-

University of Malaya

electrode dielectrophoresis or known as carbon-DEP has been documented in numerous applications due to the advantages offered compare to traditional DEP. The ability to be developed in high aspect ratio with inexpensive and simplicity of their fabrication has greatly improved the yield and efficiency of the DEP device by decreasing the mean distances of particles to the closest electrode surface. Carbon-DEP becomes as an alternative electrode material for DEP because it combines the advantages of metal-based DEP and iDEP. For instance, because of the carbon electrode feature a wider electrochemical stability window, a higher electric field can be applied without electrolyzing the sample, an advantage mutual with iDEP. While an advantage mutual with metal-based DEP, instead of hundreds or thousands of volts required in iDEP to induce DEP, the carbon electrode can taking low voltages in the range of ten volts to be polarized and generate an appropriate electric field for DEP. Additionally, glass-like carbon is chemically inert in solvents, make it resistant from strong acids such as hydrofluoric, nitric, sulfuric, and other corrosive substances. Significantly, glassy-like carbon has outstanding biocompatibility that allows its application in biomedical studies including implants, scaffolds, and as the substratum for cell culture.

These DEP-based cell patterning techniques can be efficient, high throughput, and reproducible, but it is necessary to identify the critical parameters as depicted in Table 2.2 to conserve the cell viability and functionality.

University of Malaya

Table 2.2: Comparison of electrode design parameters for DEP-based liver cell patterning.

Electrode Geometry	**Electrode Configuration**	**Electrode Material**	**Electrode Structure**	**Voltage Applied (V)**	**Electric Field Generated (V/m)**	**Electrode Resistivity (Ω·m)**	**Cell Viability**	**Reference**
Concentric-stellate-tip	Horizontal pDEP	Metal: Platinum	2D	5	6×10^{9}	10^{-7}	95%	(C.-T. Ho et al., 2006)
Radially geometric	Vertical nDEP	Metal: Titanium	2D	2	2×10^{11}	10^{-7}	92%	(Puttaswamy et al., 2010)
Lobule-mimetic-stellate	Vertical nDEP	Metal: Platinum	2D	5	1×10^{11}	10^{-7}	N/A	(R.-J. Chen & Liu)
Hepatic radial electrode	Vertical pDEP	Polymer (PEG-DA) + Titanium electrode	3D	7	N/A	N/A	N/A	(Y.-S. Chen, Ke, & Liu, 2011)
Parallel sidewalls electrode	Horizontal pDEP	Insulator (COC) + Gold Electrode	3D	200	2×10^{5}	10^{-9}	90%	(Schütte et al., 2011)
Lobule-mimetic-stellate	Vertical pDEP	Metal: Platinum	2D	5	3×10^{4}	10^{-7}	95%	(Ho et al., 2013)
Multi-layer conductive scaffold	Vertical pDEP	Conductive Polymer (CB- PDMS)	3D	60	2×10^{4}	10	77%	(Chu, Huan, Mills, Yang, & Sun, 2015)
Multi-layer hexagonal electrode	Vertical pDEP	Titanium electrode + Hydrogel (GelMa)	3D	7	2×10^{6}	N/A	95%	(Y.-S. Chen et al., 2015)

University of Malaya

2.6 Carbon MEMS (CMEMS)

Carbon MEMS can be referred to as microfabrication technology involve the set of methods to derive glass-like carbon structures from patterned organic polymers. Commonly, the CMEMS process includes two phases: 1) micro- and nano-fabrication techniques including machining, stamping, casting, and lithography 2) follows by pyrolysis to derive glass-like carbon structures. Herein, photolithography is utilized to pattern the polymer using light, due to the ability to finely control the final dimension and complexity of the precursor polymer structure. Photolithography of SU-8

The organic polymer that commonly used as a carbon precursor is SU-8, an epoxy-based negative photoresist. It was developed by IBM back in the late 1970s, composed of dissolution of EPON® SU-8 resin in an organic solvent (such as propylene glycol methyl ether acetate, PGMEA, cyclopentanone or gamma-butyrolactone, GBL) and an additional 5% to 10% in weight of salt (triarylsulfonium hexafluoroantimonate) as a photoinitiator (Ito, 1997). The viscosity of the photoresist is distinct by the ratio of SU-8 resin to the solvent, enable the range of resist film thickness. Due to its low absorption in the ultra-violet (UV) spectrum, it allows to pattern high aspect ratio structure with closely vertical sidewalls. The cross-linking of the SU-8 initiate upon the irradiation by UV light, generation of strong acid that opens the epoxy rings and acid-catalyzed activated during the post-exposure bake. However, the properties of the SU-8 are very subtle to the variations of the processing parameter (Feng & Farris, 2002).

Typically, SU-8 photolithography involves a set of processing steps: photoresist coating, soft bake, exposure, post-exposure bake, and developing. This entire process should be optimized for the specified application. A photomask is designed to enable the selective passage of UV light through the photoresist layer and changes its chemical composition by cross-linking according to the desired pattern. Cross-linking of the

University of Malaya

photoresist influenced by the combination of exposure dose (energy and time) and post-exposure bake time and temperature. The detail on SU-8 photolithography processing steps is presented in Section 3.3.3.1.

2.6.1 Pyrolysis and Glassy Carbon

Upon photolithography, carbon structures are obtained through a pyrolysis process. Pyrolysis or also known as carbonization is a thermochemical decomposition process to convert photosensitive polymer into carbon in an inert atmosphere. During carbonization, several chemical reactions happen such as condensation, dehydrogenation, hydrogen transfer, and isomerization. (Fitzer, Mueller, & Schaefer, 1971; Jenkins & Kawamura, 1976; Rodrigo Martinez-Duarte, 2014). Table 2.3 resumes the chemical reactions happen during three major steps of the pyrolysis process.

Table 2.3: Chemical reactions during the carbonization process.

Step	**Pre-carbonization (<300°C)**	**Carbonization (300°C-500°C)[1] (500°C- 1200°C)[2]**	**Annealing (>1200°C)**
Reactions	Elimination of molecules of solvent and unreacted monomer of the polymer	[1]Elimination of oxygen, nitrogen, chlorine. Form conjugated carbon system and hydrogen atoms being removed. [2]Completely eliminate all the elements and interconnect the aromatic network.	Graphitic zones start to form. Eliminate any structural defects and evolve further impurities.

The resulting carbon material for the process above is usually glassy carbon (GC). Glass-like appearances such as smooth, shiny, and conchoidal fracture surely reflect the name. GC has a carbon allotrope that exhibits excellent properties such as wider

University of Malaya

electrochemical, high impermeability, and high conductivity (Mardegan et al., 2013). This carbon network is self-polymerize and depends on several factors that may modify the graphitization including the chemical structure of the polymer precursor, fabrication technique, and pyrolysis condition. For example, Mardegan et al. (2013) found that electrochemical performance has improved by extending the dwell times from 1 hour to 8 hours. However, there is no increase in graphitic content observed using Raman spectroscopy and X-ray diffraction (XRD) due to the low sensitivity for small sample volume such as thin carbon films. On the other hand, as the thickness of the carbon film decrease, the resistance increase and no longer suitable for electrochemical applications.

The SU-8 patterned shrink during pyrolysis due to the mass loss when the elimination of elements such as oxygen and hydrogen. The shrinkage commonly involving both vertical and lateral while holding the SU-8 original shape. Vertical shrinkage percentage varies from 37% to 86% and is found to be inversely proportional to the height of SU-8 and directly proportional to the pyrolysis temperature (Martinez-Duarte et al., 2011). However, shrinkage obtained in the lateral plane is lesser than the vertical plane because the SU-8 patterned are attached to the substrate surface and avoids further shrinkage of the diameter. Shrinkage of the free-standing SU-8 structure has been shown to be isometric (R Martinez-Duarte, Madou, Kumar, & Schroers, 2009).

This shrinkage has been shown repeatable for specific dimensions of the SU-8 pattern and the pyrolysis protocol. Though, there are several parameters that give impacts on the shrinkage of the polymer. Ranganathan, Mccreery, Majji, and Madou (2000) reported that besides different temperatures, different ambient atmospheres also affect the shrinkage process; nitrogen generally initiated more shrinkage as compared to the vacuum atmosphere. Other authors also showed that the shrinkage influenced by the temperature, as the temperature increase from 600 ℃ to 1000 ℃ the shrinkage is slightly increased

University of Malaya

(Park, Taherabadi, Wang, Zoval, & Madou, 2005; Singh, Jayaram, Madou, & Akbar, 2002). The effect of initial dimensions was studied by Natu, Islam, and Martinez-Duarte (2016), who reported that the shrinkage depends on the area accessible for degassing during carbonization. Hence, the ratio of the lateral and vertical surface area is significantly influenced. Recently, they also showed that the geometry of the pattern plays a major role in determining the shrinkage of the polymer (Natu, Islam, Gilmore, & Martinez-Duarte, 2018). Thus, once the shrinkage is characterized appropriately, it can be reproducible for a production process.

2.6.2 Internal Resistance of Carbon Electrode

In an electrode material, there is a voltage drop due to the internal resistance of the material. High internal resistance plays a role affecting the DEP performance as the current to the electrical potential becomes larger according to Ohm’s law in Eq. (2.4):

$$E = IR \tag{2.4}$$

where E is the electrode potential, R is the resistance and I is the current. One potential disadvantage of the 3D carbon electrode is it has a voltage drop due to the Ohmic resistance. This resistance is generated by the thin connecting leads at the base of the 3D structure as well as from the function generator, hence requiring higher voltage than those applied in the metal electrode. Nevertheless, a voltage range of 20 V has been verified to be adequate to generate an appropriate DEP force for biological cell manipulation when using carbon electrodes (Rodrigo Martinez-Duarte, Gorkin III, Abi-Samra, & Madou, 2010; Martinez-Duarte et al., 2011).

Towards minimizing the internal resistance, introducing nanostructure such as graphene can be promising. Graphene is one of the highest studied materials over a decade since it has remarkable properties (Geim, 2009). The integration of the carbon

University of Malaya

nanostructures onto the carbon electrode shows many advantages, i.e. increase surface area, enhanced conductivity, and improved optical properties. One method was to integrate graphene nanosheets through both photolithography and electrostatic spray deposition (ESD) processes onto the carbon micropillar array (Penmatsa et al., 2012). The main parameters such as deposition time, substrate temperature, and nozzle-substrate distance were shown to have a morphology effect of the layered graphene film. This graphene/carbon micropillar shows a significant increase in effective surface area which is favorable to improve the electrical functionality of the electrochemical device. In another study, the ESD technique was also used to deposit graphene/enzyme onto the 3D carbon microstructures (Song, Chen, & Wang, 2015). This excellent integration exhibited almost seven times of improved power density as compared to the bare carbon microstructures.

To the best of the author’s knowledge, there are no publications on the graphene-based 3D carbon electrode for DEP applications. It will be incredible to further enhance the performance of DEP manipulations with the integration of graphene into the 3D carbon electrode. Besides, other efforts are on the patterning of carbon electrodes on top of metal leads to extra minimize the voltage requirements.

2.7 Summary

This chapter highlighted several works of literature related to this study. First, brief detail about liver structure and functions have been discussed. Several of engineering approaches for in vitro liver cell culture to treat liver disease and failure were outlined where micropatterning by DEP was highlighted. Next, the theory on DEP phenomena was presented along with a discussion about types of electrode usually used for DEP. Finally, reviewed on CMEMS microfabrication technology to fabricate the proposed

University of Malaya

carbon electrode that will be used in this study for potential dielectrophoretic hepatic cell patterning.

University of Malaya

CHAPTER 3: METHODOLOGY

3.1 Introduction

This chapter generally discussed the design, simulation, microfabrication process, and characterization of the fabricated 3D carbon-DEP system for the use in particle patterning as summarized in the flowchart shown in Figure 3.1 below:

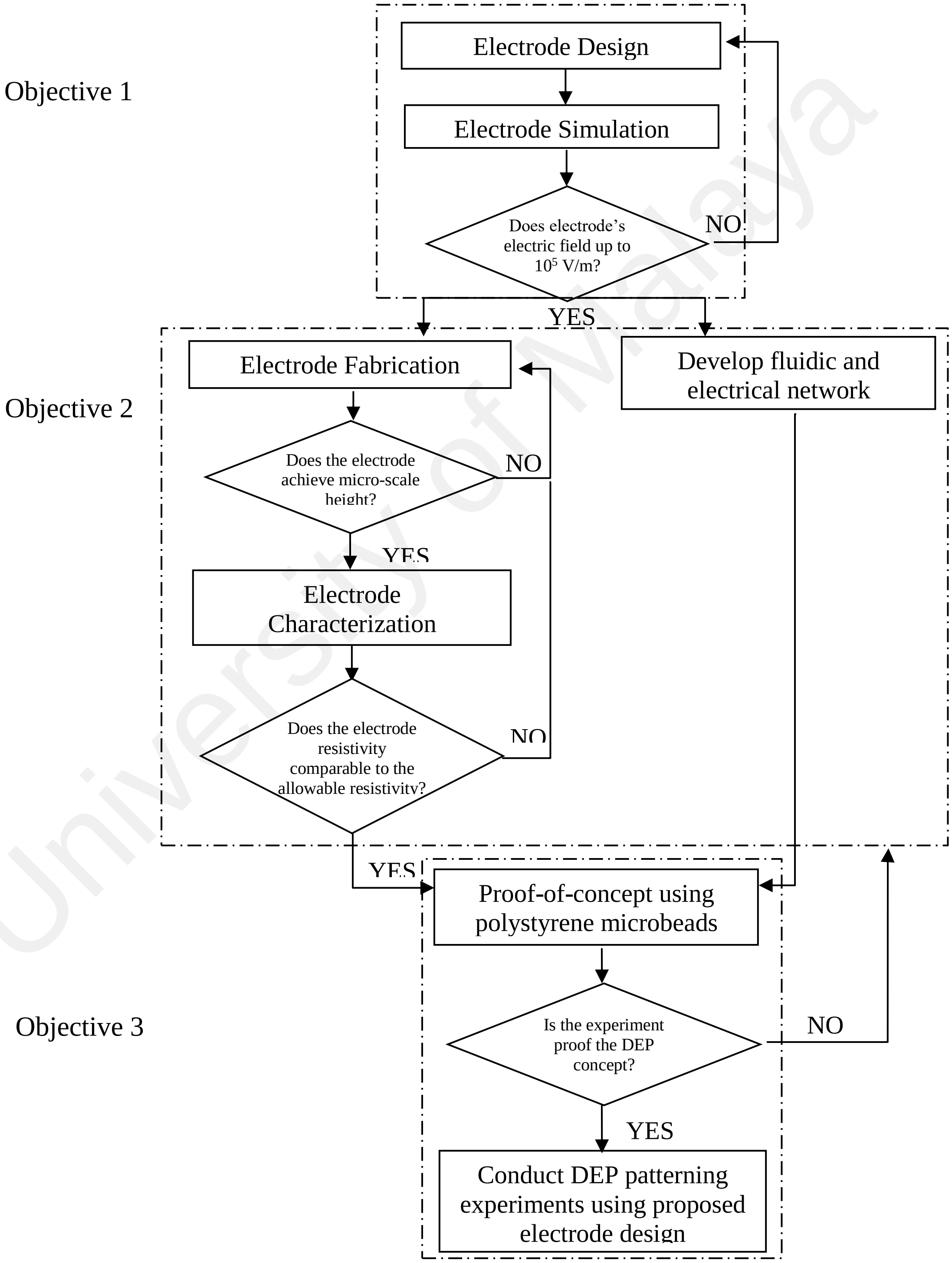

Figure 3.1: Flowchart of methodology.

University of Malaya

First, the system begins with electrode design and geometry which are the crucial part of the application in cell patterning. The design will be optimized by numerical analysis using COMSOL 4.2a in order to achieve a high throughput of DEP effects. Next come in the CMEMS microfabrication process which is divided into two sub-process which are photolithography and pyrolysis. There are three types of sample: Sample 1, Sample 2 and Sample 3. Fabrication process for each type of sample is repeated for three times and the results are averaged. Thus, in total there are nine samples to be examined. To complete this LOC system, the microfluidic platform, the electrical and fluidic connection will be designed and fabricate accordingly. Furthermore, this chapter also explains how to characterize the fabricated carbon electrode and describe in detail the experimental setup for DEP proof-of-concept and microbeads patterning. One representative sample for each type of sample has been used for the DEP experiments. Each experiments were repeated for three times to get the averaged measurements.

3.2 Design and Optimization of Electrode Based on Simulation Analysis

3.2.1 Electrode Design

Regardless of the electrode material, cell patterning for tissue engineering using DEP is strongly dependent on the design and configuration of the electrode. The idea of closely mimic the biological design of tissue or organ is reflected in the electrode shape. Hence, based on the literature review specifically on the design parameters as can be referred in Table 2.2, a microarray of the hexagonal radiating-strips electrode is designed to reflect the hepatic plates of the biological liver as depicted in Figure 3.2a below.

The liver consists of over a million of hepatic lobules which are morphologically shaped approximately like an array of hexagon plate. Each lobule contains cords of liver parenchymal cells, they are hepatocytes, radiating from the central vein and separated by a hepatic sinusoid and another non-parenchymal lining of cells as illustrated in Figure 3.2a.

University of Malaya

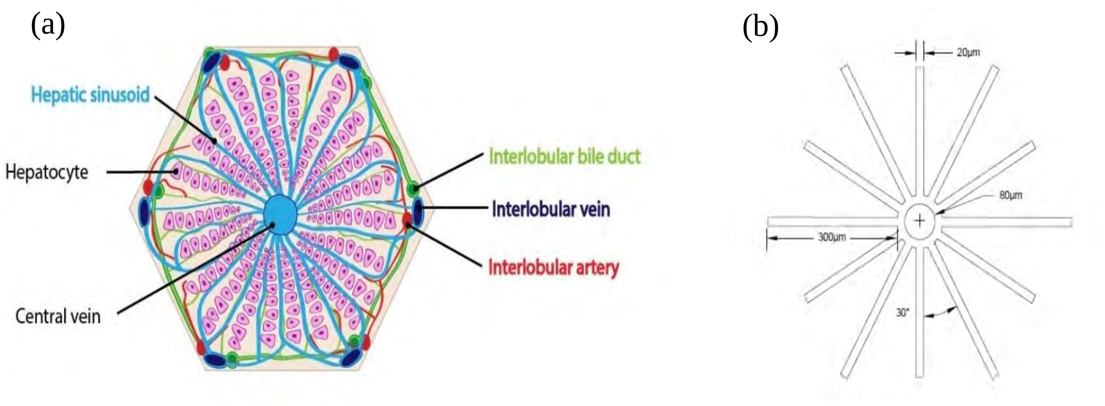

Figure 3.2: (a) Illustration of a single unit hepatic lobule. (b) Electrode design of a unit of the hexagonal radiating-strips electrode array.

University of Malaya

Hepatocytes are organized in such complex and unique structure for the reason of optimal contact with the interlobular vein, artery, bile ducts as well as other cells. This is essential for the liver to perform the broad range of liver function hence the significance of the hepatic cell patterning (Stevens et al., 2013).

The basic unit of the electrode design is to mimic the morphology shape of the native hepatic lobule. To form the radial pattern of the biological lobule, the hexagonal radiating-strips electrode is designed with each strip has the width of 20 µm and length of 300 µm radiating the connecting 80 µm circular electrode in the center with 30° angle as shown in Figure 3.2b. Each strip extends out from the center to the length of 300 µm for capturing about 20 - 25 hepatocytes in the case of an adult liver (Fausto & Campbell, 2003). To create a 3D patterning effect, the proposed design is extruded to a certain height relative to a constant 100 µm of chamber height. Table 3.1 below shows the design specifications to optimize the hexagonal radiating-strips electrode and further details on electrode geometry and configuration will be discussed in Section 3.2.2.

Table 3.1: Design specifications for hexagonal radiating-strips electrode optimization.

Parameter	**Value**
Electric field, *E*	10^5 V/m
Voltage applied range, *V*	1-20 V
Frequency range, ω	5 kHz – 200 MHz
Electrode width, *w*	20 µm
Electrode gap, *g*	10 – 40 µm
Electrode height, h	20 – 80 µm

3.2.2 Electrode Simulation by COMSOL

Electrode configuration strongly affects the DEP force acts on the particles. Therefore, designing an appropriate electrode configuration is an essential step to archive an efficient DEP patterning. Equation 2.1 shows among other parameters, DEP force, F_{DEP} is a function of electric field gradient, ∇E^2. Thus in the order to simulate the cell trajectories, the spatial variation of ∇E^2 which denotes the root-mean-squared of AC potential must be identified. For the simulation works obtainable here, the electric field is determined by the Laplace equation which can be expressed as in Eq. (3.1):

$$\nabla^2 V = 0 \tag{3.1}$$

where *V* denotes the AC voltage applied to the electrode. The subsequent electric field is as in Eq. (3.2):

$$E = -\nabla V \, . \tag{3.2}$$

In this study, the electric field intensity of two electrode configurations was determined and compared in terms of uniformity that will contribute to better cell patterning. Using

University of Malaya

the most uniform DEP configuration, electrode geometries were then optimized to enhance the electric field thus DEP effects to cell manipulation.

The method used for modeling and simulating the novel designed electrode was numerical technique. COMSOL Multiphysics 4.2a, the finite element software was used and the AC/DC module was selected. The application was in 3D mode and a steady-state electric field current module was used to simulate the electric field at a specific frequency. A block dimension of $2.0 \times 2.0 \times 0.1$ mm^3, defined as deionized (DI) water was designed on top of the electrodes as the conducting media and representing the microfluidic channel, *H*. DI water relative permittivity and conductivity were set to 78 and 2×10^{-4} S/m, relatively while GC was defined as the electrode metal. Suitable boundary conditions were applied to the simulation models. Extra fine tetrahedral meshing was performed to segment the geometry into smaller domains called elements. To simplify the numerical computation, a few assumptions are used as follows:

i. The simulation was done only for a single unit since the electrodes are distributed periodically.
ii. The electrodes are assumed to be perfect conductors and the effect of inductive of the system is neglected.
iii. Laplace equation (Equation 3.1) is used and it is assumed that there are no electric charges inside the channel.

3.2.2.1 **Uniform Electric Field Distribution**

This simulation was performed to observe which configurations generate a more uniform electric field for the novel electrode design. Figures 3.3a and b illustrate the vertical configuration of the microfluidic system with a single GC as the working electrode while on top of the microfluidic channel is the indium tin oxide (ITO) layer as the counter electrode with the dimension of $2.5 \times 2.5 \times 0.01$ mm^3. Figures 3.3c and d

University of Malaya

illustrate the horizontal configuration of the microfluidic channel featuring GC as both working and counter electrodes. This configuration displays where the counter electrode was designed to interdigitate the working electrode to generate the non-uniform electric field. The boundary of the electrodes was set to 10 V and -10 V as shown in the figure and the frequency was set to 100 MHz to induce pDEP. The channel height, *H* was set to be 100 μm, and electrode thickness, h was 20 μm for both configurations. In order to analyze the distribution and difference between two electrode configurations, the intensity profile of the electric field was presented on a cut-line (z = 0 mm) from point A to B as shown in Figures 3.3a and d. Cut-plane as shown in Figure 3.3c was used to optimize the electrode height.

University of Malaya

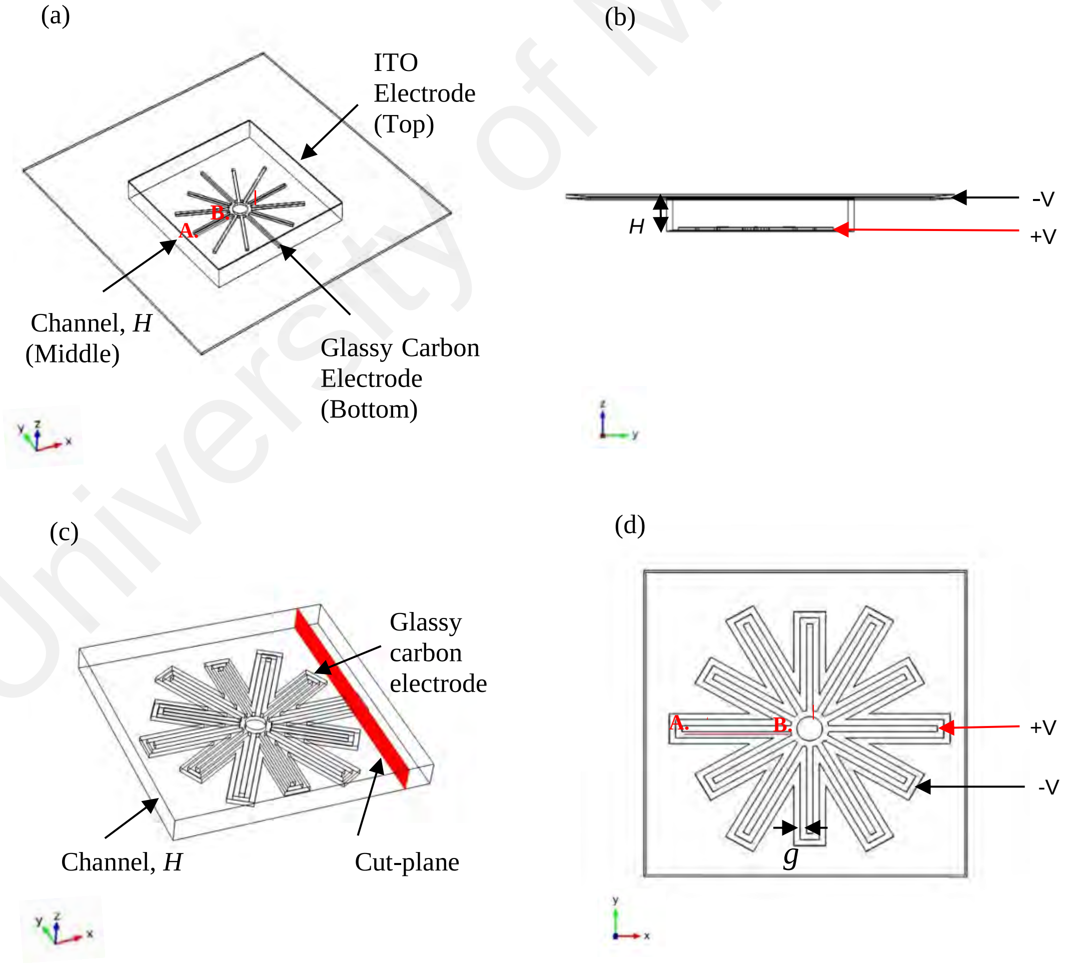

Figure 3.3: Electrode setup and boundary condition exerted for numerical simulation. (a) and (b) 3D and side view of vertical configuration, respectively. (c) and (d) 3D and top view of horizontal configuration, respectively.

3.2.2.2 Optimization of Electrode Design

The gradient of the generated electrical field which determines the DEP force on cells depends on several factors such as electrode geometry and applied voltage. In order to optimize the selected electrode structure for optimum dielectrophoretic cell patterning, the distribution of the electric field in various electrode gaps and electrode heights were compared. The electrode gap was varied from 10 μm, 20 μm to 40 μm with a constant electrode height of 20 μm, and the surface electric field distribution was plotted. The simulation was continued by varying the electrode height from 20 μm, 50 μm to 80 μm with a constant electrode gap of 20 μm at the cut-plane shown in Figure 3.3c. Using the selected optimum geometry, the effect of voltages applied on electric field strength is attained for different applied voltages and discussed.

3.3 Fabrication and Characterization of 3D Carbon Electrode for Lab-on-a-chip (LOC) Development

The LOC system comprising 3D carbon electrode arrays was fabricated using the CMEMS process comprising standard photolithography technology and thermochemical decomposition of a polymer called pyrolysis as illustrated in Figure 3.4. This microfluidic system consists of three layers where the bottom part comprised electrode arrays with respective connecting leads and insulating layers, the top part act as a cover with a fluid port feature, and the middle part is the chamber where the experiment takes place. A schematic diagram of the microfluidic system is shown in Figure 3.5.

University of Malaya

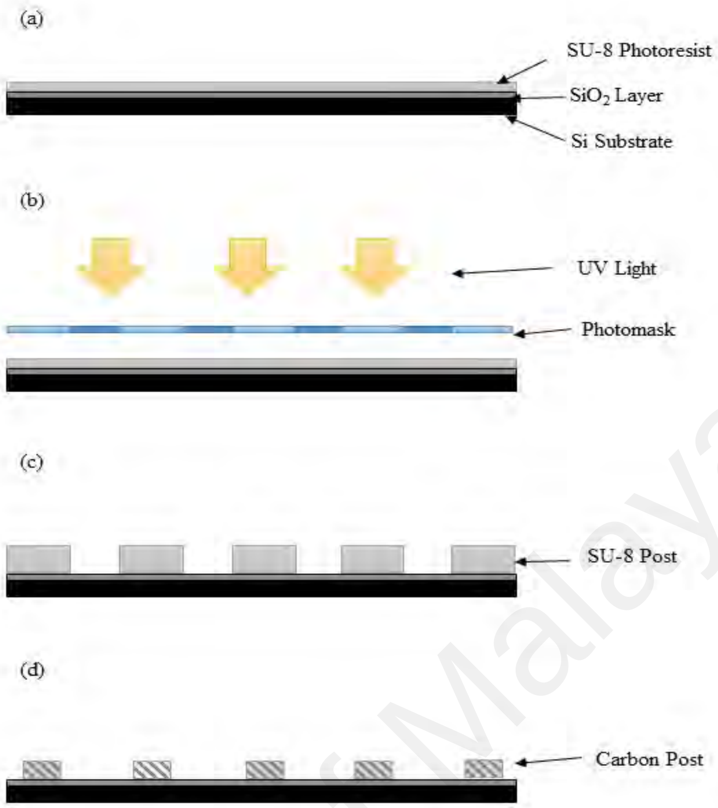

Figure 3.4: The flow of the CMEMS fabrication process. (a) Spin coating of SU-8 polymer onto silicon dioxide substrate, (b) UV exposure through photomask for polymer cross-linking, (c) development of crosslinked SU-8 post, and (d) 3D carbon post after pyrolysis.

University of Malaya

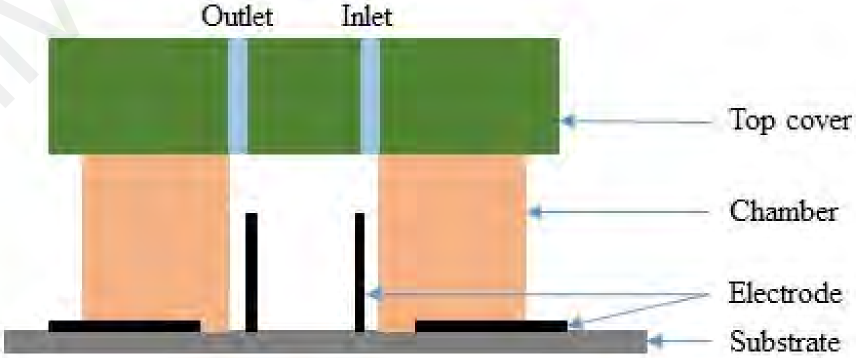

Figure 3.5: A schematic diagram of the microfluidic system for DEP cell patterning.

3.3.1 Photomask Design

Prior to the electrode fabrication procedure, a photomask is necessary to transfer the electrode pattern on the photoresist. The electrode geometry was designed using AutoCAD® software (Autodesk Inc, California, USA) according to the results obtained in the simulation part and in a way that matches with negative photoresist as depicted in Figure 3.6.

(a)

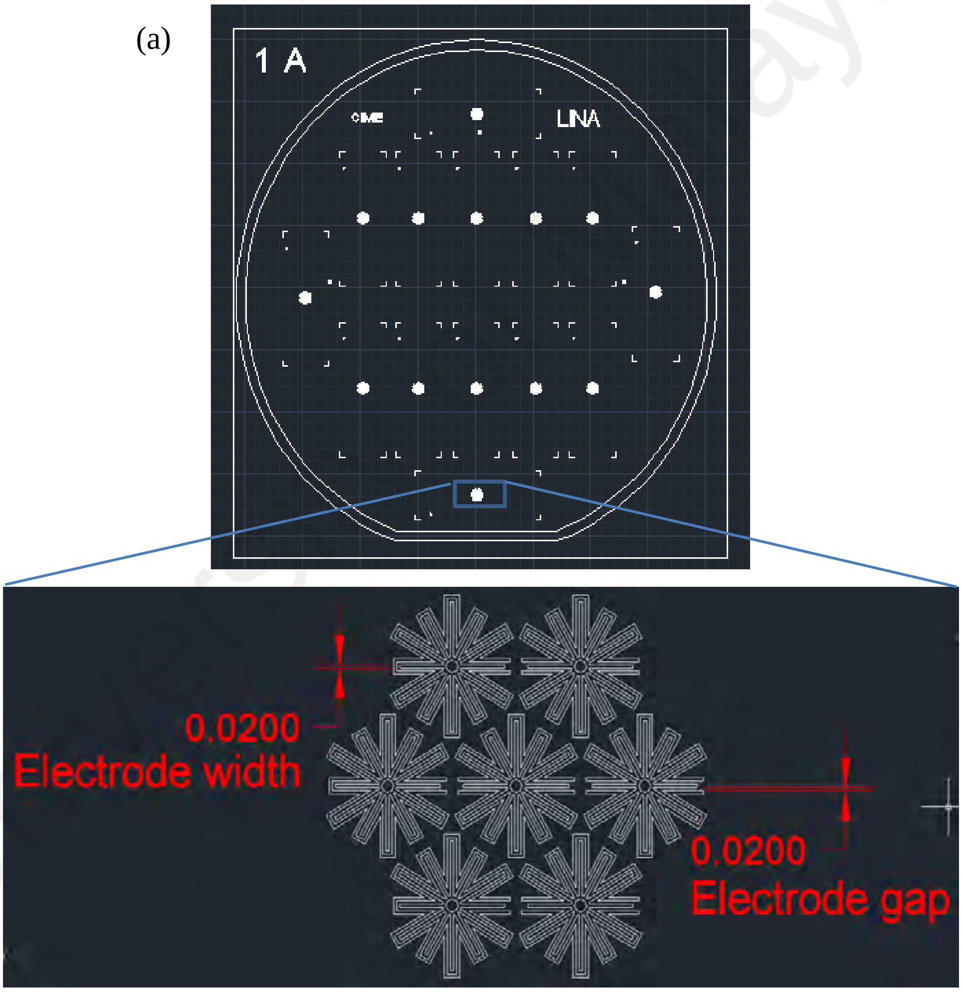

University of Malaya

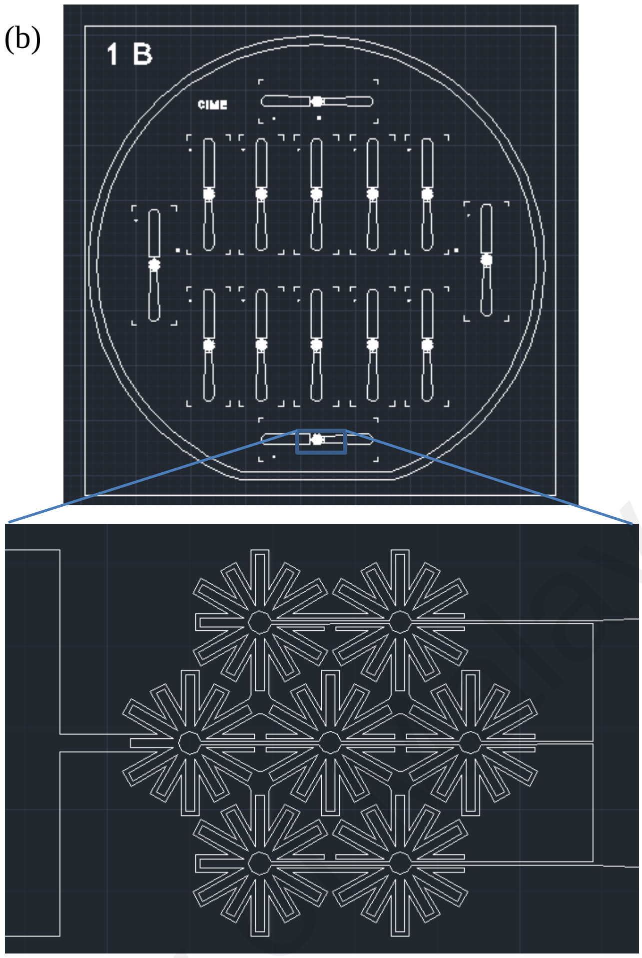

Figure 3.6: Photomask designed using AutoCAD (dimension in mm), (a) 3D pattern structures, and (b) connecting leads for electrical connection.

In the case of negative photoresist, the white area on the photomasks will be cross-link upon UV exposure and remain after the SU-8 developing process. Since there are two photomasks, alignment marks are crucial to accurately align both photomasks. Four squares surrounding one cross shape marks were placed at each corner of the photomasks as shown in Figure 3.7.

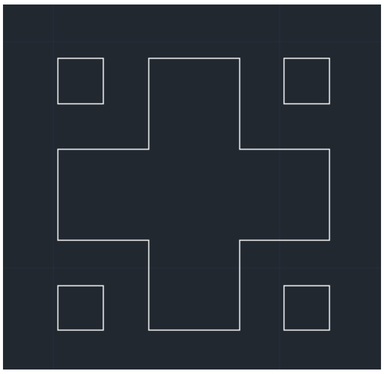

Figure 3.7: Alignment mark for photomasks alignment.

University of Malaya

3.3.2 Substrate Treatment

Silicon dioxide, SiO_2 (100 mm diameter with 5000 Å of O_2 thermally deposited) wafers were used as the substrates for the entire CMEMS (photolithography and pyrolysis) process. The oxide layer acts as an insulator to the contacts and electrodes from the underlying silicon. An epoxy-based negative photoresist, SU-8 from MicroChem, US was chosen as the carbon precursor of the electrode material.

The wetting behavior of the substrate surface is crucial to obtain well substrate-resist adhesion. Upon substrate cleaning, the substrate surface was likely to be hydrophilic because of all the solvents used. Besides, the humidity of the environment also gives a hydrophilic effect on the surface properties and its impact on adhesion (Luo & Wong, 2005). Such behavior generates a layer of moisture which triggering the delamination of the coated photoresist from the substrate and consequently thwart the entire photolithography proses. The main method used to evaluate the wettability of the solid substrate surface is the contact angle. By means of contact angle, it defines the behavior of a liquid droplet on a surface in air and is described as the angle between the tangent at the three-phase point and the surface.

For optimum performance and reliability of the substrate, appropriate surface treatment before photoresist coating is a key requirement. In this study, the treatment is to dehydrate the substrate in an oven for some time at 120 °C. Prior to that, it is essential to analyze the surface wettability of the SiO_2 substrate during high humidity (78%) and low humidity (58%) using a water contact angle. This is to determine in which humidity condition is the best to work at. Static contact angle measurements with sessile drop (4 µl) technique were performed at room temperature using an OCA-20 contact angle meter and analyzed using a SCA20 software. Reported contact angles are the average of at least 5 different points of measurements.

University of Malaya

Next, the dehydration treatment was done at the best humidity condition as has been identified earlier. After samples cleaning, three of the samples were treated in the oven at 120 °C for different periods; 30 min, 4 h, and 12 h. Another sample was untreated and set as a control sample. Right after the treatment, the water contact angle for each sample was measured and analyzed. The contact angle was measured shortly after droplet deposition on the samples to minimize the evaporation. However, enough time was allowed for the droplet to spread on the surface of the samples. The elapsed time between deposition and measurement had to be fixed and then replicated for each droplet during contact angle measurement. Ellipse fitting mode was used for the entire measurements.

Following, each sample were undergone the CMEMS microfabrication process to examine the final yield. The details of the process will be explained in the next section. The surface morphology of the pyrolyzed SU-8 was then analyzed using Scanning Electron Microscope (SEM) (Phenom ProX). These procedures were repeated three times for each sample, and both the average value and standard deviation were attained.

3.3.3 Electrode Microfabrication

3.3.3.1 SU-8 Photolithography

. Two different viscosities that are SU-8 2015 and SU-8 2025 were used to fabricate the connecting leads and the 3D pattern structures, respectively. Spin coating of the photoresists was done using a Laurell spin coater and an MDA-400M (MIDAS, Korea) mask aligner was used for UV exposure and aligning.

Two-step of the photolithography process was done as the first layer for the connector while the second layer for the 3D structure as shown in the flowchart of Figure 3.8. The process parameters to fabricate 2D and 3D SU-8 structures on SiO_2 substrate are summarized in Table 3.2 and 3.3. This process is repeated three times for each sample and the result is averaged.

University of Malaya

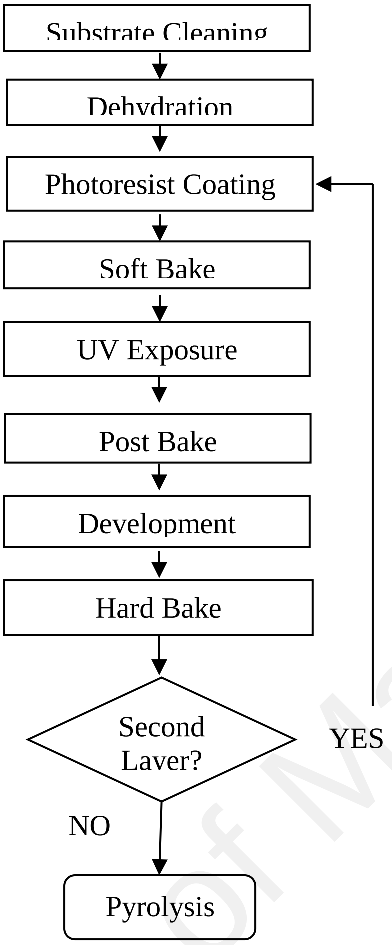

Figure 3.8: Flowchart of the SU-8 photolithography process.

Table 3.2: Spin programs and resultant SU-8 layer.

Sample	**SU-8**	**First step - spread**			**Second step – thickness definition**			**T_{SU-8} (µm)**
		***s* (rpm)**	***a* (rpm/s)**	***t* (s)**	***s* (rpm)**	***a* (rpm/s)**	***t* (s)**	
First layer (connecting lead)								
1	2015	500	200	15	4000	350	45	13
2	n/a	n/a	n/a	n/a	n/a	n/a	n/a	n/a
3	2015	500	200	15	4000	350	45	13
Second layer (electrode structure)								
1(3D)	2025	500	200	15	1000	350	45	38
2 (2D)	2015	500	200	15	4000	350	45	13
3 (3D)	2025	500	200	15	1000	350	45	38

Notes: *s* = speed, *a* = acceleration, *t* = time, T_{SU-8} = expected thickness of the SU-8 layer

University of Malaya

Table 3.3: Fabrication process for all structures.

Sample	**Soft bake (minutes)**		**Exposure**		**PEB (minutes)**		**Development (minutes)**
	At 65°C	**At 95°C**	**Dose (mJ.cm^{-2})**	**Time (s)**	**At 65°C**	**At 95°C**	
First layer (connecting lead)							
1	3	3	130	30	2	2	3
2	n/a	n/a	n/a	n/a	n/a	n/a	n/a
3	3	3	130	30	2	2	3
Second layer (electrode structure)							
1(3D)	3	5	160	40	2	4	5
2 (2D)	3	3	130	30	2	2	3
3 (3D)	3	5	160	40	2	4	5

(a) ***Substrate Cleaning and Dehydration***

Several ranges of cleaning techniques are available depending on the substrate and contaminants. Herein, a SiO_2 wafer as purchased from University Wafer (South Boston, MA), was washed under a stream of DI water, rinsed with acetone and isopropyl alcohol (IPA), and dried using a nitrogen gun, in that sequence. The acetone used to remove organic impurities, followed by IPA which removes contaminated acetone before it can form smudges on the substrate. In order to increase yield, prior to spin coating of photoresist, the cleaned wafer was then dehydrated in a convection oven set at 190 °C overnight.

(b) ***Photoresist Coating***

Multiple of SU-8 photoresist viscosity were used to fabricate patterns of different film thicknesses on a substrate. SU-8 2015 was used to fabricate the first layer that becomes

University of Malaya

the connecting leads and pads while SU-8 2025 was used to fabricate the second layer that forms patterns for the 3D structure.

The most common technique to deposit photoresist under 1mm thickness is spin coating since the spin coater is programmable and easy to optimize until the desired of the film thickness is achieved. The optimal volume of photoresist is deposited directly from the bottle to the center of the substrate as shown in Figure 3.9. Spin speed, spin acceleration, and spin duration were set to a value suggested in the processing datasheet provided by MicroChem to achieve certain film thickness and were optimized accordingly. The substrate is held in place by a vacuum-actuated chuck and centrifugal force acting during spinning helps to spread the photoresist uniformly. Table 3.3 presenting all the spin programs and resultant layer thickness used in this work.

University of Malaya

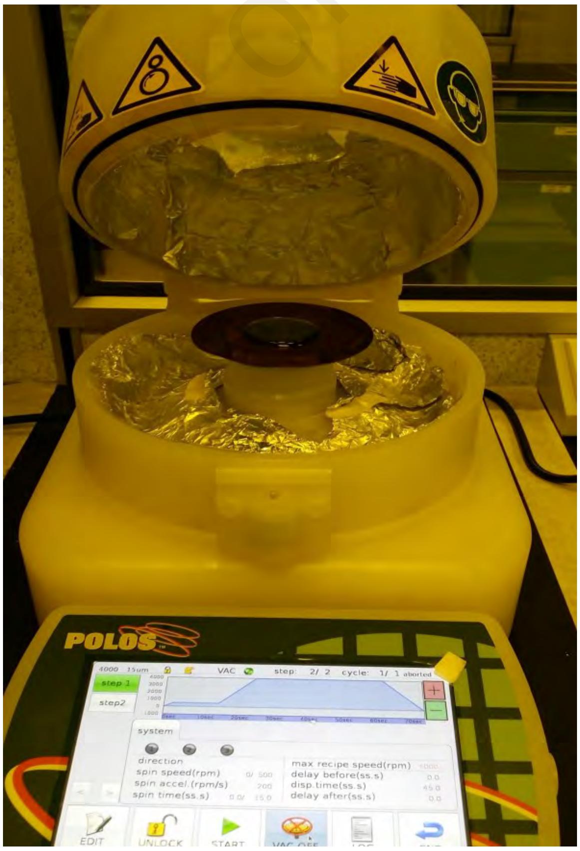

4000 15um VAC step: 2/ 2 cycle: 1/ 1 aborted

spin speed(rpm) 0/ 500
spin accel.(rpm/s) 200
spin time(ss.s) 0.0/ 15.0
delay before(ss.s) 0.0
disp.time(ss.s) 45.0
delay after(ss.s) 0.0

Figure 3.9: Photoresist coating using a spin-coater.

(c) ***Soft Bake***

Soft bake also known as pre-exposure bake is a step to evaporate the solvent in photoresist coating the substrate. The soft bake process was done using a hotplate set at 65 °C and 95 °C. These two steps baking is to reduce thermal stress and to control the evaporation rate. Baking times vary from 1 to 60 minutes subject to the type of SU-8 and layer thickness. Apparently, the thicker layer required longer baking time to completely remove the solvent, since incomplete evaporation of the solvent will interrupt during the exposure step. Besides, the use of a hotplate instead of a convection oven also aids to evaporate faster, well-regulated and minimizing trap solvent especially for the thick layers (C. Wang et al., 2005). While in the convection oven, the solvent at the surface is evaporated first, creating an impenetrable resist skin and trapping the residual solvent inside. Table 3.3 includes the soft bake times and temperatures used in this work depending on the type of SU-8 and layer thickness.

(d) ***UV Exposure***

Next, the soft baked substrate is transferred to the exposure system (mask aligner) as shown in Figure 3.10 where it is aligned to the patterns on a photomask as illustrated in Figure 3.6. The duty of the exposure system is to provide UV light with optimal intensity, uniformity, and directionality across the substrate, letting a close to perfect transfer of the mask pattern on to the photoresist. Upon UV light is exposed, the photoacid generator (triarylsulfonium hexafluoroantimonate salt) is activated to initiate the polymerization of SU-8 during the post-bake step. The light intensity created by the mask aligner is fixed at 4.5 mW•cm^{-2}. Exposure dose, *D*, used to determine the exposure time was obtained from the MicroChem processing datasheet, is related as in Eq. (3.3).

$$Exposure\ time\ (s) = \frac{Exposure\ Dose\ (mJ.cm^{-2})}{Light\ Intensity\ (mW.cm^{-2})} \tag{3.3}$$

University of Malaya

Underexposed of the photoresist causes the pattern obtained is imperfect. The pattern could either lift off or dissolve during development since the cross-linking acid concentration was low to begin polymerizing the photoresist all the way down to the bottom substrate. On the other hand, overexposed can cause photoacid diffusion that polymerized a thin layer along the top surface of the photoresist that is not exposed, commonly known as *T-topping*. Moreover, it can also cause light diffraction resulting in severe pattern distortions and broadening.

Figure 3.10: Mask aligner for UV light exposure.

(e) ***Post-Bake***

After the UV exposure, post bake also known as a post-exposure bake (PEB) is a must to finalize the cross-linking of the polymer. The degree of chemical reactions initiate during exposure could be enhanced by baking at 65 °C and 95 °C on a hotplate for different times. As for PEB, the precise control of times and temperatures are critical to determining the following development. In general, longer times at low temperatures are suggested. Thermal stress is likely to occur at high temperatures and extended baking time causing patterns cracking, bending, or even peeling off from the substrate. In contra, insufficient of PEB temperature and times produce incomplete cross-linked patterns and

Universiti Malaya

can be destroyed by the developer. This outcome either very high surface roughness of complete dissolution of the photoresist. Thus, the heating and cooling ramp rate of PEB had been optimally controlled according to layer thickness as shown in Table 3.3.

(f) ***Development and Drying***

The next step is the development where the dissolution of un-polymerized SU-8 to transforms the underlying resist, formed during UV exposure, into a relief image as presented in the photomask. Generally, two main techniques are available for photoresist development: wet development and dry development. This study used wet development that requires the substrate to be immersed in Propylene Glycol Methyl Ether Acetate, PGMA (supplied by MicroChem as SU-8 developer). During the immersion in SU-8 developer, those areas that were not cross-linked dissolve and followed by rinsing using the developer. Different times applied to different thicknesses, in general, long time benefit for thicker layer as shown in Table 3.3. The resulting SU-8 pattern after development is then rinsed with IPA using a normal rinse bottle and blown dried using a nitrogen gun.

(g) ***Hard Bake***

Samples were hard bake to removes all residual solvent and developer, improve the interfacial adhesion of the resist that has been weakened during the developing process. However, hard bake does resist shrinkage and stress if it occurs at improper temperature and time. Thus, all samples were hard baked for 30 min at 90 °C using an oven.

3.3.3.2 **Pyrolysis**

Pyrolysis of the SU-8 pattern was conducted on an open-ended quartz tube furnace (Naberthem, Germany) under a constant nitrogen gas flow at 2000 mL/min as shown in Figure 3.11. The pyrolysis protocol featured five stages: (i) the temperature ramp from room temperature at 23 °C to 300 °C at 20 °C/min; (ii) 30 min dwell at 300 °C to allow

University of Malaya

residual oxygen to be eliminated from the chamber; (iii) a temperature ramp from 300 °C to 900 °C at 10 °C/min; (iv) another 60 min dwell at 900 °C to complete the carbonization; and (v) the samples were then cooled down to room temperature naturally which took approximately 8 hours. Figure 3.12 shows the graph of the heating protocol. In this study, 900 °C was used as the final temperature since most applications of carbon structure achieve at this temperature (Amato et al., 2015; Sharma, Sharma, & Madou, 2010; C. Wang et al., 2005).

University of Malaya

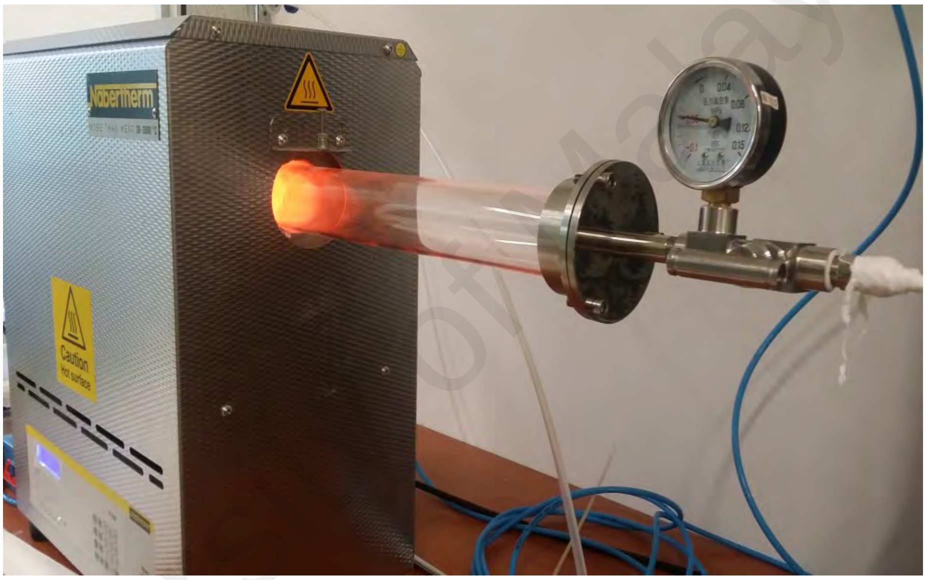

Figure 3.11: Pyrolysis conducted in a quartz tube furnace.

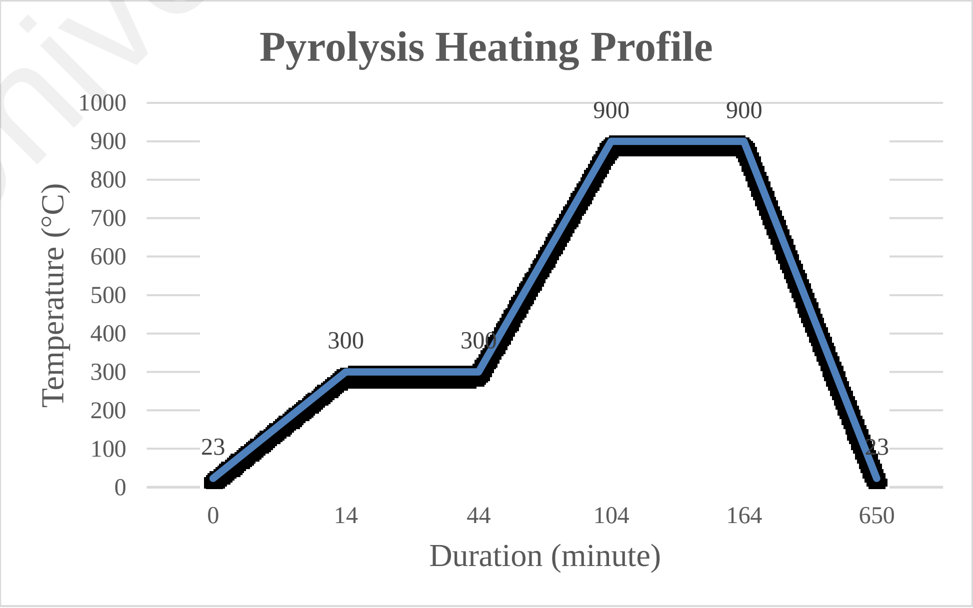

Figure 3.12: Pyrolysis heating profile.

The characteristic dimension, D of the SU-8, and carbon structures were analyzed using field emission scanning electron microscopy (FESEM). Three structures were measured for each data point reported in the results section. The percentage shrinkage was calculated using Equation 3.4, where the dimensions can be either height, H, or diameter/width, D/W of the structure.

$$Percentage\ Shrinkage\ (\%) = \frac{Dimension\ SU8 - Dimension\ Carbon}{Dimension\ SU8}\ x\ 100 \quad (3.4)$$

3.3.4 Fluidic and Electrical Network

3.3.4.1 **Microfluidic Platform**

The developed microfluidic in this work featured two layers: the top layer and the channel layer. The top layer was fabricated from 1mm thick of polymethyl methacrylate (PMMA) using a Computer Numerical Control (CNC) machine (VISION 2525, Vision Engraving and Routing System, USA). Two 1mm holes were drilled for fluids inlet and outlet ports.

The second layer is the channel where the DEP procedure takes place. The channel of the network was cut out from a 100 µm thick of double-sided pressure-sensitive adhesive (FLEXmount DFM 200 Clear V-95 150 POLY H-9 V-95 4 FLEXcon, MA, USA) using a cutter plotter machine (PUMA II, GCC, Taiwan). A 3.6 mm × 10.0 mm hole was introduced at the middle part to allow approximately 3 µl of fluid flow.

The PMMA and adhesive layers are then aligned and adhered together manually. This 2-layers stack is then manually aligned to the fabricated carbon electrode as previously displayed in Figure 3.5. The inlet and outlet were connected by polytetrafluoroethylene (PTFE) tubing for supplying the solution and particles to be tested. This microfluidic

University of Malaya

platform was designed to have a perfect seal and no leakage of flows. Despite the simple fabrication technique, the cost is greatly reduced since no additional photolithography process involves as in polydimethylsiloxane (PDMS) and SU-8 channel circumstances.

3.3.4.2 **Electrical Connection**

The electrical connection was made by depositing silver conductive paste on the carbon pads using a syringe. Metal wires AWG18 were then sealed to the silver paste and were allowed to fully cure at room temperature for 24 h. Unfortunately, a significant problem arising from the use of silver paste that introduces under layer reaction and causes carbon pads to detach from the substrate.

As an alternative, copper adhesive tape was used by easily cut into the desired dimension, remove the protective film, and laid on to the carbon pads. It should be done smoothly to avoid wrinkles to develop, or air to become trapped between the adhesive and the carbon pad surface. Small pressure was applied to the part being attached in order to stabilize the flow throughout the surface and create a slight fillet in the edges. Metal wire with clips was then attached to the adhesive tape and connected to the function generator.

3.3.5 Characterization of Carbon Electrode

3.3.5.1 **Microstructure**

The microscopic morphology of patterns obtained on the silicon wafers was characterized before and after pyrolysis using an optical microscope and FESEM. The percentage of shrinkage after pyrolysis can be determined from the FESEM results.

3.3.5.2 **Electrical**

The resistivity of two different thicknesses of the carbon films was calculated using a two point probe measurement unit (Keithly Sourcemeter, 4200-SCS) as illustrated in

University of Malaya

Figure 3.13. The applied DC range of 1 µA to 4 mA and applied voltage range of -1.0 V to +1.0 V. The distance between probes is fixed to approximately 200 µm. The probes are manually positioned with the assistance of a microscope. Measurements were repeated three times for each film.

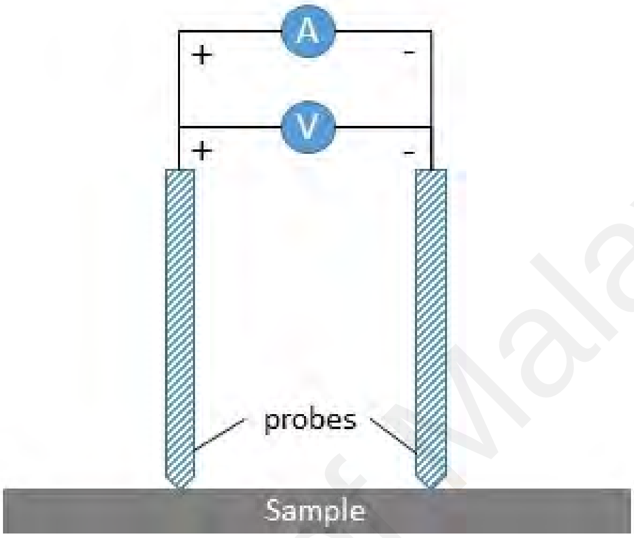

Figure 3.13: A two point probe resistivity test setup.

The resistance of the sample is given by Eq. (3.5):

$$R = \frac{V}{I} \tag{3.5}$$

where *R* equals to resistance (ohm, Ω), *V* is voltage (volt, V) measured and *I* is current (ampere, A) applied. By knowing the sample's resistance and dimensions, the sample's resistivity, ρ (ohm.meter, Ω.m) can be calculated as Eq. (3.6):

$$\rho = R\frac{A}{L} \tag{3.6}$$

where *A* is the cross-sectional area (width, *w* times thickness, *t*) and *L* is the length of the sample. In addition, the conductivity of the sample is simply the inverse of the resistivity.

University of Malaya

3.4 Dielectrophoresis (DEP) Experiments

3.4.1 Proof-of-concept

To test the fabricated LOC system, polystyrene microbeads were used to conduct the DEP experiment as it has been widely used in DEP and their dielectric properties are well characterized. To accelerate the proof-of-concept of the carbon-DEP devices, a simpler pattern of carbon electrode was implemented to dielectrophoreticly pattern the polystyrene microbeads as shown in Figure 3.14. The fabrication details were given in Table 3.2 and 3.3 and numbered as Sample 1.

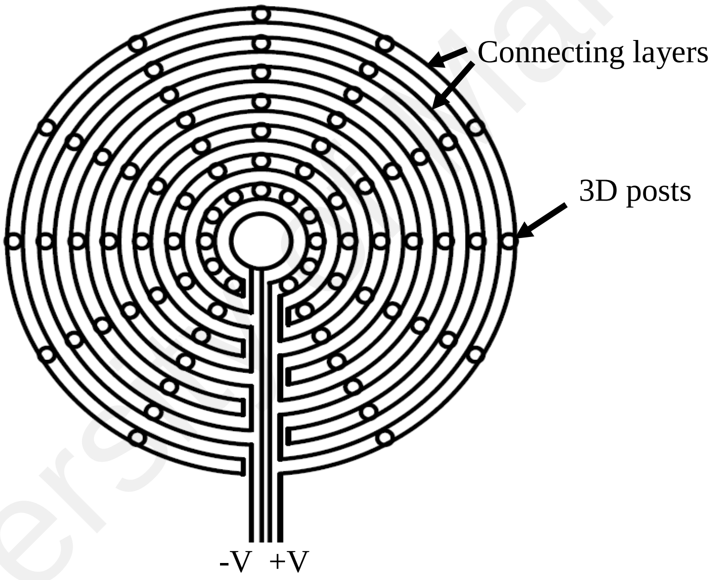

Figure 3.14: Concentric 3D post array electrode for proof-of-concept experiment.

3.4.1.1 **Microbeads Preparation**

Aqueous microbeads suspension with diameter 5 µm (Thermo Scientific, USA) was used and diluted with DI water in volume ratios of 1:3. Prior to experimentation, samples were thoroughly mix using Vortex mixer (Thermo-line, HYQ-3110) to gain homogenous microbeads distributions. 3 µl of the microbeads suspension was pipetted into the channel via the input port.

University of Malaya

3.4.1.2 Experimental Setup

A function generator (GFG-8255A, Good Will Instrument, Taiwan) was used as an AC power supply to polarized the carbon electrode. The LOC device is positioned on the stage of an optical microscope as shown in Figure 3.15 and the motions of the microbeads were monitored and recorded by the couple-charged device (CCD) camera. The images were captured and stored on the personal computer (PC). The overall setup is represented in Figure 3.16.

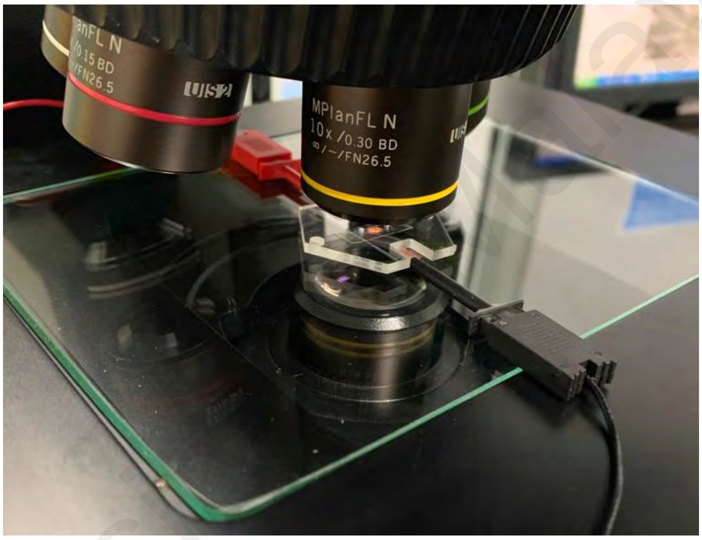

Figure 3.15: The LOC device placed on the microscope stage during DEP experiments.

Figure 3.16: Experiment setup for DEP experiments.

Universiti Malaya

An AC signal of 20 V peak to peak was applied over a range of frequencies. The voltage was fixed at 15 V peak to peak and the frequency was varied from 5 kHz to 50 MHz. Prior to loading the microbeads suspension into the LOC device, the function generator and amplifier were powered on but the outputs were set to the lowest. This is to ensure no generation of bubbles inside the channel by electrolysis. The experiment time at each frequency was 30 s and was repeated for three times, and images were captured before and after signal application. The DEP response of manipulation at a given frequency was determined by qualitatively.

3.4.2 Microbeads Patterning

The developed LOC device was specifically designed to dielectrophoretically pattern hepatic cells. To end this study, polystyrene microbeads were used as a substitute for hepatic cells for the sake of demonstration. The novel design of electrode, IRSE as shown in Figure 3.17 was used to pattern microbeads and expected to mimic simulation results.

To experimentally evaluate the advantage of 3D electrode design for patterning of particles, the trapping efficiency of microbeads was compared between 2D and 3D electrodes by using Sample 2 and Sample 3, respectively. The amplitude of the AC signal was set to 15 V while the frequency was set to 50 MHz. This amplitude and frequency were chosen to maximize the pDEP response on polystyrene microbeads while minimizing the risk of electrolysis. In this experiment, microbeads with a diameter of 10 µm were used because this size is nearly comparable to the size of hepatic cells. The suspension was diluted in DI water to get a volume ratio of 1:5, which gave a concentration of about 10^6 beads/ml. This experiment was repeated three times to get the averaged and the concentration was determined using a hemocytometer (Neubauer) for both samples.

University of Malaya

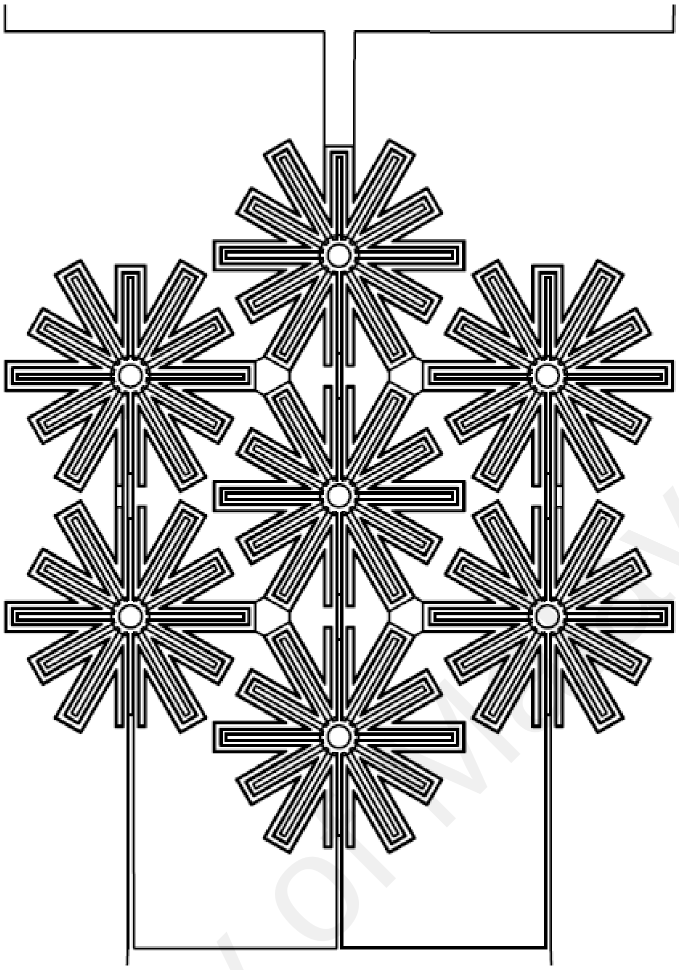

Figure 3.17: An array of IRSE for the DEP patterning experiment.

Hence the trapping efficiency can be calculated by Eq. (3.7):

$$Trapping\ efficiency\ (\%) = 1 - \frac{C_o}{C_i}\ x\ 100 \tag{3.7}$$

where C_o and C_i are the concentration of microbeads at the outlet and inlet, respectively.

3.5 Summary

This chapter begins with an electrode design that mimicking the biological shape of liver tissue. The new electrode design was then numerically simulated using COMSOL to optimize the best electrode configuration and geometry prior to the real fabrication. Following that is the CMEMS fabrication process featuring photolithography and

University of Malaya

pyrolysis procedure to fabricate the IRSE carbon electrode based on the results of the simulation. The development of the LOC device was then completed by the fluidic and electrical setup. Moreover, the fabricated carbon electrode was characterized using FESEM for microstructure and 2-point probe for electrical properties. In order to confirm the application of the developed LOC device, proof-of-concept of DEP manipulation was conducted using concentric 3D post arrays. Finally, is the DEP patterning experiment using a new design electrode, IRSE, and comparing the patterning efficiency between 2D and 3D electrode structures.

University of Malaya

CHAPTER 4: RESULTS AND DISCUSSION

4.1 Introduction

This chapter presents the results and discussion obtained throughout this study. Simulation results by COMSOL will be presented to compare and determine the best configuration for uniform dielectrophoretic cell patterning. Besides, optimization of the electrode geometry had been done and presented. Next, the outcome from the microfabrication electrode trough the CMEMS process is shown. Microstructural and electrical characterization of the fabricated carbon electrode will be presented and discussed as well. Finally, the results of the DEP experiment that were conducted as proof-of-concept are presented and discussed.

4.2 Results of Design and Optimization of Electrode Based on Simulation Analysis

4.2.1 Electrode Simulation

4.2.1.1 Comparison of Electric Field Distributions for Vertical and Horizontal Configurations

Simulation results of the comparison between electrode configurations are presented in Figure 4.1 which strong electric field implied by the red and weaker field by blue. Figures 4.1a and b illustrate the surface plot of electric field distributions produces by vertical and horizontal electrode configuration, respectively, at the xy-plane with an operating voltage of 10 V and frequency of 100 MHz. The vertical configuration shows the non-uniform distribution of the electrical field and produces a strong electrical field at every tip of the strips with a maximum of 6.01×10^{5} V/m as shown in Figure 4.1a. The value rapidly decreases along the strips toward the center of the electrode with a minimum of 1.45×10^{-64} V/m. On the other hand, horizontal configuration shows uniform distribution of the electrical field along every strip with a strong reading of 1.18×10^{6}

University of Malaya

V/m at the edges of the electrodes as shown in Figure 4.1b. However, the center of the electrode still showing a weak electric field but with a minimum of 2.03 x 10^{-6} V/m which is significantly higher than the minimum value of the vertical configuration.

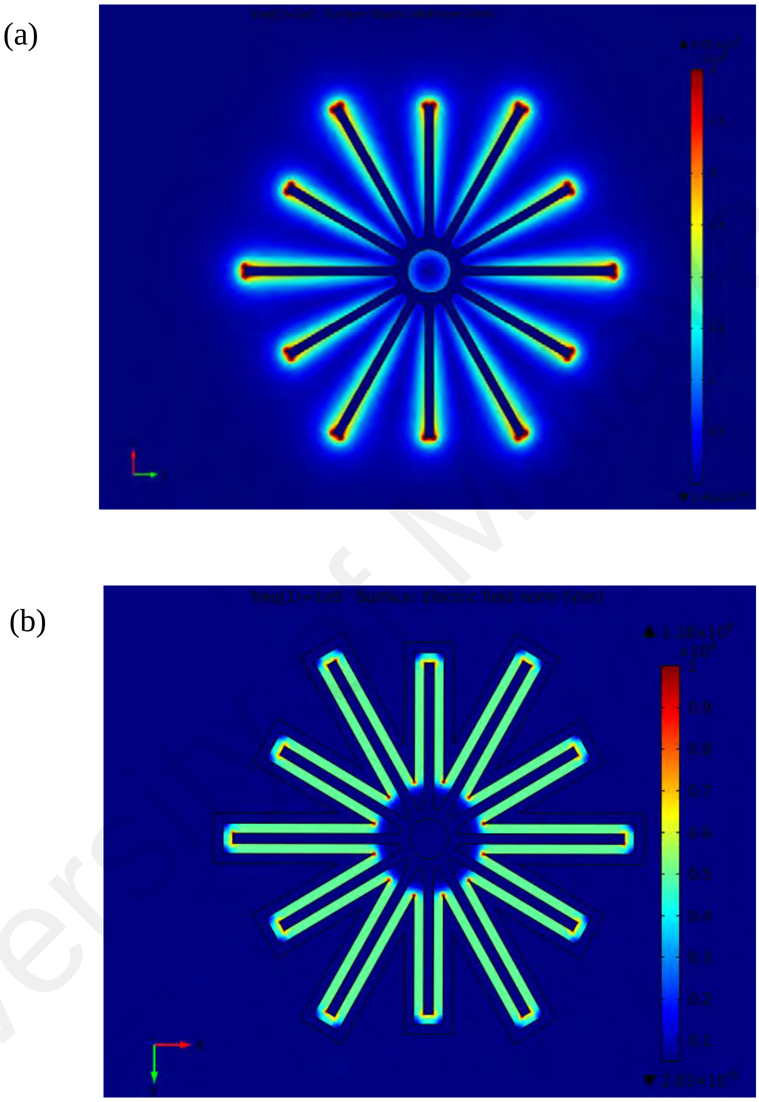

Figure 4.1: Surface plot of electrical field distribution (a) vertical configuration (b) horizontal configuration.

The vertical configuration is able to create a vertical electric field for 3D DEP force (R.-J. Chen & Liu; Lin, Ho, Liu, & Chang, 2006). However, given the complexity of the electrode design, the generated electric field distribution is not uniform along the strips, which takes the maximum value only at the end of the strips. For further comparison, Figure 4.2 shows the changes of the electric field at the cut line across the strip from Point A to Point B produced by the vertical and horizontal electrode configuration, respectively

University of Malaya

as shown in Figures 3.3a and d. The x-axis represents the non-dimensional length of the cut-line while the y-axis represents the magnitude of the electric field. Vertical configuration is shown gradually decrease of the electric field as the line move towards the center, as it reduces from a peak value of 1.78 × 10^5 V/m at Point A to 0.29 × 10^5 V/m at Point B. This can be explained by the low signal-to-noise ratio when the diffusion layers of the individual strips are overlapped as it goes from Point A to Point B. Because at Point B, the gap between strips are smaller thus decreasing the overall current and consequently electric field (Stulík, Amatore, Holub, Marecek, & Kutner, 2000). In comparison, horizontal configuration shows there are no significant changes in the electric field with a peak value of 5.05 × 10^5 V/m at Point A and 4.93 × 10^5 V/m at Point B. This configuration impressively eliminates the issue of overlap diffusion layer between adjacent electrodes.

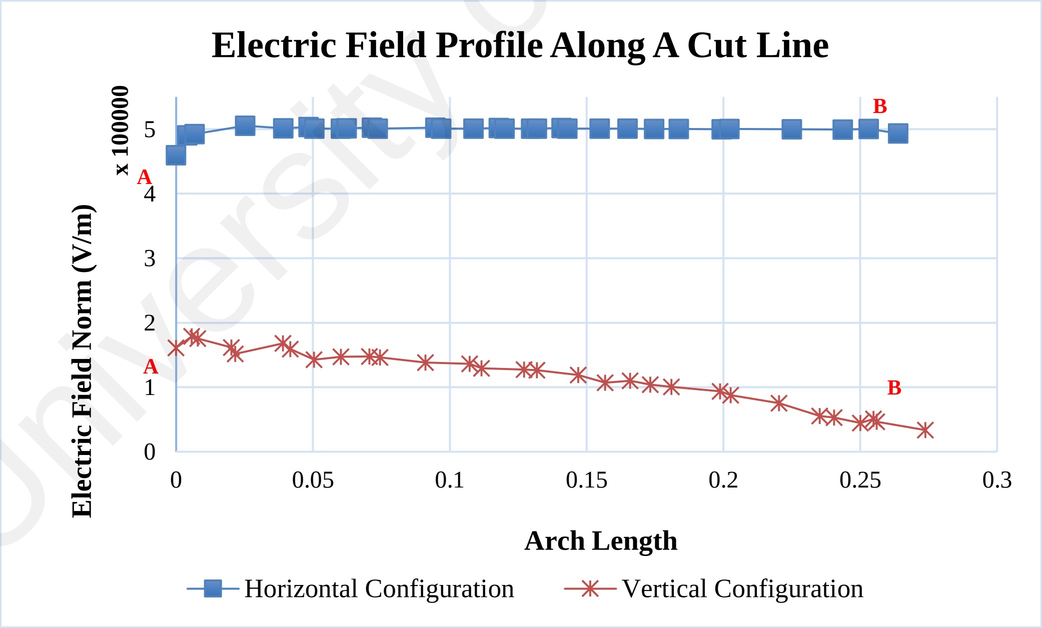

Figure 4.2: Comparison profile of electric field from Point A (left) to Point B (right) along a cut line of z=0mm for vertical configuration and horizontal configuration.

With those comparisons, horizontal electrode configuration obviously shows better uniformity for the electric field distribution as compared to the vertical configuration. For the vertical case, the distribution of the electric field was concentrated on the end of the

University of Malaya

strips, but the horizontal case shows uniformly distributed along the radiating-strips electrode. Uniform distributed electric field will appear in uniform DEP force for patterning cells according to the designed electrode and avoid unprecedented assemble at the distinct location along the strips. Nevertheless, this electrode design is novel and sufficiently intricate that tough to analytically specify the field between the electrodes.

The horizontal configuration is essentially designed to interdigitate the original hexagonal radiating-strips electrode since interdigitated configurations are very well known for its versatility in manipulating cells and flexibility in designing the geometry (Cao, Cheng, & Hong, 2008). Hence, this new 3D interdigitated radiating-strips electrode (IRSE) has been suggested to be further optimized to increase the efficiency of designing the 3D DEP cell patterning chip.

4.2.1.2 **Effect of Electrode Gap**

Variations in the electric field magnitude can also be seen in varied electrode height and spacing between electrodes. Since the horizontal configuration has better electrical field uniformity than vertical configuration, the discussion ahead will only be focused on the horizontal configuration, IRSE. Based on the electric field gradient simulation result shown in Figure 4.3, a stronger electric field generated on the electrode surface but weaker electric field when it is distant from the electrode. Increasing gaps from 10 μm to 20 μm and 40 μm generate lower electric field but improved electric field gradient. This is showing that significant factor ∇E^2 depends on the electrode gap. As has been analyzed by (Clague & Wheeler, 2001), when the width of the electrode, *w* is equal to the gap, *g* between the electrode, the ∇E^2 is given by the following Eq. (4.1):

$$|\nabla E^2|_{\frac{g}{w}=1} \sim \left(\frac{g}{w}\right)^{-1.69} \tag{4.1}$$

University of Malaya

As *g* is decreased below 2*w*, the electric field intensity increase exponentially. This result discloses that for all electrodes width, the electric field intensity is dependent on the gap between the adjacent electrodes. Hence, it is presumed that DEP strength can be improved by the reduction of the electrode gap (B Yafouz, Kadri, & Ibrahim, 2012). However, among the three, an electrode gap of 20 μm was chosen to avoid the merging of the electric field between the adjacent electrodes, while generating a strong electric field and consequently DEP force. Moreover, considering cell size it compromises enough space for cell immobilization between the electrodes under pDEP force without clogging.

(a)

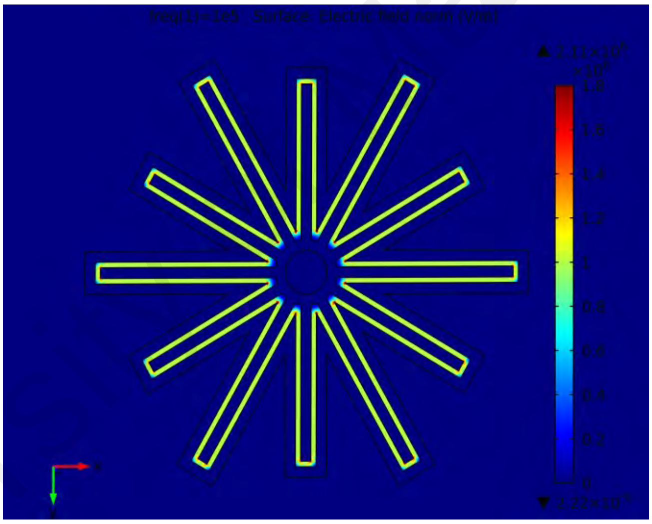

(b)

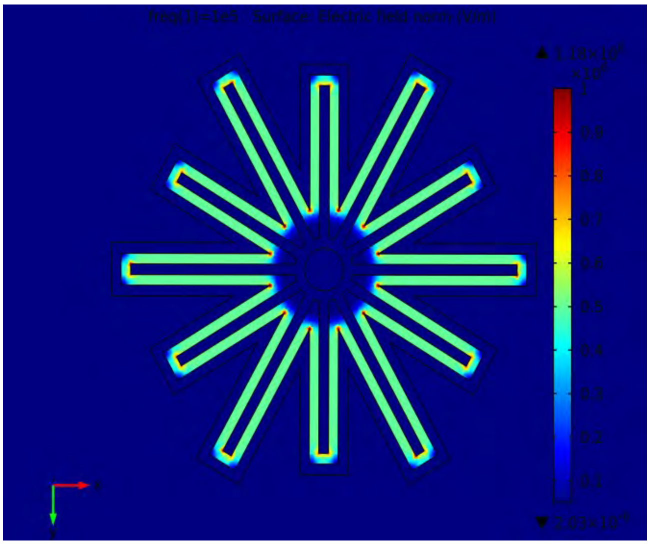

University of Malaya

(c)

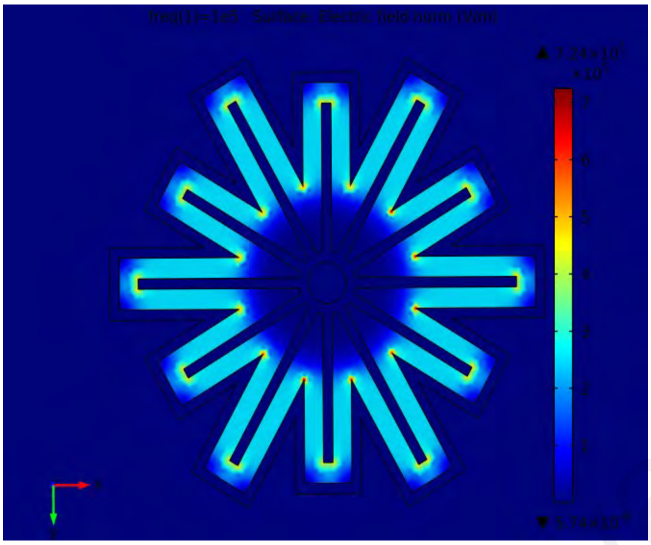

Figure 4.3: Surface plot of electric field distribution of horizontal configuration, IRSE with different electrode gap. (a) 10 µm, (b) 20 µm, and (c) 40µm.

4.2.1.3 Effect of Electrode Height

Figure 4.4 shows the variation of the electric field across the microchannel at the height of 0, 10, 20, 50, 80, and 100 µm at zy-plane, produced by the electrode height of 20 µm, 50 µm, and 80 µm, respectively. In Figure 4.4a clearly shows the gradual reduction of the electric field along with the height, as it reduces from a peak value of 7.07 × 10^5 V/m at z= 0.02 mm, 3.47 × 10^5 V/m at z= 0.03 mm, 0.81 × 10^5 V/m at z=0.05 mm to 0.24 × 10^5 V/m at z=0.08 mm and 0.16 × 10^5 V/m at the top of the channel. The electric field strength is more homogeneous near the top of the channel. In comparison, Figures 4.4b and c show a minor decreasing in the electric field along with the height of the microchannel. For better illustration of the electric field distribution, the inserted figures containing 2D surface plot were included to correspond the each plotted line graph. This suggests that as the electrode height increase, it provide larger exposure of the generated electric field over the microchannel allowing greater DEP effect on cells. Which is in line with an exponential decrease in electric field intensity as distance increase from the electrode surface by $E \propto \exp(-2\pi H)$ (N. G. Green, Ramos, & Morgan, 2002).

University of Malaya

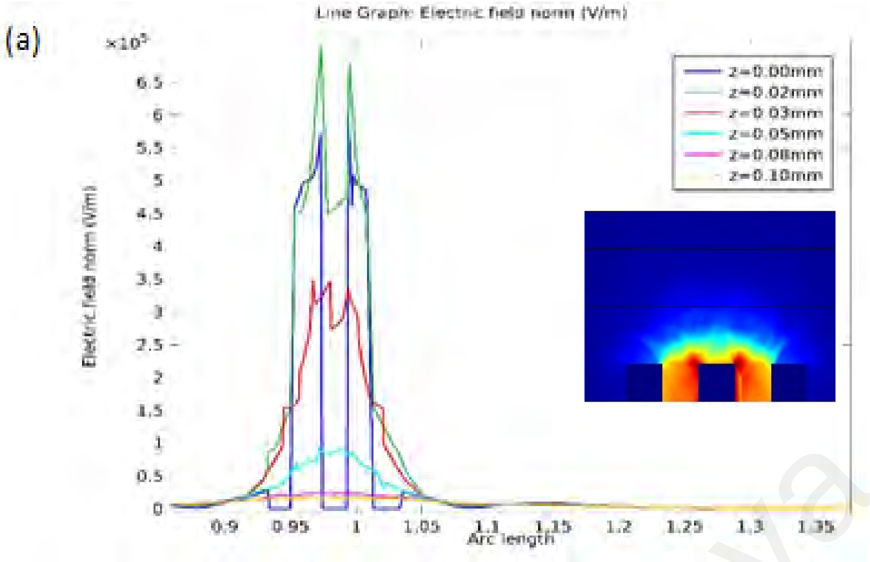

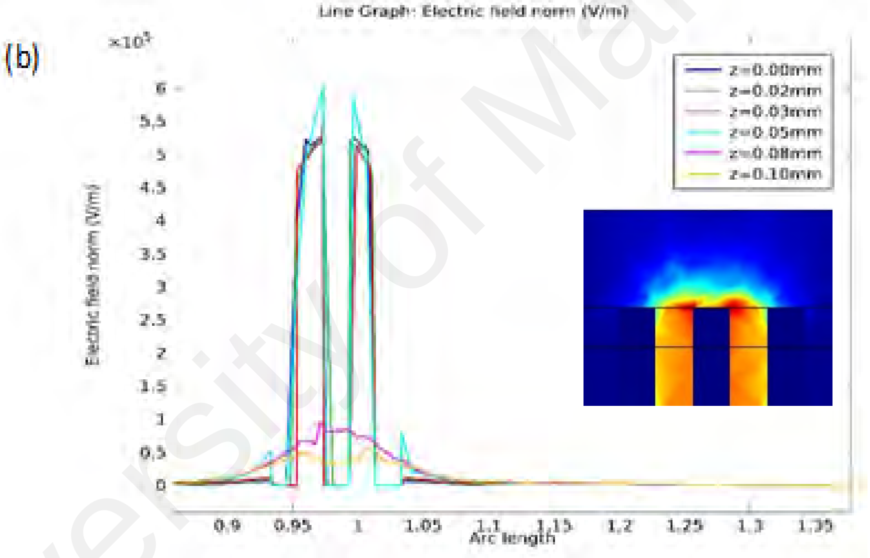

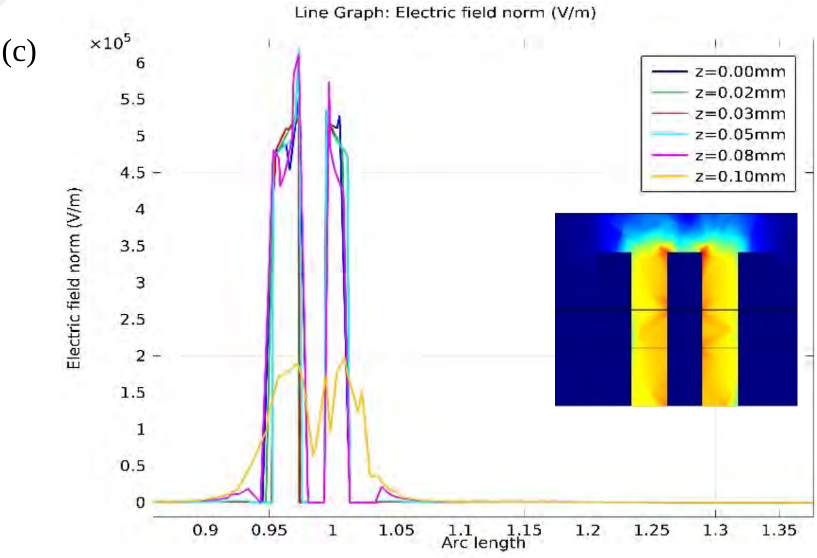

University of Malaya

Figure 4.4: Plotted line graph of the electric field generated at various elevations of the microchannel for different electrode height (a) 20 µm, (b) 50 µm, and (c) 80 µm. Insert figures are showing the 2D surface plot with lines corresponds to each plotted line graph.

As illustrated in Figure 4.5, the schematic diagram shows that 3D electrodes are more effective than 2D electrodes for DEP-based particle manipulation. The 80 µm height electrode, therefore, provides better non-uniform electric field distribution, yet, by concerning fabrication challenges, 50 µm is selected (Rouabah et al., 2011).

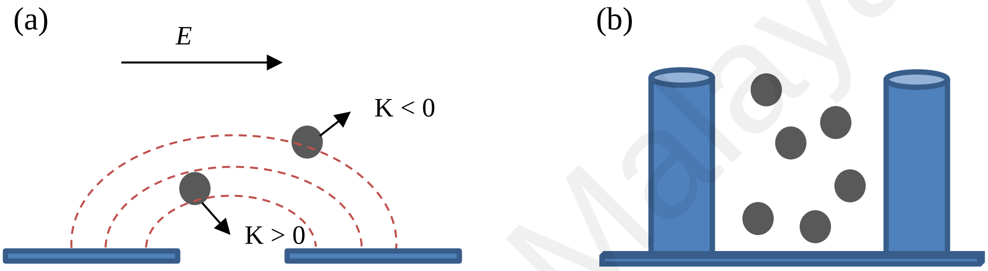

Figure 4.5: Schematic diagram of DEP manipulation. (a) Schematic of DEP manipulation in 2D planar electrode with K > 0 and K < 0 signifying pDEP and nDEP, respectively. (b) Schematic of particles in 3D electrode configuration.

4.2.1.4 Effect of Applied Voltage

The electric voltage effect on electric field magnitude is illustrated in Figure 4.6. The maximum value varies from 1.06×10^6 V/m for 5 V, 2.11×10^6 V/m for 10 V, 3.17×10^6 V/m for 15 V to 6.35×10^6 V/m for 30 V. It can be observed that increasing the voltage leads to a stronger electric field and therefore leads to a quadratic increase of DEP force that would be enforced on cells. To support this result, it is helpful to make an order of magnitude approximation of Equation 2.1 to estimate the expected dependency. By altering all length scales in Equation 2.1 dimensionless with the particle radius, *r* the magnitude in the DEP force scale is as in Eq. (4.2) (Bahaj & Bailey, 1979):

$$F_{DEP} \propto \frac{V^2}{L^3} \qquad (4.2)$$

V is the amplitude of the applied voltage and L is a length scale for a given electrode. In Figure 4.6, for all voltages tested, the electric field intensity showed a squared dependence of the DEP force on the applied voltage:

$$\nabla E \sim V^2 \tag{4.3}$$

This result is in agreement with the scaling approximation in Equation 4.2. As a consequence, the cells will move and pattern accordingly in the shorter time but high applied voltage could damage the cell and the electrode itself as well as activate Joule heating (Tay, Yu, Pang, & Iliescu, 2007). Gascoyne et al., have reported that the mammalian cells can withstand prolonged exposure to the electric field strength less than 10^4 V/m with above 95% of cell viability (X. Wang, Yang, & Gascoyne, 1999). But as the voltage increase, the cell viability decrease. However, other groups have reported no significant damage to cells with higher applied voltage with similar electrode setup (Archer, Li, Evans, Britland, & Morgan, 1999). These diverse results are probably due to different cell types used in the studies. Thus, optimum voltage selection along with other parameters such as frequency and medium conductivity should be done with consideration of the specific cell membrane damage, dielectric failure, fluid heating and fabrication limitation.

University of Malaya

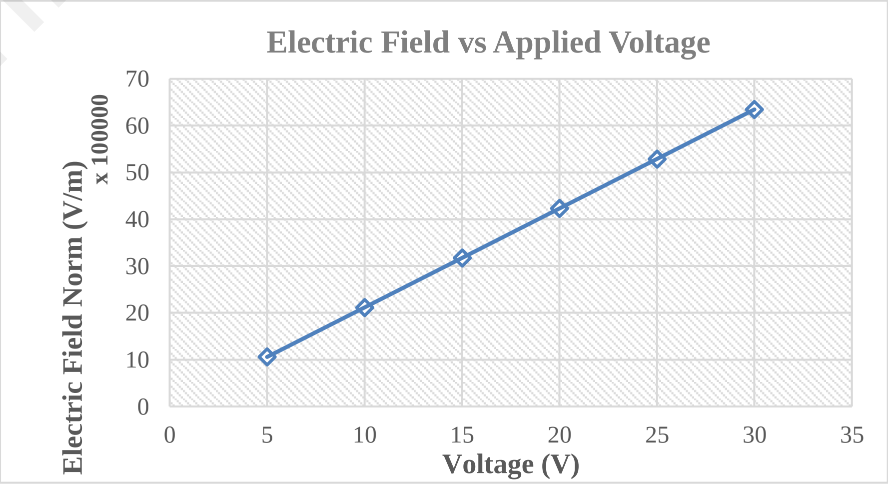

Figure 4.6: The effect of the electric field with the increasing applied voltage. The frequency is fixed at 100 MHz.

4.3 Results of Fabrication and Characterization of 3D Carbon Electrode for Lab-on-a-chip (LOC) Development

4.3.1 Substrate Treatment

4.3.1.1 Contact Angle Measurement

To investigate the surface wettability of SiO_2 in practical processing conditions for CMEMS, a water contact angle was performed and analyzed. Prior to treatment, the water contact angle was measured at two different humidity conditions. There is no exact value to identify the humidity range of high or low humidity. Hence, the humidity is a qualitative measurement in this study. At high humidity (74%), the result shows less degree in contact angle as compared to low humidity (58%) as depicted in Table 4.1.

Table 4.1: The water contact angle of SiO2 wafer at low and high humidity.

Relative humidity (%)	**Low (58%)**	**High (78%)**
Water contact angle (Degree, °)	43.86 ± 0.42	15.68 ± 0.42

The lower contact angle indicates higher hydrophilicity and a higher wetting of the surface (Kibria, Zhang, Lee, Kim, & Howlader, 2010). This happens because SiO_2 forms polar hydroxyl (-OH) bonds on their surface after extensive exposure to high humidity. Besides, a high humidity atmosphere slowing the water evaporation since the presence of water molecules in the air is high (Chhasatia, Joshi, & Sun, 2010). The substrate is thereby hydrophilic and therefore shows a poor affinity for the non-polar resin molecules of the photoresist. Thus, in order to make the substrate surface hydrophobic (water-repellent) and hence photoresist-attractive, dehydration treatment was executed. In addition, the treatment was performed at low humidity conditions since results before shown lower hydrophilicity.

University of Malaya

SiO_2 samples were dehydrated at different duration to indicate the effects and optimum treatment time; untreated (as control), 30 min, 4 h, and 12 h under low humidity (51%) condition. Figure 4.7 shows the contact angle values after each different time of dehydration treatment. Even though the contact angle measurement was conducted at a low humidity condition, the untreated sample was still hydrophilic with a contact angle of 17.08 ± 2.14°, which relevant to the nature of the SiO_2 wafer. As for the sample which treated for 30 min, the value increases to 21.52 ± 1.07°, 27.44 ± 2.00° when treated for 4 h and increase to 34.22 ± 0.82° when treated for 12 h. This shows that as the dehydration duration increase the water contact angle increase, they adsorbed water is continuing been removed which making the sample lean towards the hydrophobic surface. Thus, 12 h of dehydration treatment was applied for all the samples in this study to achieve optimum performance of the SiO_2 substrate.

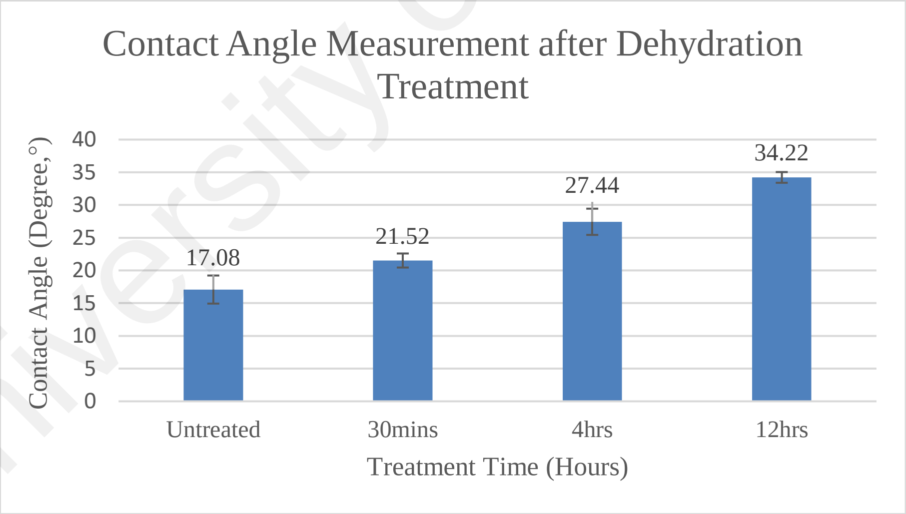

Figure 4.7: Water contact angle measurements after dehydration treatment in a low humidity condition.

4.3.1.2 SEM Characterization

CMEMS microfabrication process had been carried out for each sample to produce planar interdigitated structures. The SEM characterization with a high resolution of 10 kV was performed to study the surface morphology of the pyrolyzed samples as depicted in Figure 4.8.

University of Malaya

All of the SU-8 structures become glass-like carbon structures after the pyrolysis process as has been discussed in Section 2.6.1 with the retained pattern. Figure 4.8a and b show most of the structures were fractured and peeled off from the substrate. While structures still intact for longer dehydration time as shown in Figure 4.8c and d. However, for the sample dehydrated for 4hours, there are some cracked shown on the contact pad area as depicted in Figure 4.9. This shows that as dehydration time longer, the adhesion of SU-8 to the SiO_2 substrate gets stronger since more water molecules had been eliminated.

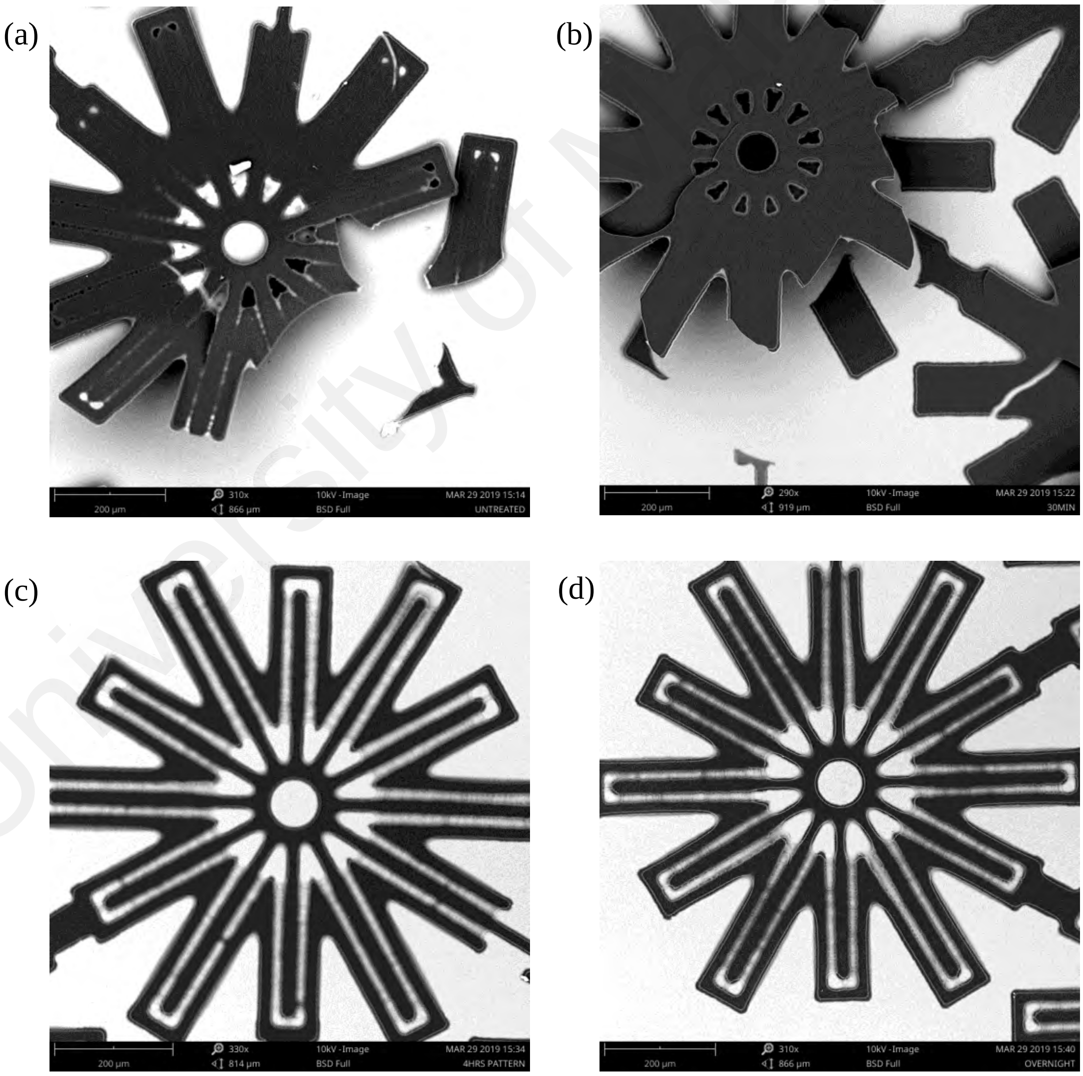

Figure 4.8: SEM images of the pyrolyzed samples dehydrated at different times. (a) Untreated, (b) 30 minutes, (c) 4 hours and (d) 12 hours.

University of Malaya

University of Malaya

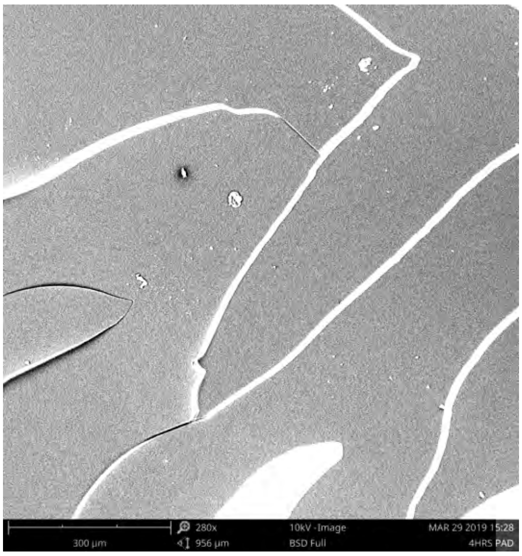

Figure 4.9: Fractures on the contact pad of the carbon structure at 4 hours of dehydration time.

4.3.2 Electrode Microfabrication

The carbon electrode, required to generate a non-uniform electric field for DEP application, was fabricated using the CMEMS microfabrication process as detailed in Subsection 3.3.3. The output of the fabricated carbon electrode is shown in Figure 4.10.

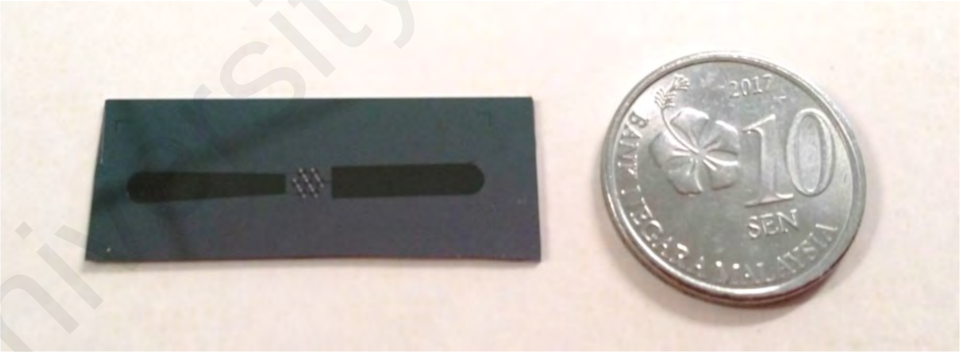

Figure 4.10: The fabricated carbon electrode in comparison with Malaysian 10 cents coin.

4.3.2.1 SU-8 Photolithography Process

Substrate cleaning is the first and significant step in the photolithography process, as the adhesion of the photoresist, SU-8 to the substrate could be thoroughly liaised by the presence of contaminants. Contaminants could be from solvent stains (acetone or IPA) and airborne dust possibly from operators, process equipment, attire, and others as shown in Figure 4.11. This will cause poor adhesion and leaks between the substrate and SU-8 interface hence affect the performance of the microfluidic device.

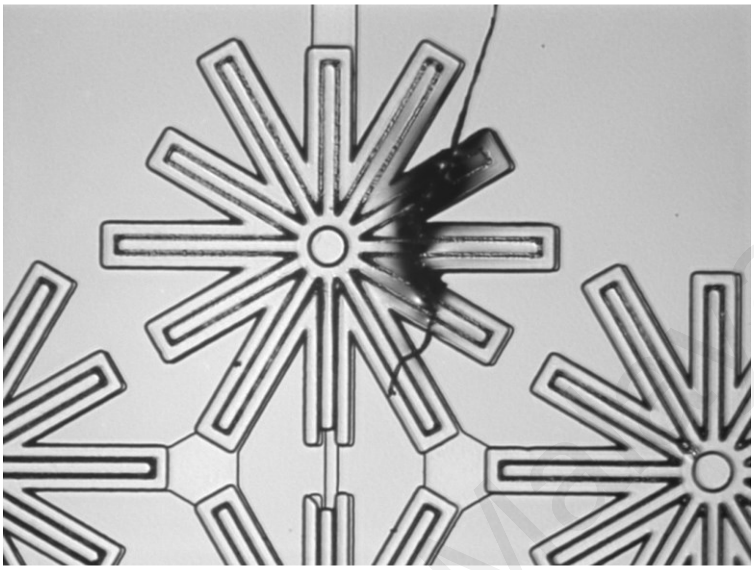

Figure 4.11: Example of airborne dust compromised with the pattern SU-8.

The fabrication of the 3D carbon electrode involved two-steps of the photolithography process, the first layer (bottom) for the connector lead and the second layer (top) for 3D structure. One of the challenging parts is to precisely align the top pattern with an underlayer pattern. The choice of exposure mode is crucial to avoid air gaps between the substrate and the mask that introduce misaligning during exposure of the light as can be seen in Figure 4.12. In this study, vacuum contact mode was chosen given the finest resolution is 1 μm as stated in the manual report by the manufacturer.

Besides, the alignment technique must be improved to avoid distortion that could lead to both patterns overlap since this is a fully manual mask aligner. Good control of X and Y direction as well as rotation are necessary in order to achieve high alignment accuracy. Since the electrode gap is 20 μm, it is critical to not let both layers to be overlap. Thus the accuracy of ±2 μm is tolerable to proceed with the next procedure.

.

University of Malaya

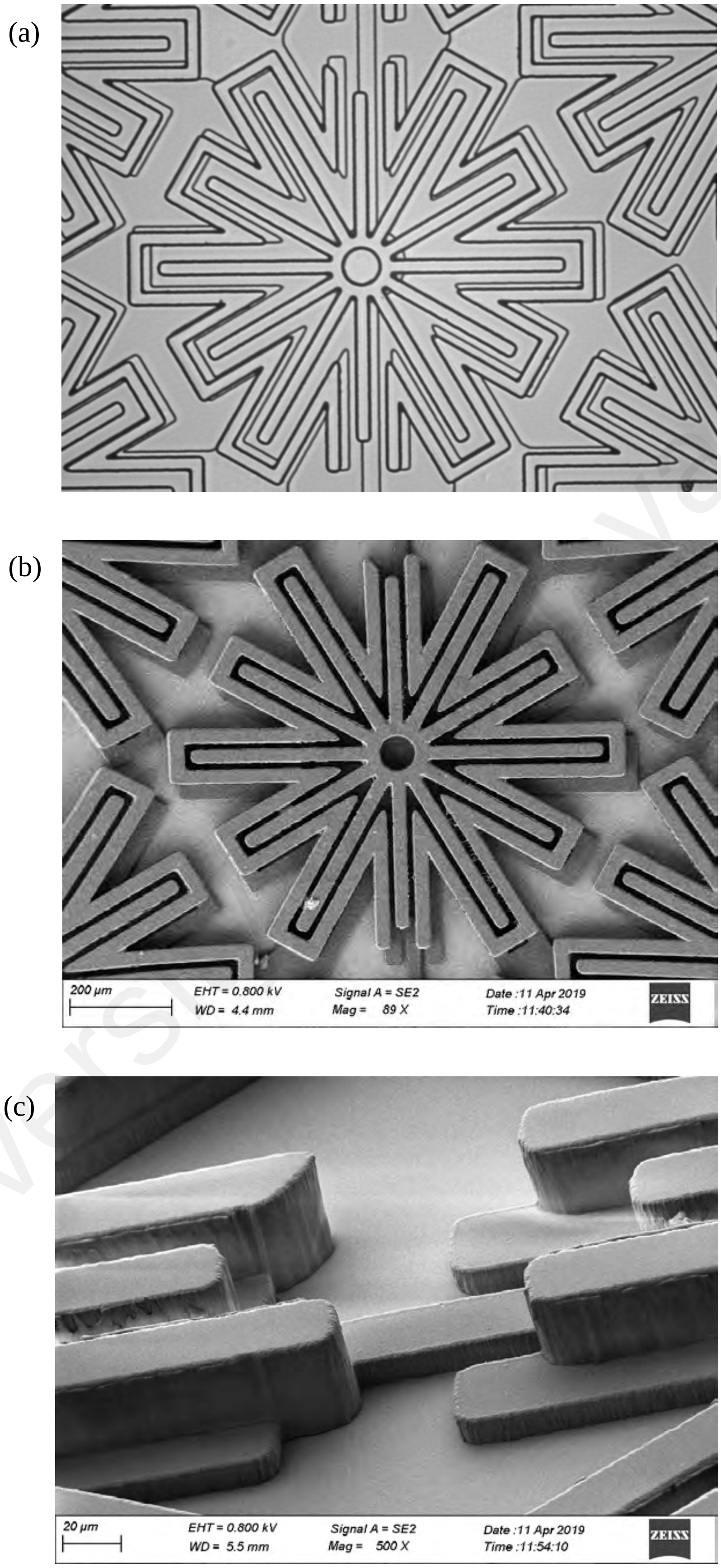

Figure 4.12: Examples of misaligned patterns. (a and b) Top view image of 3D IRSE taken using microscope and FESEM, respectively, and (c) close up FESEM image of misaligned strips of 3D IRSE.

Another major problem involves during photolithography is known as *T-topping* or Fresnel diffraction as shown in Figure 4.13. The photoresist features are narrowing toward the substrate and create a thin layer on the top surface of the photoresist film that causes mechanical contact between neighboring structures. This effect happened because of the UV exposure was carried out in proximity mode, where the photoresist's top surface is 10 to 20 µm away from the photomask. The air gaps cause pattern broadening since the refractive index of air and SU-8 is different. Thus, as compared to the contact mode (soft and hard), vacuum mode is the better choice to minimize the air gap while maximizing the intensity of UV exposure. Besides, the introduction of a filter can be employed to match the refractive index (Chuang, Tseng, & Lin, 2002; R. Yang & Wang, 2005).

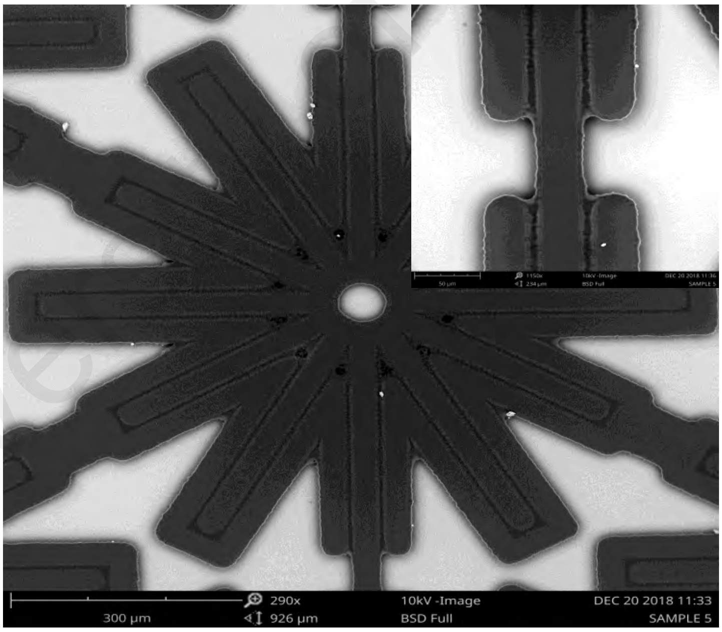

Figure 4.13: Example of *T-topping* effect.

4.3.2.2 **Pyrolysis Process**

Examples of 3D SU-8 and resulting carbon electrode are shown in Figure 4.14. The SU-8 precursor structure shrinks during pyrolysis as it can be observed by comparing the resultant carbon structure and the footprint left by the precursor SU-8 structure (red dashed line). Shrinkage phenomena are related to the degasification of SU-8 as has been

University of Malaya

explained in Section 2.6.1. When the gasses escape from the top surface area, they result in vertical shrinkage; when they escape from the lateral surface area, lateral shrinkage happens. The amount of shrinkage depends on the dimension of the SU-8 precursor and can be calculated using Equation 3.4.

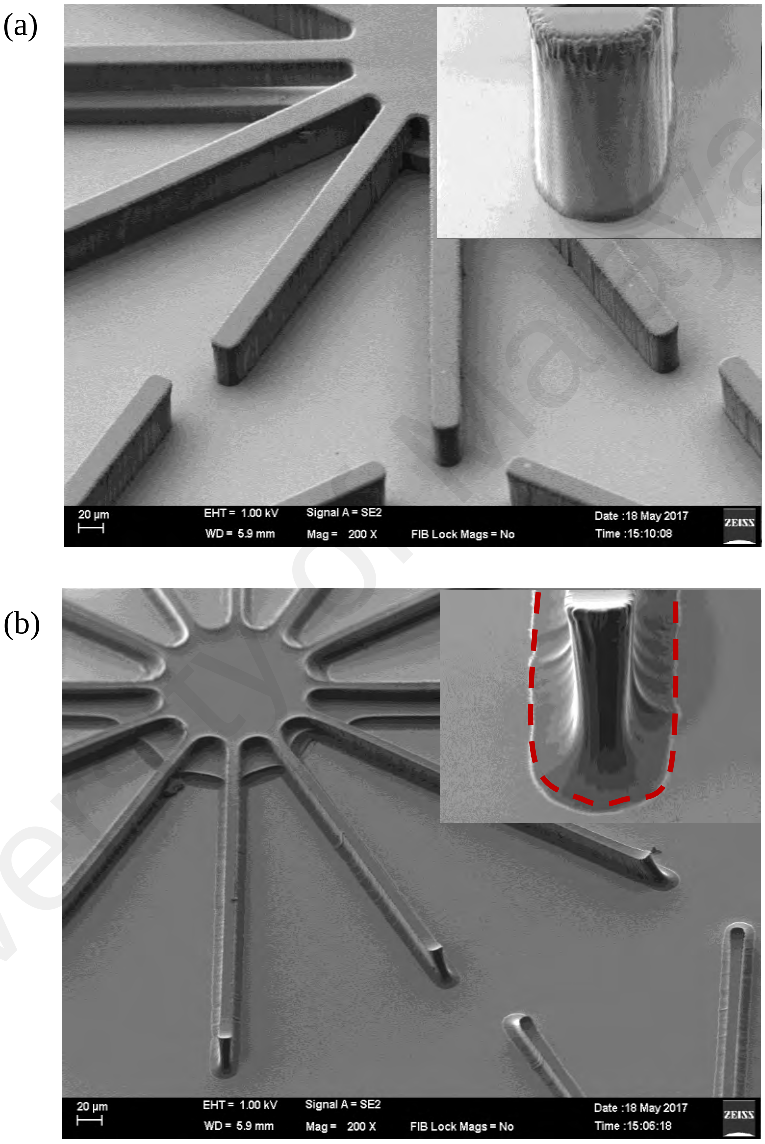

Figure 4.14: Example of pyrolysis result (a) SU-8 structure (b) carbon electrode structure. Insert figures show an enlarged view of the structures (red dashed line represents the footprint left by the original SU-8).

Table 4.2 shows the dimensions of all actual SU-8 structures and the resulting carbon structure fabricated in this study. The fabrication process of all SU-8 structures leading to the carbon structures can be found in Table 3.2 and 3.3 by correlating the Sample number (first column) of both tables. Shrinkage up to 86% is present when pyrolyzing

University of Malaya

planar structure with a height of 13.4 µm. Vertical shrinkage is high at a low aspect ratio (Sample 2) and decreases as the aspect ratio increase (Sample 3). Though, the shrinkage obtains at all dimensions is non-isometric since the height and lateral (diameter/width) of the structures do not shrink in the same proportion. As for Sample 1, the shrinkage in diameter (49%) is bigger than in height (30%). For samples 2 and 3, the shrinkage in width goes increasing with the aspect ratio. When comparing the total surface area of different SU-8 patterns, the lateral shrinkage goes on decreasing with the increase in surface area. This is shown in the case of Sample 1 and 3 with both heights near 30 µm. These results suggest that, as the lateral surface area of the structure increase, the gasses trap at the central cause it is hard to escape from the lateral areas, resulting in less lateral shrinkage (Natu et al., 2016). In addition, the carbon sidewalls were curved as compared to the vertical sidewalls of the SU-8 structure caused by volume shrinkage force during pyrolysis. However, volume shrinkage of carbon structure relative to the initial SU-8 structure is varied by the precursor shapes and thickness due to different surface-to-volume ratios (J. A. Lee, Lee, Lee, Park, & Lee, 2008). The volume ratio of circular carbon posts will be 1.5 times less than a long strip.

4.3.3 Fluidic and Electrical Network

The microfluidic platform was designed to be a companion with the fabricated carbon-DEP electrode while minimizing the fabrication challenges, cost, and time as shown in Figure 4.15. This 2-layer design featured an adhesive layer patterned with a 3.6 mm × 10.0 mm wide channel to contain the carbon electrode array. The thickness of the adhesive layer indicates the channel height which is 0.1 mm that yields fabricated channel volume equal to 3.6 µl. The adhesive layer was then aligned and adhered to a piece of 1mm thick PMMA previously drilled with two 1 mm holes. This 2-layer stack was then manually aligned to fabricated carbon electrode to yield the LOC device and used for both proof-of-concept and patterning setup.

University of Malaya

University of Malaya

Table 4.2: Dimensions of all fabricated SU-8 and carbon structures.

Sample	SU-8 (µm)			Carbon (µm)			Shrinkage (%)	
	H	D/W	AR	H	D/W	AR	H	D/W
Connecting Lead								
1	10.28 ± 0.52	n/a	n/a	6.15 ± 0.40	n/a	n/a	41	n/a
2	n/a	n/a	n/a	n/a	n/a	n/a	n/a	n/a
3	8.60 ± 0.92	n/a	n/a	5.20 ± 0.35	n/a	n/a	40	n/a
Electrode Structures								
1(3D)	33.48 ± 1.01	64.31 ± 1.05	0.52	23.77 ± 0.97	33.05 ± 1.10	0.72	30	49
2 (2D)	13.40 ± 0.85	21.47 ± 1.41	0.57	1.82 ± 1.12	11.16 ± 1.13	0.15	86	53
3 (3D)	31.04 ± 0.52	24.21 ± 1.81	1.44	17.59 ± 0.90	8.95 ± 1.32	1.97	44	58

Notes: H = height, D = diameter, W = width, AR = aspect ratio, n/a = not applicable

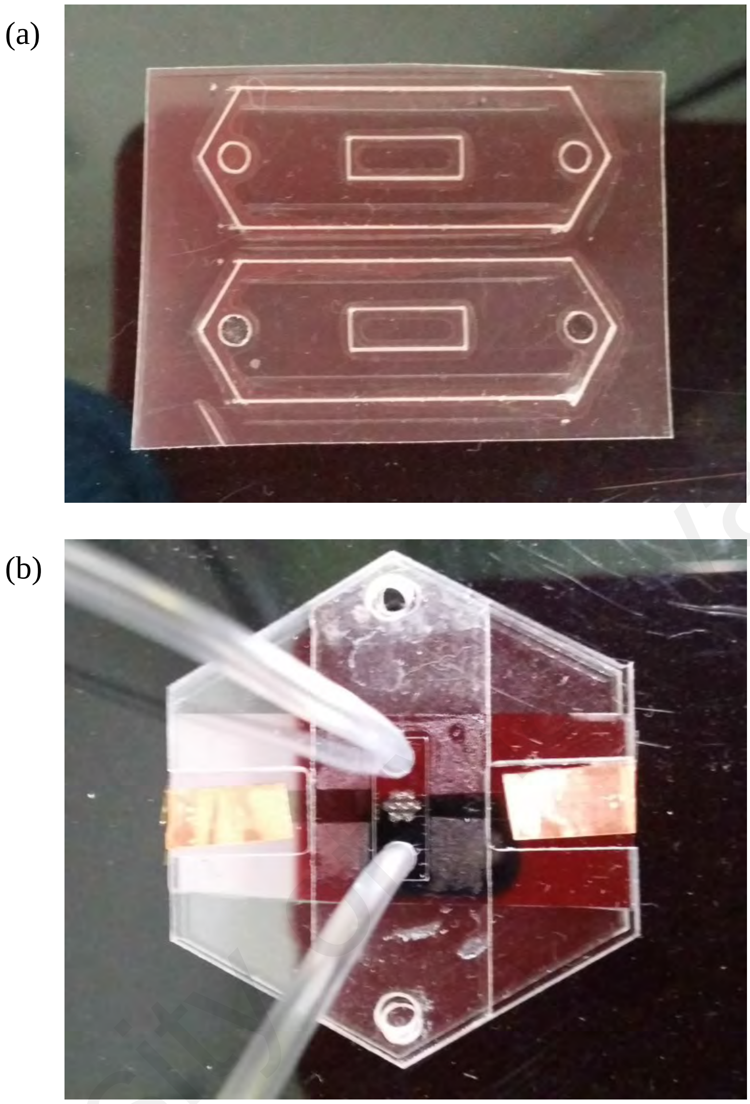

Figure 4.15: Microfluidic platform. (a) Channel and (b) top view of LOC device.

Figure 4.16a shows a reaction upon depositing silver paste on the carbon pad. The swelling effect caused a short circuit or completely disabled the electrical connection when the carbon pad detaches off the substrate. This happens due to the humid atmosphere, where the adhesive absorbs water during curing causing poor wettability (De Vries & Caers, 2011). The alternative solution by using copper adhesive tape has greatly improved the system reliability that eliminates the swelling effect on the carbon pad as shown in Figure 4.16b. This adhesive tape offers several advantages over the adhesive paste, particularly in controlling the amount of adhesive that deposited and assuring full coverage. With adhesive paste, errors often happen in excessive or fewer dispensing adhesives. With the little amount, there will be a lack of complete coverage, which

University of Malaya

decreases the bond strength; excessive adhesive flows over the sides of the contact pad and may contaminate the electrode. Besides, unlike adhesive paste, adhesive tape is already in a solid-state. This strongly avoids the issues of handling and dispensing of the paste. More importantly, it can be used in ambient conditions without disturbing their properties and has a long shelf life. Hence by using copper adhesive tape to make good electrical connections, the flexibility, no curing time, offer exclusive access to efficiency and effectivity to induce the DEP force.

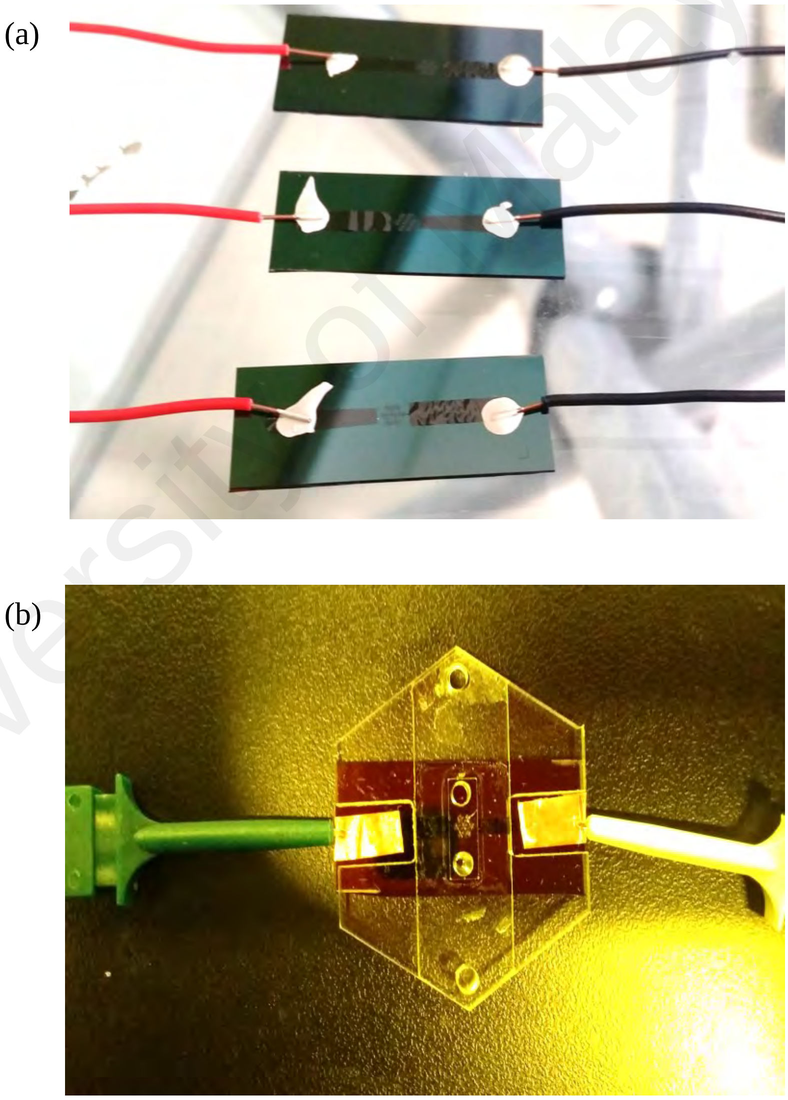

Figure 4.16: Electrical connection using (a) silver adhesive paste and (b) copper adhesive tape.

University of Malaya

4.3.4 Characterization of Pyrolyzed Carbon

In this section, the morphology of the patterns obtained on the SiO_2 substrate was characterized before and after pyrolysis with optical and electron microscopy. The electrical resistivity of all samples after pyrolyzed was also examined before the DEP experimentation.

4.3.4.1 Physical Microstructure Properties

Figure 4.17 shows the resultant SU-8 structure of Sample 1, concentric 3D post arrays after photolithography steps. All of the 3D posts were successfully aligned on top of the planar connecting leads as depicted in Figure 4.17a. Besides, uniform structures were obtained with straight sidewalls and smooth top surface as shown in Figure 4.167. This result proves that all the photolithography steps were optimized properly mainly UV exposure dose and PEB time.

(a)

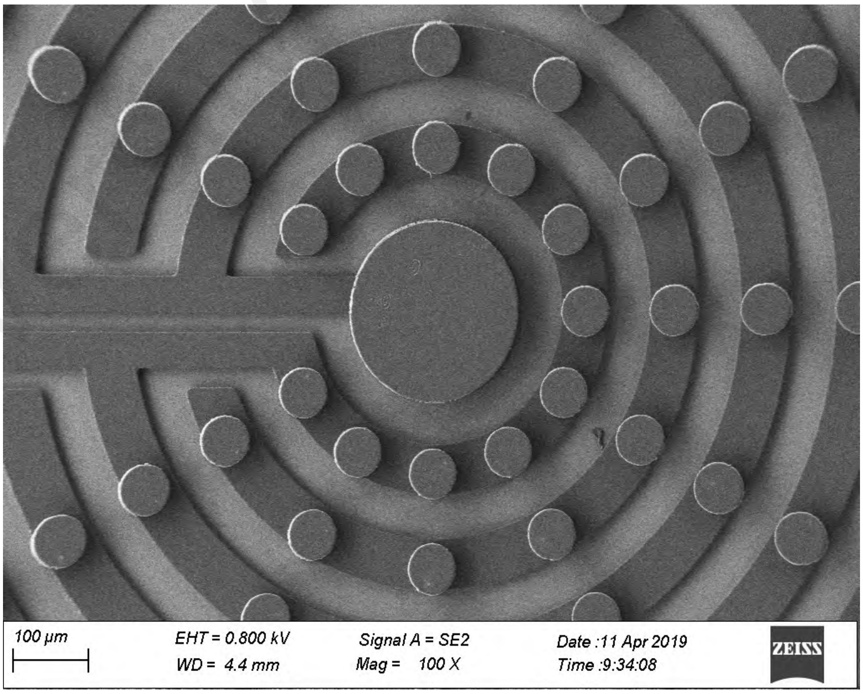

University of Malaya

(b)

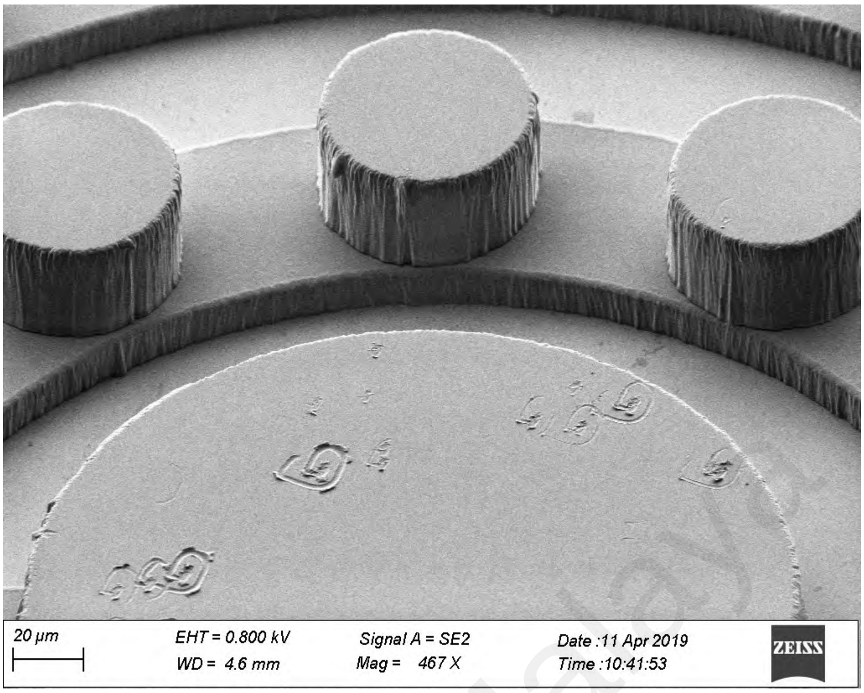

Figure 4.17: FESEM images of the SU-8 structure of Sample 1 after the photolithography process. (a) top view showing concentric 3D post arrays and (b) tilted view showing individual 3D posts on planar connection lead.

Shrinkage caused by pyrolysis clearly seen in Figure 4.18a, where the original dimensions of the SU-8 structure were decreased but still maintain the pattern. However, the bigger 3D post in the middle was detached from the substrate. This is because the shrinkage force is stronger than the adhesion force on a larger surface area. Therefore the diameter of the structure is inversely relative to the structure thickness (Teixidor, Zaouk, Park, & Madou, 2008). This suggests that structures that require high surface areas such as connection pads benefit from the use of planar structure. Besides, the competition between shrinkage and adhesion force is also responsible for the distinctive curved wall at the base of the carbon post as can be observed in Figure 4.18b. In addition, sagging at the top surface of the carbon post was observed where the edges are seen to protrude as compared to the central area. This sagging special effect occurs was believed due to the residual stress developed during degassing which appears in other polymers as well (Ferracane, 2005). However, these effects are decreasing as the aspect ratio increase since degassing mainly occurs through the lateral surface area (Natu et al., 2018).

University of Malaya

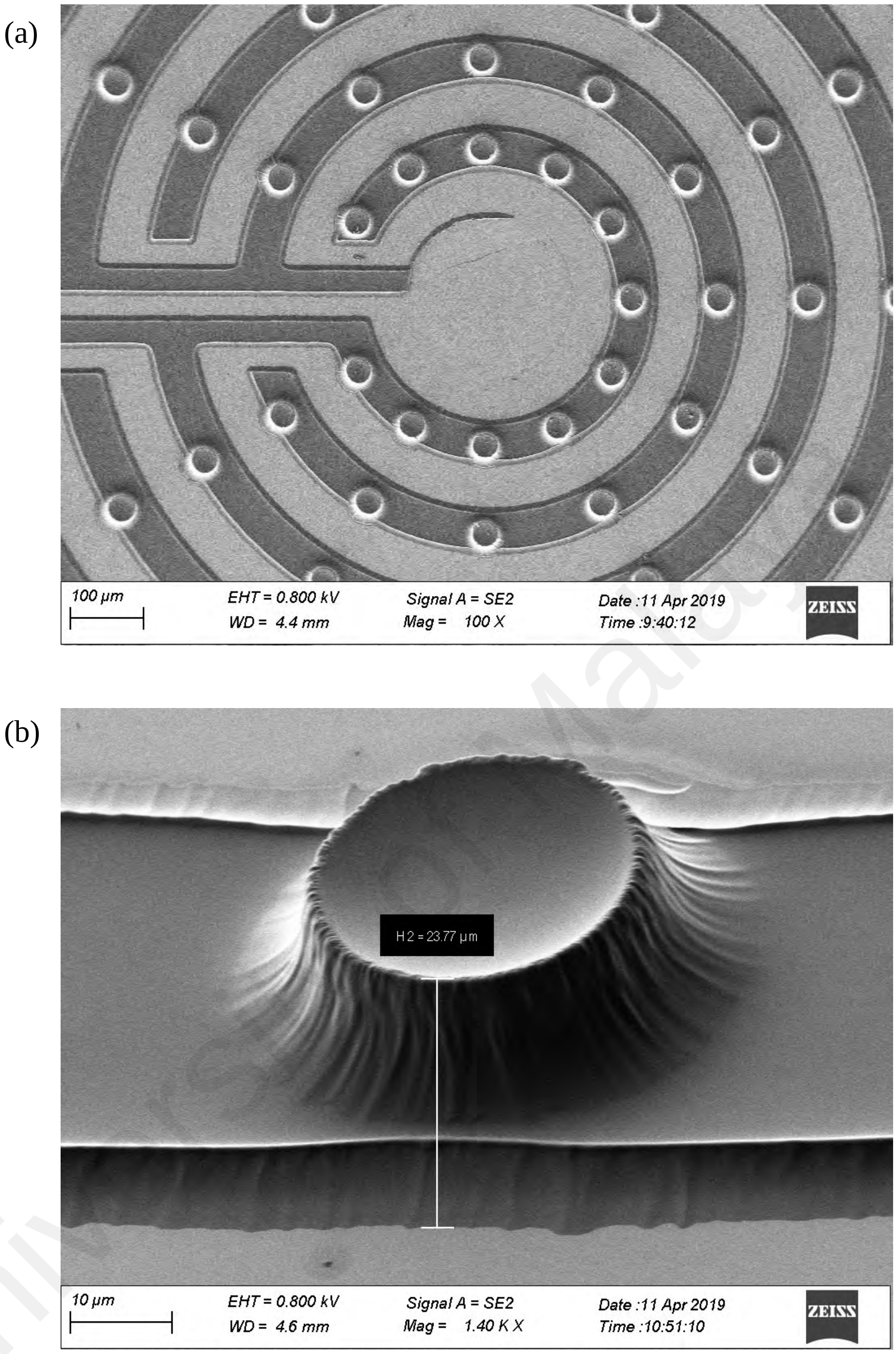

Figure 4.18: FESEM images of the carbon structure of Sample 1 after the pyrolysis process. (a) top view showing shrank concentric 3D post arrays and (b) tilted view showing shrank individual 3D post with sagging effect and curved wall.

Figure 4.19 and 4.20 display the FESEM images of the SU-8 structures after the photolithography steps of samples 2 and 3, respectively. The thickness after the photolithography was compatible with the nominal thickness (13 µm for Sample 2 and 38 µm for Sample 3) of the spin-coated SU-8. In particular, the resulted thickness is 13.40 ± 0.85 µm for sample 2 and 31.04 ± 0.52 µm for sample 3 based on three times of measurements. Table 4.3 reports the data of the dimensional analysis of the SU-8 and carbon structures.

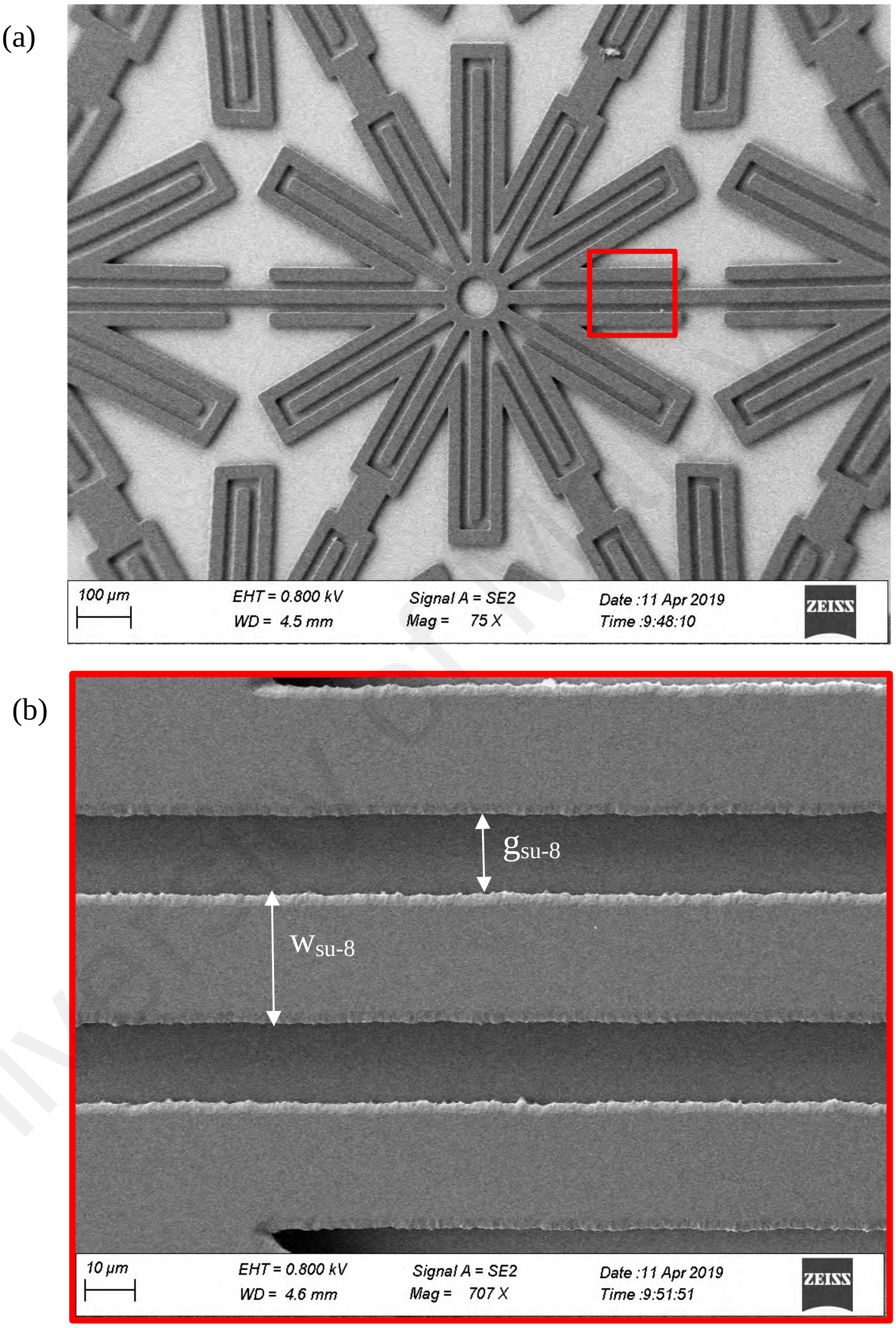

Figure 4.19: FESEM images of the SU-8 structure of Sample 2 after the photolithography process. (a) top view showing planar IRSE and (b) close-up view of the strips (red box) showing the dimension of width (w_{su-8}) and gap (g_{su-8}).

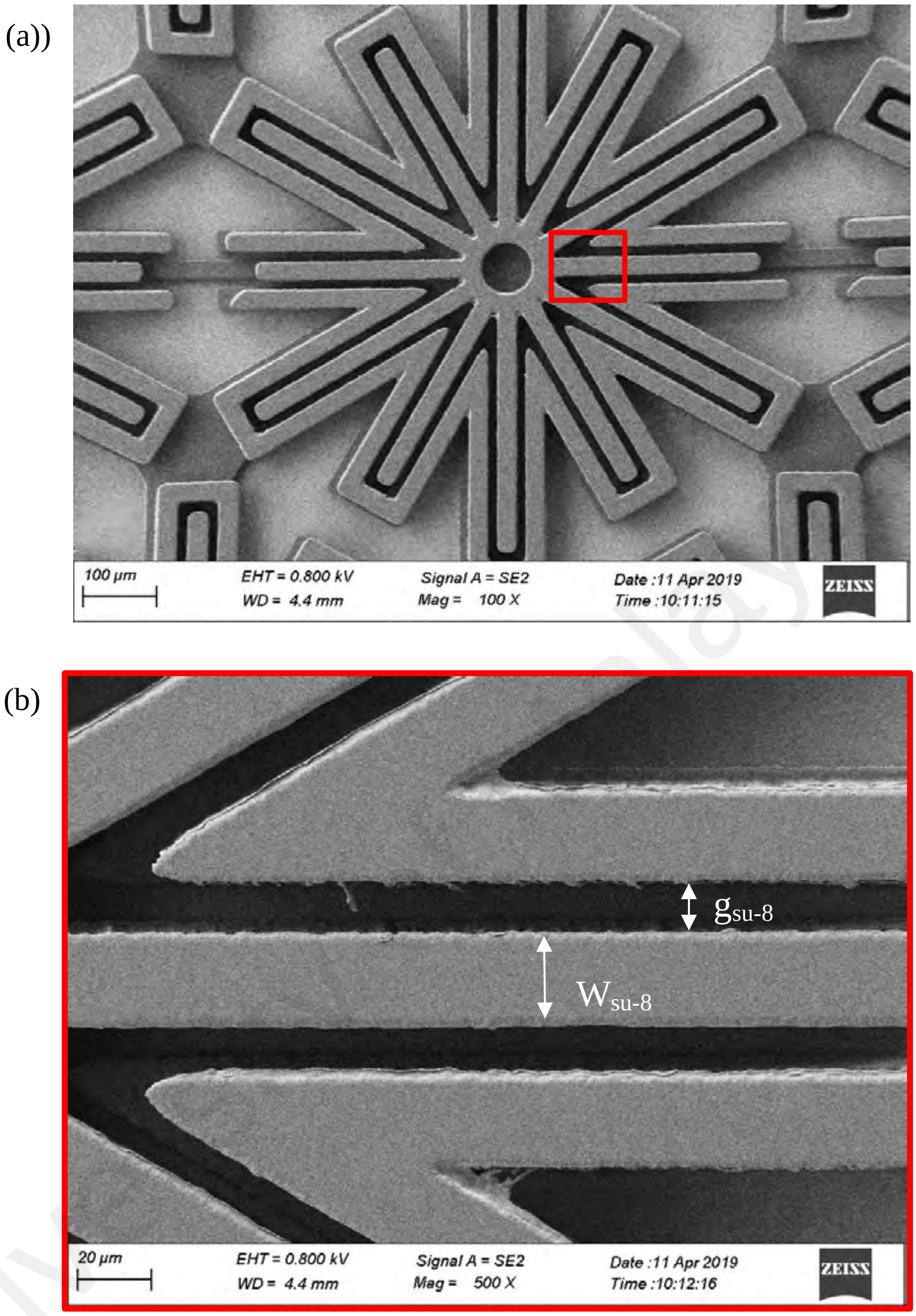

Figure 4.20: FESEM images of the SU-8 structure of Sample 3 after the photolithography process. (a) top view showing 3D IRSE and (b) close-up view of the thick strips (red box) showing the dimension of width (w_{su-8}) and gap (g_{su-8}).

Table 4.3: Nominal structure of samples and resulting dimensions of SU-8 (after photolithography) and carbon (after pyrolysis).

Sample	w_o	w_{su-8}	w_c	g_o	g_{su-8}	g_c
2	20.0	21.47 ± 1.41	11.16 ± 1.13	20.0	15.47 ± 1.11	28.23 ± 1.62
3	20.0	24.21 ± 1.81	8.95 ± 1.32	20.0	13.4 ± 1.91	35.79 ± 1.51

Notes: w_o=nominal width, w_{su-8}=SU-8 width, w_c=carbon width, g_o=nominal gap, g_{su-8}=SU-8 gap and g_c=carbon gap.

The data state the difference between the nominal widths and gaps (w_o, g_o), the actual obtained after photolithography ($w_{su\text{-}8}$, $g_{su\text{-}8}$), and after pyrolysis (w_c, g_c). The difference shows a slight increase in width compares to nominal as a result of *T-topping*. This occurs regularly to high aspect ratio structure during exposure, where the absorbance of the UV light from the top to the bottom layer gradually decreases. Besides, the pattern broadening can also due to the poor exposure setup, which introduces air gaps between the photomask and photoresist. The air gaps increase light diffraction and cause pattern broadening; increase in width, $w_{su\text{-}8,}$ and decrease in the gap, $g_{su\text{-}8}$.

Figures 4.21 and 4.22 show the FESEM images of the carbon structure after the pyrolysis process of samples 2 and 3, respectively. As has been reported in Table 4.3, more significant dimensional differences obtained after the pyrolysis. The differences are resulting from the shrinkage occurring during degassing. Shrinkage in width is more dominant for high aspect ratio as has been discussed in section 4.3.2.2. The higher lateral surface area making degassing easier hence decreasing the width, $w_{c,}$ and certainly increasing the gap, $g_{c.}$

University of Malaya

(a)

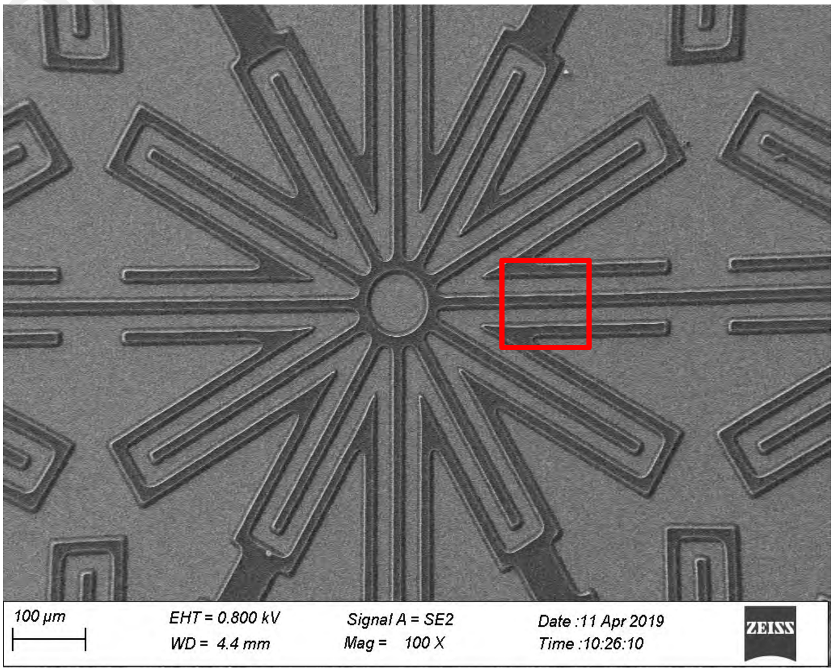

(b)

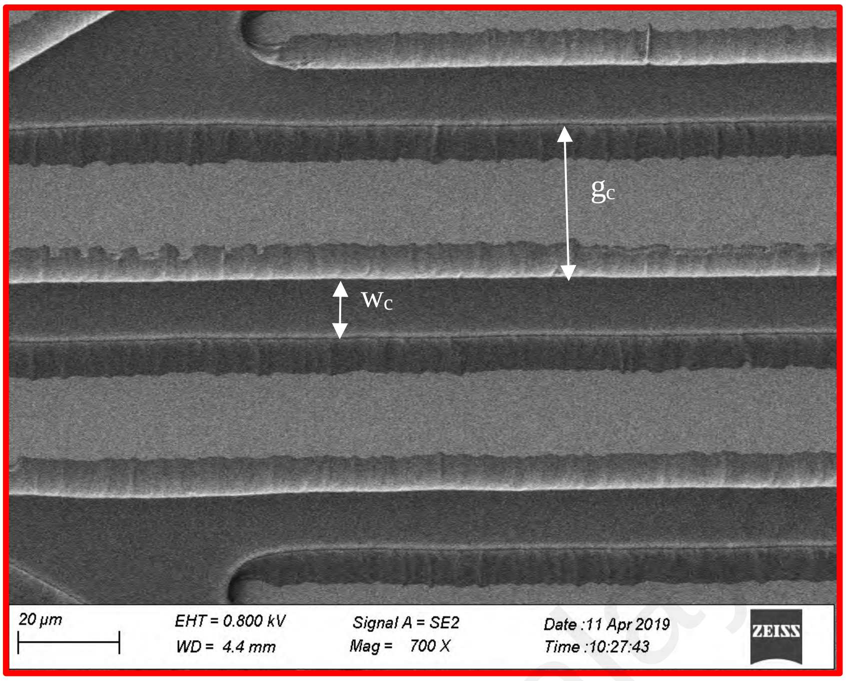

Figure 4.21: FESEM images of the carbon structure of Sample 2 after the pyrolysis process. (a) top view showing planar IRSE and (b) close-up view of the strips (red box) showing the dimension of width (w_c) and gap (g_c).

(a)

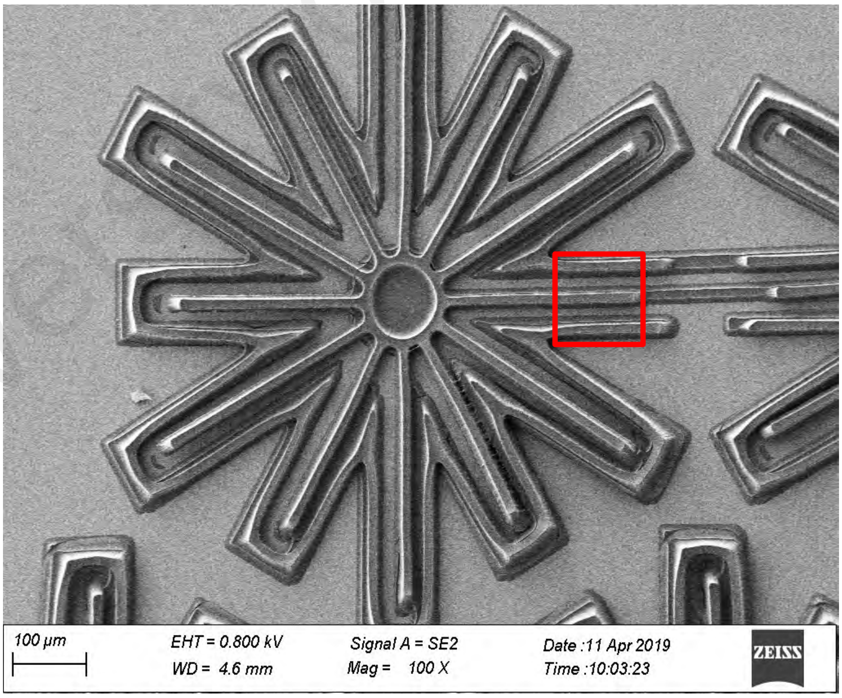

University of Malaya

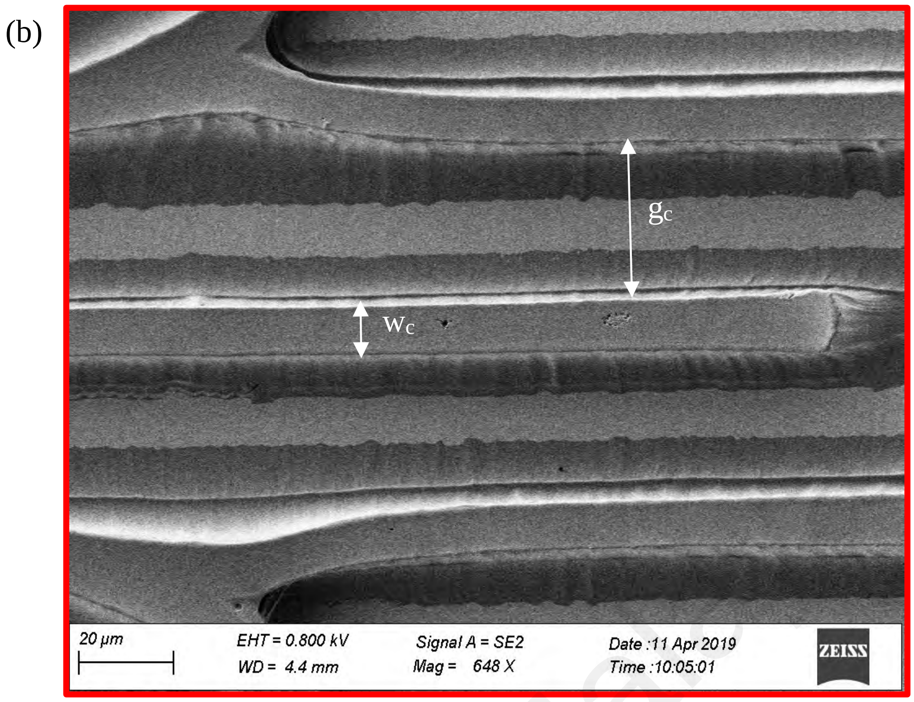

Figure 4.22: FESEM images of the carbon structure of Sample 3 after the pyrolysis process. (a) top view showing 3D IRSE and (b) close-up view of the thick strips (red box) showing the dimension of width (w_c) and gap (g_c).

4.3.4.2 Electrical Properties

Figure 4.23 shows the resistance measured over two different thicknesses of the film; 1.8 µm and 18.0 µm. The resistance of the carbon films decreases as the thickness increase. Thus it is definitely an added value to the 3D electrode as compared to the 2D electrode. This is also applicable to the connection pad, where a thicker connection pad can reduce up to 70% of the resistance. However, the surface area of the connection pad must be balanced to avoid their detachment from the substrate since wide structures benefit from the use of low thickness.

Multiple voltage and current measurements were conducted on carbon films of different thicknesses to acquire the resistance, R as detailed in Table 4.4 and the resistivity can be calculated by using Equation 3.6.

University of Malaya

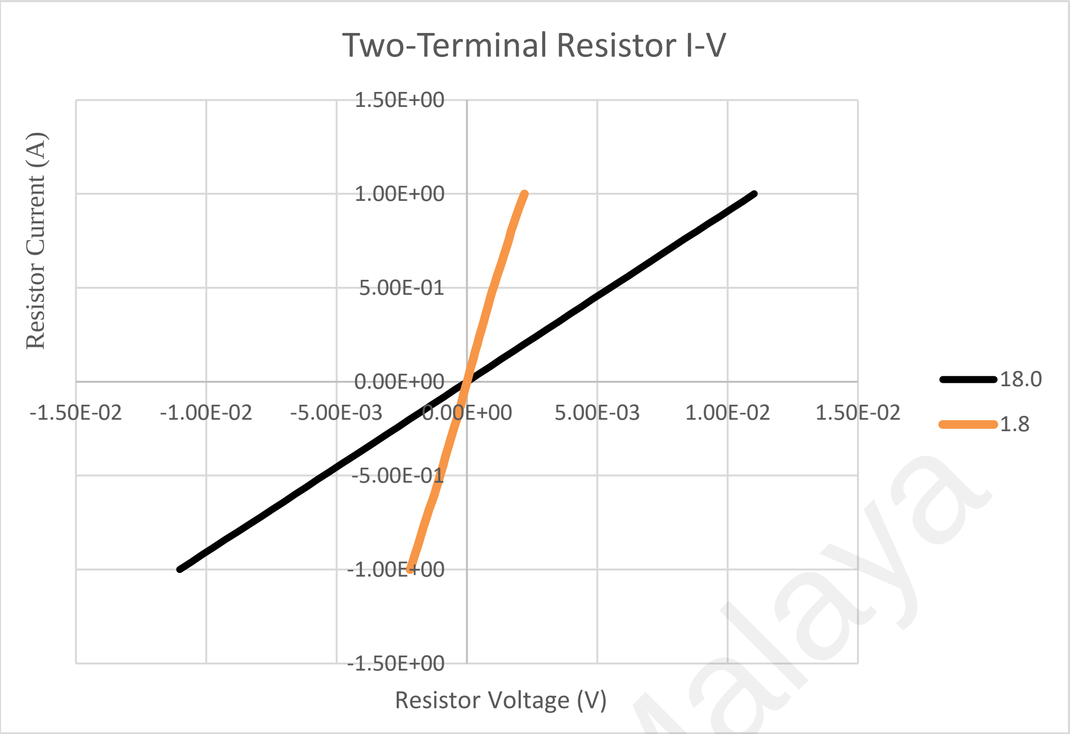

Figure 4.23: I-V graph of two-terminal resistors for two different thicknesses of carbon films.

Table 4.4: Resistivity characterization of carbon films for different thicknesses.

Measurement	**Resistance, R (Ω)**	**Resistivity, ρ (Ω.m)**
film thickness = 1.8 μm		
1	276.3 ± 8.3	4.97 ± 0.33 x 10^{-4}
2	150.5 ± 7.7	2.71 ± 1.13 x 10^{-4}
3	281.4 ± 10.3	5.07 ± 0.63 x 10^{-4}
film thickness = 18.0 μm		
1	89.1 ± 3.8	16.04 ± 1.72 x 10^{-4}
2	94.9 ± 5.6	17.08 ± 1.83 x 10^{-4}
3	90.4 ± 9.3	16.27 ± 1.33 x 10^{-4}

University of Malaya

The resistivity of the carbon films is independent of the film thickness and the average value obtained in this study is $10.36 \pm 1.19 \times 10^{-4}$ Ω·m. This value is slightly large than previously obtained, which is 1.04×10^{-4} Ω·m, but is still low enough to generate an electric field for DEP applications using ten of volts (Park et al., 2005).

4.4 Results of Dielectrophoresis (DEP) Experiments

4.4.1 Proof-of-concept

In order to confirm the application of the fabricated LOC device, the manipulation of polystyrene microbeads was conducted using DEP. As has been explained in Section 2.5, DEP refers to the motion of polarizable particles suspended in a medium, induced by the applied non-uniform electric field. Polystyrene microbeads will exhibit pDEP when they are more polarized than the surrounding medium and move toward the regions with a strong electric field. Otherwise, they will exhibit nDEP if they are less polarizable than the medium and repel from the region with a strong electric field (Khoshmanesh et al., 2010).

The qualitative characterization of the DEP response of polystyrene microbeads is presented in Table 4.5 below. pDEP is observed at various frequencies in the range of 50 MHz to 500 kHz. At 50 kHz to 5 kHz the microbeads begin to show nDEP response.

Table 4.5: Qualitative characterization of DEP response to manipulate polystyrene microbeads in a range of frequency at 15V applied voltage.

Frequency	**MHz**			**kHz**		
	50	**5**	**1**	**500**	**50**	**5**
DEP Response	pDEP	pDEP	pDEP	pDEP	nDEP	nDEP

University of Malaya

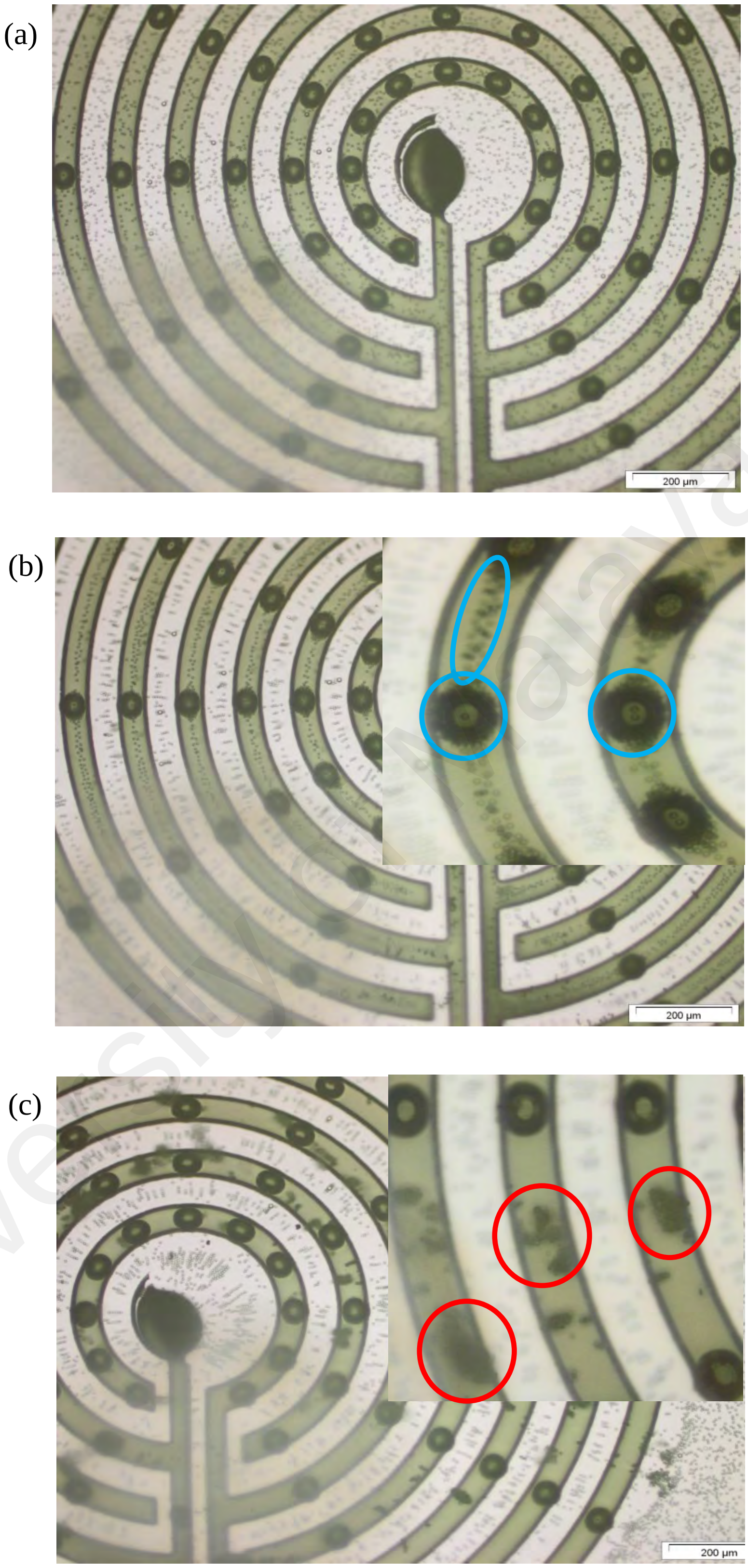

University of Malaya

Figure 4.24: Manipulation of 5 µm polystyrene microbeads based on DEP force. (a) Homogenous distribution of polystyrene microbeads before application of electric field, (b) pDEP effect after applying 50 MHz signals (blue circles), and (c) nDEP effect after applying 5 kHz signal (red circles).

Figure 4.24 shows the 5 µm polystyrene microbeads response when subjected to the DEP force. As shown in Figure 4.24a, the microbeads were homogeneously distributed all over the electrode array prior to the application of the electric field. When a 50 MHz AC signal was applied, the microbeads were attracted to the edges of the electrodes as depicted in Figure 4.24b (blue circles marks). This behavior was in response to the pDEP effect in which particles move toward the strong electric field region. In addition, there were microbeads that aggregated along the connection leads due to the dipole-dipole interactions of the neighboring microbeads as clearly seen in the enlarged image of Figure 4.24b (blue oval marks). On the other hand, under 5 kHz applied AC signal, the microbeads were repelled from the electrode edges as depicted in Figure 4.24c (red circles marks). This shows that the microbeads were under the nDEP effect where they move away from the strong electric field region. The microbeads were forced to accumulate between the electrodes and levitated to a certain height above the electrodes as shown in the enlarged image of Figure 4.24c (the out-of-focus are the electrodes). However, under both conditions, there are lateral pearl chains forming at the bottom of the gap between connecting leads. This happens due to the additional electric field created by the connecting leads. These effects could be significantly reduced by pattern a thin layer of SU-8 around the 3D carbon electrodes to electrically insulate the connection leads (Martinez-Duarte et al., 2011).

University of Malaya

By decreasing the applied frequency to 500 Hz, electrolysis was induced as shown in Figure 4.25 where the microbeads were drifted away and randomly distributed through the suspension of the media as well as air bubbles began to develop (yellow circles). However, by increasing the frequency, this effect will reduce. This effect was influenced by the frequency of the AC electric field, the voltage applied to the electrodes, and the ion concentration of the medium (S. Li et al., 2013). Hence, suitable frequency and voltage should be chosen wisely according to the desired DEP response and to avoid potential electrolysis.

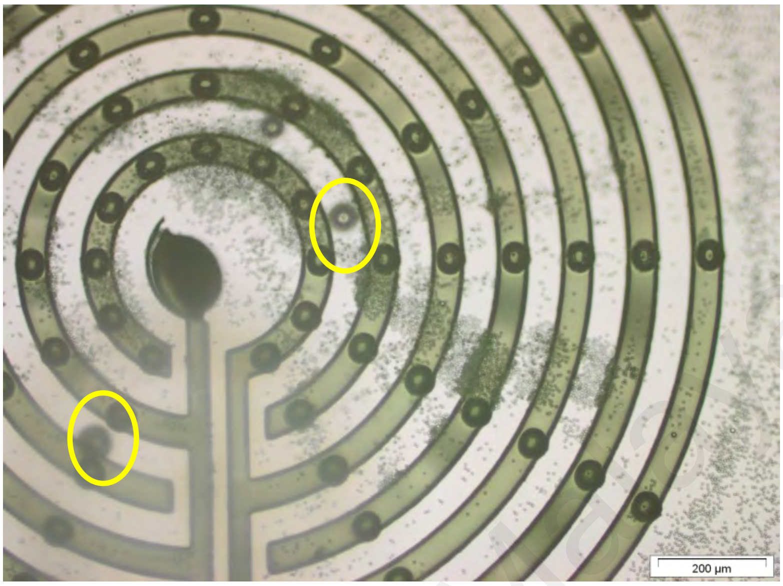

Figure 4.25: Electrolysis effect which creates air bubbles (yellow circles marks) under 500 Hz applied frequency.

This result indicates that the fabricated LOC device featuring a carbon electrode is successfully manipulated the polarized polystyrene microbeads by using nDEP and pDEP effect. Thus, it is expected that this LOC could be used for a newly designed electrode named IRSE and potentially used for hepatic cells patterning.

4.4.2 Microbeads Patterning

Upon the proof-of-concept experiment, the DEP patterning experiment was conducted on polystyrene microbeads in order to achieve the final objective of this study, which is to pattern microbeads using the proposed electrode design. This is to demonstrate the potential application of this LOC device to pattern hepatic cells using DEP force mimicking the natural architecture of biological hepatic lobule. The results and discussion of the microbeads patterning using both 2D and 3D IRSE electrode were presented in Figure 4.26 below.

University of Malaya

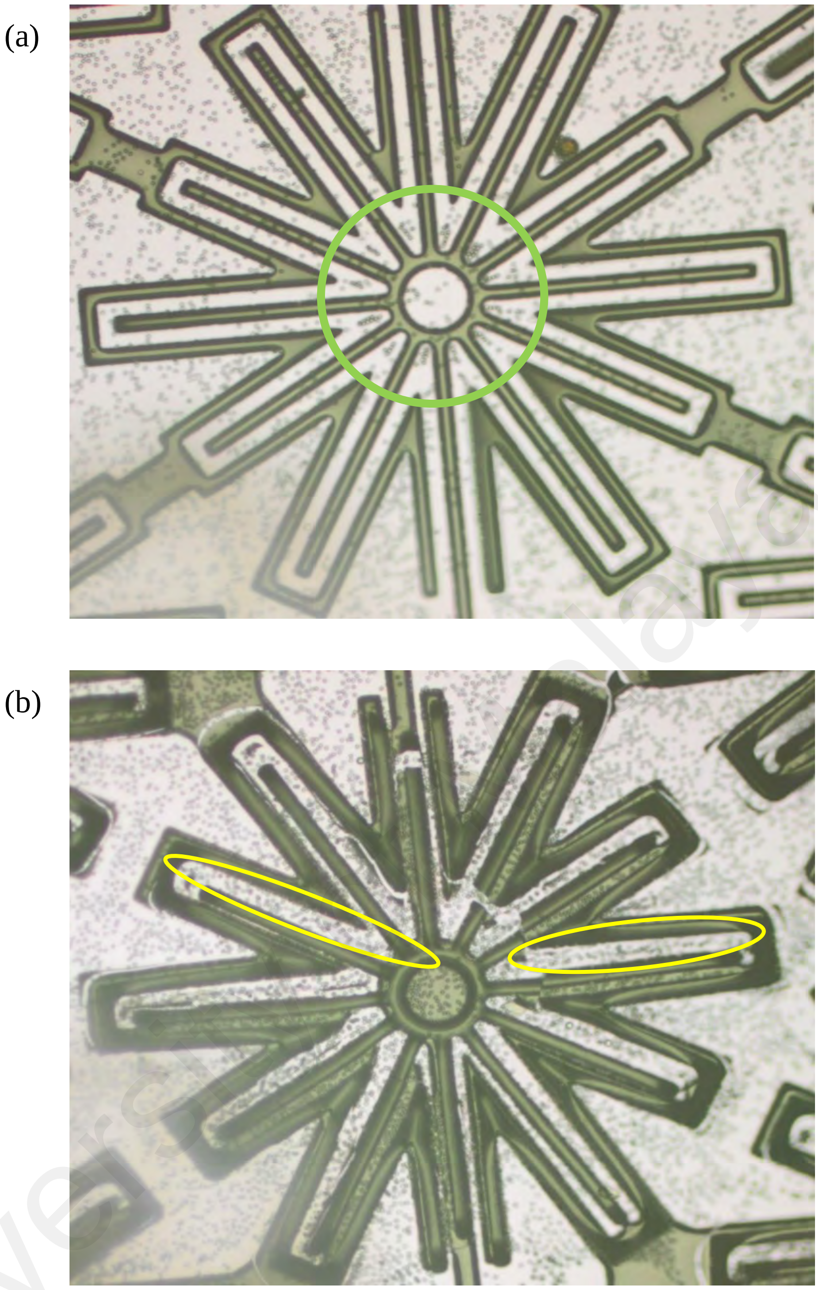

Figure 4.26: Manipulation of 10 µm polystyrene microbeads based on pDEP force at 15 V and 50 MHz on (a) 2D IRSE and (b) 3D IRSE.

Figure 4.26a and b show the pDEP response of polystyrene microbeads when 15 V of AC potential was applied at 50 MHz frequency on 2D and 3D IRSE, respectively. Figure 4.26a shows weak pDEP force limited the trapping of microbeads at the beginning of the strips near the center, as shown with the green circle. However, the 3D IRSE demonstrated better trapping efficiency, as evidence by patterns of microbeads along the strips, as shown in Figure 4.26b (yellow ovals).

University of Malaya

By using Equation 3.7, trapping efficiency for 2D IRSE is 15% ± 3% while 3D IRSE is 82% ± 8% given an increase of 67%. This shows that the trapping efficiency is increasing as the electrode height increase. Such an improvement is mainly attributed to the fact that the DEP force is proportional to the gradient of the square of the electric field (Equation 2.1). An increased electrode height leads to a larger volume of DEP force over the channel, resulting in an improved trapping efficiency which consistent with the simulation results earlier (Section 4.2.1.3). Besides, the low trapping efficiency of 2D IRSE is due to the interference of the levitation force along the channel when the microbeads pass through the planar electrode.

Nevertheless, although the trapping efficiency is relatively high and microbeads pattern mainly along the strips, there is a significant number of untrapped microbeads shown by 3D IRSE. This might be because of unbalanced microbeads concentration as compared to channel total area that affects the trapping volume, hence optimization on microbeads concentration should be carried out to increase the efficiency of DEP effects (Jaramillo, Torrents, Martínez-Duarte, Madou, & Juárez, 2010). Moreover, after 1 minute of applied voltage, the 3D IRSE was spotted to be shifted and a few of the strips were broken. Possible contributing reasons to this effect include electro-thermal, electro-osmotic, or even low surface adhesion between the carbon electrode and the SiO_2 substrate.

In short, these results show that the new design electrode, IRSE is successfully able to pattern particles via DEP mimicking the complex architecture of the biological hepatic lobule. Additionally, a 67% increase in microbeads trapping is presented for the case of 3D IRSE as compared to the 2D IRSE. This suggests that the 3D IRSE has high potential to be applied for 3D hepatic cell patterning.

University of Malaya

4.5 Summary

In this chapter, the results of the developed LOC device were presented and analyzed. In the beginning, simulation results by COMSOL have suggested that horizontal configuration is better than vertical configuration to generate a uniform distribution of electric field over the new design electrode. Furthermore, the electrode with a horizontal configuration named as IRSE was optimized geometrically and agreed to the optimum dimension of 20 µm:50 µm (gap: height) with a 20 µm electrode width. Thus, this IRSE has been proposed to be fabricated for the dielectrophoretic cell patterning application. Next, outcomes of LOC development were presented featuring electrode microfabrication and fluidic and electric network. Errors that occurred during the CMEMS process were detailed as well for future improvement. In addition, characterization results show the microstructure of the fabricated carbon electrode and their resistivity value, which is significant to generate the electric field. In order to confirm the application of the fabricated LOC device, the manipulation of polystyrene microbeads was conducted using DEP. DEP effects including pDEP and nDEP were obtained once the AC signal was applied for a range of frequency, indicating that the fabricated LOC device is function properly and can be utilized for dielectrophoretic cell patterning. Lastly, the fabricated LOC device featuring the proposed new electrode design, IRSE was successfully patterning polystyrene microbeads according to the desired pattern resembling simulation results. Other advantages also have been highlighted by comparing 2D and 3D structures. Thus, this LOC device is shown to be effective at manipulating and patterning particles into the desired pattern, specifically mimicking the architecture of the biological hepatic lobule.

University of Malaya

CHAPTER 5: CONCLUSION AND FUTURE WORK

5.1 Conclusion

A LOC device featuring a 3D carbon electrode potentially for hepatic cell patterning based on DEP was designed, simulated, fabricated, and its performance was tested utilizing microbeads particle. A new design of electrode has been proposed called IRSE that mimicking the hepatic plates of the biological liver. The simulation results of the IRSE configuration showed a uniform distribution of the electric field with the value up to 10^6 V/m that could generate even DEP effects of particles. Furthermore, the numerical modeling was used to optimized the electrode geometry parameters given a result of 20 µm:50 µm (gap: height) with a 20 µm electrode width.

Using the CMEMS fabrication technique, both 2D and 3D carbon electrodes have been successfully fabricated. The fabricated carbon electrodes have been characterized both microstructure and electrical ($10.36 \pm 1.19 \times 10^{-4}$ Ω·m) to show its capability in implementing DEP proses efficiently. Although the electrical resistivity value is slightly higher than in literature but is still low enough to generate an electric field for DEP applications using ten of volts. Moreover, to complete the LOC device, the carbon electrode was assembled with a compatible fluidic and electrical network. The developed fluidic platform was designed to reach simple fabrication, low cost, leakage-free flow, and reusable. The electrical network also has been improvised to achieve better electrical connections between the carbon electrode and the function generator.

A proof-of-concept experiment was conducted to confirm the functionality of the completed LOC device. The experiment's finding has qualitatively confirmed the capability of polystyrene microbeads manipulation by utilizing both nDEP and pDEP. In addition, another experiment was conducted to prove the ability of the proposed IRSE to dielectrophoretically patterning the polystyrene microbeads. This experiment was also to

University of Malaya

compare the trapping efficiency of both 2D and 3D IRSE. The result shows that an increase of 67% of trapping efficiency yield by the 3D IRSE showing that the region affected by the DEP is dependent on the height of the electrode, hence provide improvement in particle trapping and patterning. As expected, this LOC device could be used for a newly designed electrode and has the potential to be used for hepatic cells patterning.

This carbon-DEP has been demonstrated as a new alternative to present DEP technologies that offer several advantages: 1) wider electrochemical stability window than metal electrodes that minimizing the possibility of electrolysis; 2) carbon is biocompatible and highly inert, and 3) the use of low voltage (tens of volts) to polarize carbon electrode array is enough to generate a DEP force. Furthermore, CMEMS fabrication offers an inexpensive high-yield process for 3D carbon electrodes.

University of Malaya

5.2 Contribution

The following are the summary of the original contribution undertaken towards accomplishing this study:

i. Design a new electrode named IRSE which specifically designed to mimic the architecture of the biological hepatic lobule.
ii. Fabricate 3D carbon-DEP using the CMEMS microfabrication technique which is relatively simple and cost-effective as it only requires photolithography and pyrolysis process.
iii. Design and development of LOC device featuring an optimized version of IRSE based on simulation analysis using COMSOL Multiphysics software.
iv. Patterning of polystyrene microbeads using DEP force according to the desired pattern.

5.3 Future Work Recommendation

Following are some of the recommendations for future work that can be integrated with the developed LOC device:

i. DEP patterning on living hepatic cells and assessment on viability to prove the biocompatibility and evaluate the design of IRSE.
ii. Device integration such as microfluidic fluid delivery that could contribute to creating a cell culture microenvironment.
iii. Fabrication of the carbon electrodes on a transparent substrate to empowers experiment visualization.
iv. Optimization on channel total volume to enhance the DEP effect.
v. Numerical simulation of other forces contributes to DEP experimentation.

University of Malaya

REFERENCES

Abd Rahman, N., Ibrahim, F., & Yafouz, B. (2017). Dielectrophoresis for biomedical sciences applications: A review. *Sensors, 17*(3), 449.

Amato, L., Heiskanen, A., Hansen, R., Gammelgaard, L., Rindzevicius, T., Tenje, M., . . . Keller, S. S. (2015). Dense high-aspect ratio 3D carbon pillars on interdigitated microelectrode arrays. *Carbon, 94*, 792-803.

Archer, S., Li, T.-T., Evans, A. T., Britland, S. T., & Morgan, H. (1999). Cell reactions to dielectrophoretic manipulation. *Biochemical and biophysical research communications, 257*(3), 687-698.

Babensee, J. E., Anderson, J. M., McIntire, L. V., & Mikos, A. G. (1998). Host response to tissue engineered devices. *Advanced drug delivery reviews, 33*(1-2), 111-139.

Bahaj, A., & Bailey, A. (1979). Dielectrophoresis of microscopic particles. *Journal of Physics D: Applied Physics, 12*(10), L109.

Beidaghi, M., Chen, W., & Wang, C. (2011). Electrochemically activated carbon micro-electrode arrays for electrochemical micro-capacitors. *Journal of Power Sources, 196*(4), 2403-2409.

Bhatia, S., Balis, U., Yarmush, M., & Toner, M. (1998). Probing heterotypic cell interactions: hepatocyte function in microfabricated co-cultures. *Journal of Biomaterials Science, Polymer Edition, 9*(11), 1137-1160.

Bhatia, S. N., Yarmush, M. L., & Toner, M. (1997a). Controlling cell interactions by micropatterning in co-cultures: Hepatocytes and 3T3 fibroblasts. *Journal of Biomedical Materials Research: An Official Journal of The Society for Biomaterials and The Japanese Society for Biomaterials, 34*(2), 189-199.

Bhatia, S. N., Yarmush, M. L., & Toner, M. (1997b). Engineered Substrates for Controlling Cell-Cell Interactions. *ASME-PUBLICATIONS-HTD, 355*, 99-104.

Bonnans, C., Chou, J., & Werb, Z. (2014). Remodelling the extracellular matrix in development and disease. *Nature reviews Molecular cell biology, 15*(12), 786-801.

Braff, W. A., Pignier, A., & Buie, C. R. (2012). High sensitivity three-dimensional insulator-based dielectrophoresis. *Lab Chip, 12*(7), 1327-1331.

Campana, L., & Iredale, J. P. (2017). *Regression of liver fibrosis.* Paper presented at the Seminars in liver disease.

Canavan, H. E., Cheng, X., Graham, D. J., Ratner, B. D., & Castner, D. G. (2005a). Cell sheet detachment affects the extracellular matrix: a surface science study comparing thermal liftoff, enzymatic, and mechanical methods. *Journal of Biomedical Materials Research Part A: An Official Journal of The Society for Biomaterials, The Japanese Society for Biomaterials, and The Australian Society for Biomaterials and the Korean Society for Biomaterials, 75*(1), 1-13.

University of Malaya

Canavan, H. E., Cheng, X., Graham, D. J., Ratner, B. D., & Castner, D. G. (2005b). Surface characterization of the extracellular matrix remaining after cell detachment from a thermoresponsive polymer. *Langmuir, 21*(5), 1949-1955.

Cao, J., Cheng, P., & Hong, F. (2008). A numerical analysis of forces imposed on particles in conventional dielectrophoresis in microchannels with interdigitated electrodes. *Journal of electrostatics, 66*(11-12), 620-626.

Chen, R.-J., & Liu, C.-H. Liver-on-chip engineering: the rapid lobule-mimetic reconstruction of functional engineered liver tissues via dielectrophoresis-based cell patterning.

Chen, Y.-S., Ke, L.-Y., & Liu, C.-H. (2011). *3D lobule-mimetic chip via positive dielectrophoresis force with sinusoidal spacing poly (ethylene glycol)-diacrylate microwalls.* Paper presented at the 2011 16th International Solid-State Sensors, Actuators and Microsystems Conference.

Chen, Y.-S., Tung, C.-K., Ke, L.-Y., Fan, S.-K., Wang, X., & Liu, C.-H. (2015). *Using gelatin methacrylate covering and dielectrophoresis force manipulating for lobule-mimicking culture chip in vitro.* Paper presented at the 2015 Transducers-2015 18th International Conference on Solid-State Sensors, Actuators and Microsystems (TRANSDUCERS).

Chhasatia, V. H., Joshi, A. S., & Sun, Y. (2010). Effect of relative humidity on contact angle and particle deposition morphology of an evaporating colloidal drop. *Applied Physics Letters, 97*(23), 231909.

Chiou, C.-H., Pan, J.-C., Chien, L.-J., Lin, Y.-Y., & Lin Jr, -. L. (2013). Characterization of Microparticle Separation Utilizing Electrokinesis within an Electrodeless Dielectrophoresis Chip. *Sensors, 13*(3), 2763-2776.

Chou, C.-F., & Zenhausern, F. (2003). Electrodeless dielectrophoresis for micro total analysis systems. *IEEE Engineering in Medicine and Biology Magazine, 22*(6), 62-67.

Chu, H., Huan, Z., Mills, J., Yang, J., & Sun, D. (2015). Three-dimensional cell manipulation and patterning using dielectrophoresis via a multi-layer scaffold structure. *Lab on a Chip, 15*(3), 920-930.

Chuang, Y.-J., Tseng, F.-G., & Lin, W.-K. (2002). Reduction of diffraction effect of UV exposure on SU-8 negative thick photoresist by air gap elimination. *Microsystem Technologies, 8*(4-5), 308-313.

Chung, S., Sudo, R., Vickerman, V., Zervantonakis, I. K., & Kamm, R. D. (2010). Microfluidic platforms for studies of angiogenesis, cell migration, and cell–cell interactions. *Annals of biomedical engineering, 38*(3), 1164-1177.

Chung, T. W., Yang, J., Akaike, T., Cho, K. Y., Nah, J. W., Kim, S. I., & Cho, C. S. (2002). Preparation of alginate/galactosylated chitosan scaffold for hepatocyte attachment. *Biomaterials, 23*(14), 2827-2834.

University of Malaya

Clague, D., & Wheeler, E. (2001). Dielectrophoretic manipulation of macromolecules: The electric field. *Physical review E, 64*(2), 026605.

Das, T., & Chakraborty, S. (2009). Biomicrofluidics: Recent trends and future challenges. *Sadhana, 34*(4), 573.

Davalos, R. V., McGraw, G. J., Wallow, T. I., Morales, A. M., Krafcik, K. L., Fintschenko, Y., . . . Simmons, B. A. (2008). Performance impact of dynamic surface coatings on polymeric insulator-based dielectrophoretic particle separators. *Analytical and bioanalytical chemistry, 390*(3), 847-855.

De Vries, J., & Caers, J. (2011). Anisotropic conductive adhesives in electronics *Advanced Adhesives in Electronics* (pp. 53-104): Elsevier.

Dhandayuthapani, B., Yoshida, Y., Maekawa, T., & Kumar, D. S. (2011). Polymeric scaffolds in tissue engineering application: a review. *International journal of polymer science, 2011*.

Domansky, K., Inman, W., Serdy, J., Dash, A., Lim, M. H., & Griffith, L. G. (2010). Perfused multiwell plate for 3D liver tissue engineering. *Lab on a Chip, 10*(1), 51-58.

Eltom, A., Zhong, G., & Muhammad, A. (2019). Scaffold techniques and designs in tissue engineering functions and purposes: a review. *Advances in Materials Science and Engineering, 2019*.

Fausto, N. (2001). Liver regeneration: from laboratory to clinic. *Liver transplantation, 7*(10), 835-844.

Fausto, N., & Campbell, J. S. (2003). The role of hepatocytes and oval cells in liver regeneration and repopulation. *Mechanisms of development, 120*(1), 117-130.

Feng, R., & Farris, R. J. (2002). Influence of processing conditions on the thermal and mechanical properties of SU8 negative photoresist coatings. *Journal of Micromechanics and Microengineering, 13*(1), 80.

Ferracane, J. L. (2005). Developing a more complete understanding of stresses produced in dental composites during polymerization. *Dental Materials, 21*(1), 36-42.

Fitzer, E., Mueller, K., & Schaefer, W. (1971). The chemistry of the pyrolytic conversion of organic compounds to carbon. *Chemistry and physics of carbon, 7*, 237-383.

Ge, P.-L., Du, S.-D., & Mao, Y.-L. (2014). Advances in preoperative assessment of liver function. *Hepatobiliary & Pancreatic Diseases International, 13*(4), 361-370.

Geim, A. K. (2009). Graphene: status and prospects. *science, 324*(5934), 1530-1534.

Glasser, H., & Fuhr, G. (1998). Cultivation of cells under strong ac-electric field—differentiation between heating and trans-membrane potential effects. *Bioelectrochemistry and bioenergetics, 47*(2), 301-310.

University of Malaya

Glicklis, R., Shapiro, L., Agbaria, R., Merchuk, J. C., & Cohen, S. (2000). Hepatocyte behavior within three-dimensional porous alginate scaffolds. *Biotechnology and bioengineering, 67*(3), 344-353.

Gonzalez, C. F., & Remcho, V. T. (2005). Harnessing dielectric forces for separations of cells, fine particles and macromolecules. *Journal of Chromatography A, 1079*(1-2), 59-68.

Goral, V. N., Hsieh, Y.-C., Petzold, O. N., Clark, J. S., Yuen, P. K., & Faris, R. A. (2010). Perfusion-based microfluidic device for three-dimensional dynamic primary human hepatocyte cell culture in the absence of biological or synthetic matrices or coagulants. *Lab on a Chip, 10*(24), 3380-3386.

Goral, V. N., & Yuen, P. K. (2012). Microfluidic platforms for hepatocyte cell culture: new technologies and applications. *Annals of biomedical engineering, 40*(6), 1244-1254.

Green, N., Morgan, H., & Milner, J. J. (1997). Manipulation and trapping of sub-micron bioparticles using dielectrophoresis. *Journal of biochemical and biophysical methods, 35*(2), 89-102.

Green, N. G., Ramos, A., & Morgan, H. (2002). Numerical solution of the dielectrophoretic and travelling wave forces for interdigitated electrode arrays using the finite element method. *Journal of Electrostatics, 56*(2), 235-254.

Grzesiak, J. J., & Pierschbacher, M. D. (1995). Shifts in the concentrations of magnesium and calcium in early porcine and rat wound fluids activate the cell migratory response. *The Journal of clinical investigation, 95*(1), 227-233.

Hashimoto, M., Kaji, H., & Nishizawa, M. (2009). Selective capture of a specific cell type from mixed leucocytes in an electrode-integrated microfluidic device. *Biosensors and Bioelectronics, 24*(9), 2892-2897.

Hasirci, V., Berthiaume, F., Bondre, S., Gresser, J., Trantolo, D., Toner, M., & Wise, D. (2001). Expression of liver-specific functions by rat hepatocytes seeded in treated poly (lactic-co-glycolic) acid biodegradable foams. *Tissue engineering, 7*(4), 385-394.

Hassan, Y. M. (2018). Pyrolytic carbon electrodes for bioelectrochemical applications.

Hernaez, R., Solà, E., Moreau, R., & Ginès, P. (2017). Acute-on-chronic liver failure: an update. *Gut, 66*(3), 541-553.

Higgins, G. M. (1931). Experimental pathology of the liver. I. Restoration of the liver of the white rat following partial surgical removal. *Arch pathol, 12*, 186-202.

Hirose, M., Kwon, O. H., Yamato, M., Kikuchi, A., & Okano, T. (2000). Creation of designed shape cell sheets that are noninvasively harvested and moved onto another surface. *Biomacromolecules, 1*(3), 377-381.

Hirose, M., Yamato, M., Kwon, O. H., Harimoto, M., Kushida, A., Shimizu, T., . . . Okano, T. (2000). Temperature-responsive surface for novel co-culture systems

University of Malaya

of hepatocytes with endothelial cells: 2-D patterned and double layered co-cultures. *Yonsei medical journal, 41*(6), 803-813.

Ho, C.-T., Lin, R.-Z., Chang, W.-Y., Chang, H.-Y., & Liu, C.-H. (2006). Rapid heterogeneous liver-cell on-chip patterning via the enhanced field-induced dielectrophoresis trap. *Lab on a Chip, 6*(6), 724-734.

Ho, C.-T., Lin, R.-Z., Chen, R.-J., Chin, C.-K., Gong, S.-E., Chang, H.-Y., . . . Chang, S.-F. (2013). Liver-cell patterning lab chip: mimicking the morphology of liver lobule tissue. *Lab on a Chip, 13*(18), 3578-3587.

Ho, C. T., Lin, R. Z., Chang, W. Y., Chang, H. Y., & Liu, C. H. (2006). Rapid heterogeneous liver-cell on-chip patterning via the enhanced field-induced dielectrophoresis trap. *Lab Chip, 6*(6), 724-734. doi: 10.1039/b602036d

Huang, H., Hanada, S., Kojima, N., & Sakai, Y. (2006). Enhanced functional maturation of fetal porcine hepatocytes in three-dimensional poly-L-lactic acid scaffolds: a culture condition suitable for engineered liver tissues in large-scale animal studies. *Cell transplantation, 15*(8-9), 799-809.

Hughes, M. P. (2002). Strategies for dielectrophoretic separation in laboratory-on-a-chip systems. *Electrophoresis, 23*(16), 2569-2582.

Hughes, M. P., Morgan, H., Rixon, F. J., Burt, J. P., & Pethig, R. (1998). Manipulation of herpes simplex virus type 1 by dielectrophoresis. *Biochimica et Biophysica Acta (BBA)-General Subjects, 1425*(1), 119-126.

Hutmacher, D. W., Schantz, T., Zein, I., Ng, K. W., Teoh, S. H., & Tan, K. C. (2001). Mechanical properties and cell cultural response of polycaprolactone scaffolds designed and fabricated via fused deposition modeling. *Journal of Biomedical Materials Research: An Official Journal of The Society for Biomaterials, The Japanese Society for Biomaterials, and The Australian Society for Biomaterials and the Korean Society for Biomaterials, 55*(2), 203-216.

Isenberg, B. C., Tsuda, Y., Williams, C., Shimizu, T., Yamato, M., Okano, T., & Wong, J. Y. (2008). A thermoresponsive, microtextured substrate for cell sheet engineering with defined structural organization. *Biomaterials, 29*(17), 2565-2572.

Ito, H. (1997). Chemical amplification resists: History and development within IBM. *IBM Journal of research and development, 41*(1.2), 119-130.

James, T., Mannoor, M., & Ivanov, D. (2008). BioMEMS–advancing the frontiers of medicine. *Sensors, 8*(9), 6077-6107.

Jaramillo, M. d. C., Torrents, E., Martínez-Duarte, R., Madou, M. J., & Juárez, A. (2010). On-line separation of bacterial cells by carbon-electrode dielectrophoresis. *Electrophoresis, 31*(17), 2921-2928.

Jenkins, G. M., & Kawamura, K. (1976). *Polymeric carbons: carbon fibre, glass and char*: Cambridge University Press.

University of Malaya

Jubery, T. Z., Srivastava, S. K., & Dutta, P. (2014). Dielectrophoretic separation of bioparticles in microdevices: A review. *Electrophoresis, 35*(5), 691-713.

Kadota, Y., Yagi, H., Inomata, K., Matsubara, K., Hibi, T., Abe, Y., . . . Itano, O. (2014). Mesenchymal stem cells support hepatocyte function in engineered liver grafts. *Organogenesis, 10*(2), 268-277.

Kawaguchi, M., & Kataoka, H. (2014). Mechanisms of hepatocyte growth factor activation in cancer tissues. *Cancers, 6*(4), 1890-1904.

Khetani, S. R., & Bhatia, S. N. (2008). Microscale culture of human liver cells for drug development. *Nature biotechnology, 26*(1), 120.

Khoshmanesh, K., Nahavandi, S., Baratchi, S., Mitchell, A., & Kalantar-zadeh, K. (2011). Dielectrophoretic platforms for bio-microfluidic systems. *Biosensors and Bioelectronics, 26*(5), 1800-1814.

Khoshmanesh, K., Zhang, C., Nahavandi, S., Tovar-Lopez, F. J., Baratchi, S., Mitchell, A., & Kalantar-Zadeh, K. (2010). Size based separation of microparticles using a dielectrophoretic activated system. *Journal of Applied Physics, 108*(3), 034904.

Kibria, M., Zhang, F., Lee, T., Kim, M., & Howlader, M. (2010). Comprehensive investigation of sequential plasma activated Si/Si bonded interfaces for nano-integration on the wafer scale. *Nanotechnology, 21*(13), 134011.

Kikuchi, A., & Okano, T. (2005). Nanostructured designs of biomedical materials: applications of cell sheet engineering to functional regenerative tissues and organs. *Journal of Controlled Release, 101*(1-3), 69-84.

Kiss, A., Wang, N.-J., Xie, J.-P., & Thorgeirsson, S. S. (1997). Analysis of transforming growth factor (TGF)-alpha/epidermal growth factor receptor, hepatocyte growth Factor/c-met, TGF-beta receptor type II, and p53 expression in human hepatocellular carcinomas. *Clinical Cancer Research, 3*(7), 1059-1066.

Kozanoglu, E., Canataroglu, A., Abayli, B., Colakoglu, S., & Goncu, K. (2003). Fibromyalgia syndrome in patients with hepatitis C infection. *Rheumatology International, 23*(5), 248-251.

Kretschmer, R., & Fritzsche, W. (2004). Pearl chain formation of nanoparticles in microelectrode gaps by dielectrophoresis. *Langmuir, 20*(26), 11797-11801.

Kumashiro, Y., Yamato, M., & Okano, T. (2010). Cell attachment–detachment control on temperature-responsive thin surfaces for novel tissue engineering. *Annals of biomedical engineering, 38*(6), 1977-1988.

Lapizco-Encinas, B. H., Davalos, R. V., Simmons, B. A., Cummings, E. B., & Fintschenko, Y. (2005). An insulator-based (electrodeless) dielectrophoretic concentrator for microbes in water. *Journal of Microbiological methods, 62*(3), 317-326.

Lee, J. A., Lee, S. W., Lee, K.-C., Park, S. I., & Lee, S. S. (2008). Fabrication and characterization of freestanding 3D carbon microstructures using multi-exposures

University of Malaya

and resist pyrolysis. *Journal of Micromechanics and Microengineering, 18*(3), 035012.

Lee, K.-H., Lee, J., & Lee, S.-H. (2015). 3D liver models on a microplatform: well-defined culture, engineering of liver tissue and liver-on-a-chip. *Lab on a Chip, 15*(19), 3822-3837.

Lerche, C., Fautrel, A., Shaw, P. M., Glaise, D., Ballet, F., Guillouzo, A., & Corcos, L. (1997). Regulation of the Major Detoxication Functions by Phenobarbital and 3-Methylcholanthrene in Co-Cultures of Rat Hepatocytes and Liver Epithelial Cells. *European journal of biochemistry, 244*(1), 98-106.

Li, M., Li, W., Zhang, J., Alici, G., & Wen, W. (2014). A review of microfabrication techniques and dielectrophoretic microdevices for particle manipulation and separation. *Journal of Physics D: Applied Physics, 47*(6), 063001.

Li, S., Li, M., Hui, Y. S., Cao, W., Li, W., & Wen, W. (2013). A novel method to construct 3D electrodes at the sidewall of microfluidic channel. *Microfluidics and nanofluidics, 14*(3-4), 499-508.

Lin, R. Z., Ho, C. T., Liu, C. H., & Chang, H. Y. (2006). Dielectrophoresis based-cell patterning for tissue engineering. *Biotechnology Journal: Healthcare Nutrition Technology, 1*(9), 949-957.

Liska, D. J. (1998). The detoxification enzyme systems. *Altern Med Rev, 3*(3), 187-198.

Liu, K.-K., Wu, R.-G., Chuang, Y.-J., Khoo, H. S., Huang, S.-H., & Tseng, F.-G. (2010). Microfluidic systems for biosensing. *Sensors, 10*(7), 6623-6661.

Luo, S., & Wong, C. (2005). Influence of temperature and humidity on adhesion of underfills for flip chip packaging. *IEEE Transactions on Components and Packaging Technologies, 28*(1), 88-94.

Maher, J. J. (1998). The extracellular matrix in liver regeneration *Liver growth and repair* (pp. 451-464): Springer.

Manz, A., Effenhauser, C. S., Burggraf, N., Harrison, D. J., Seiler, K., & Fluri, K. (1994). Electroosmotic pumping and electrophoretic separations for miniaturized chemical analysis systems. *Journal of Micromechanics and Microengineering, 4*(4), 257.

Mardegan, A., Kamath, R., Sharma, S., Scopece, P., Ugo, P., & Madou, M. (2013). Optimization of carbon electrodes derived from epoxy-based photoresist. *Journal of The Electrochemical Society, 160*(8), B132-B137.

Martinez-Duarte, R. (2014). SU-8 Photolithography as a Toolbox for Carbon MEMS. *Micromachines, 5*(3), 766-782.

Martinez-Duarte, R., Gorkin III, R. A., Abi-Samra, K., & Madou, M. J. (2010). The integration of 3D carbon-electrode dielectrophoresis on a CD-like centrifugal microfluidic platform. *Lab on a Chip, 10*(8), 1030-1043.

University of Malaya

Martinez-Duarte, R., Madou, M., Kumar, G., & Schroers, J. (2009). *A novel method for amorphous metal micromolding using carbon MEMS.* Paper presented at the Solid-State Sensors, Actuators and Microsystems Conference, 2009. TRANSDUCERS 2009. International.

Martinez-Hernandez, A., & Amenta, P. S. (1995). The extracellular matrix in hepatic regeneration. *The FASEB journal, 9*(14), 1401-1410.

Martinez-Duarte, R., Renaud, P., & Madou, M. J. (2011). A novel approach to dielectrophoresis using carbon electrodes. *Electrophoresis, 32*(17), 2385-2392.

Masuda, S., Itagaki, T., & Kosakada, M. (1988). Detection of extremely small particles in the nanometer and ionic size range. *IEEE transactions on industry applications, 24*(4), 740-744.

Materne, E.-M., Maschmeyer, I., Lorenz, A. K., Horland, R., Schimek, K. M., Busek, M., . . . Marx, U. (2015). The multi-organ chip-a microfluidic platform for long-term multi-tissue coculture. *JoVE (Journal of Visualized Experiments)*(98), e52526.

Matsue, T., Matsumoto, N., & Uchida, I. (1997). Rapid micropatterning of living cells by repulsive dielectrophoretic force. *Electrochimica Acta, 42*(20-22), 3251-3256.

Mazza, G., Al-Akkad, W., Rombouts, K., & Pinzani, M. (2018). Liver tissue engineering: From implantable tissue to whole organ engineering. *Hepatology Communications, 2*(2), 131-141.

Michalopoulos, G. K. (2017). Hepatostat: liver regeneration and normal liver tissue maintenance. *Hepatology, 65*(4), 1384-1392.

Min, H.-S., Park, B. Y., Taherabadi, L., Wang, C., Yeh, Y., Zaouk, R., . . . Dunn, B. (2008). Fabrication and properties of a carbon/polypyrrole three-dimensional microbattery. *Journal of Power Sources, 178*(2), 795-800.

Mironov, V., Boland, T., Trusk, T., Forgacs, G., & Markwald, R. R. (2003). Organ printing: computer-aided jet-based 3D tissue engineering. *TRENDS in Biotechnology, 21*(4), 157-161.

Natu, R., Islam, M., Gilmore, J., & Martinez-Duarte, R. (2018). Shrinkage of SU-8 microstructures during carbonization. *Journal of analytical and applied pyrolysis, 131*, 17-27.

Natu, R., Islam, M., & Martinez-Duarte, R. (2016). Shrinkage analysis of carbon micro structures derived from SU-8 photoresist. *ECS Transactions, 72*(1), 27-33.

Odde, D. J., & Renn, M. J. (1999). Laser-guided direct writing for applications in biotechnology. *TRENDS in Biotechnology, 17*(10), 385-389.

Ozuna-Chacón, S., Lapizco-Encinas, B. H., Rito-Palomares, M., Martínez-Chapa, S. O., & Reyes-Betanzo, C. (2008). Performance characterization of an insulator-based dielectrophoretic microdevice. *Electrophoresis, 29*(15), 3115-3122.

University of Malaya

Palakkan, A. A., Hay, D. C., & Ross, J. A. (2013). Liver tissue engineering and cell sources: issues and challenges. *Liver international, 33*(5), 666-676.

Pan, P., Wang, W., Ru, C., Sun, Y., & Liu, X. (2017). MEMS-based platforms for mechanical manipulation and characterization of cells. *Journal of Micromechanics and Microengineering, 27*(12), 123003.

Park, B. Y., Taherabadi, L., Wang, C., Zoval, J., & Madou, M. J. (2005). Electrical properties and shrinkage of carbonized photoresist films and the implications for carbon microelectromechanical systems devices in conductive media. *Journal of the Electrochemical Society, 152*(12), J136-J143.

Penmatsa, V., Kim, T., Beidaghi, M., Kawarada, H., Gu, L., Wang, Z., & Wang, C. (2012). Three-dimensional graphene nanosheet encrusted carbon micropillar arrays for electrochemical sensing. *Nanoscale, 4*(12), 3673-3678.

Pesch, G. R., Kiewidt, L., Du, F., Baune, M., & Thöming*, J. (2016). Electrodeless dielectrophoresis: Impact of geometry and material on obstacle polarization. *Electrophoresis, 37*(2), 291-301.

Pohl, H. A. (1951). The motion and precipitation of suspensoids in divergent electric fields. *Journal of Applied Physics, 22*(7), 869-871.

Powers, M. J., Domansky, K., Kaazempur-Mofrad, M. R., Kalezi, A., Capitano, A., Upadhyaya, A., . . . Kamm, R. (2002). A microfabricated array bioreactor for perfused 3D liver culture. *Biotechnology and bioengineering, 78*(3), 257-269.

Pucihar, G., Kotnik, T., Kandušer, M., & Miklavčič, D. (2001). The influence of medium conductivity on electropermeabilization and survival of cells in vitro. *Bioelectrochemistry, 54*(2), 107-115.

Puttaswamy, S. V., Sivashankar, S., Chen, R. J., Chin, C. K., Chang, H. Y., & Liu, C. H. (2010). Enhanced cell viability and cell adhesion using low conductivity medium for negative dielectrophoretic cell patterning. *Biotechnology journal, 5*(10), 1005-1015.

Ranganathan, S., Mccreery, R., Majji, S. M., & Madou, M. (2000). Photoresist‐derived carbon for microelectromechanical systems and electrochemical applications. *Journal of the Electrochemical Society, 147*(1), 277-282.

Rhim, J. A., Sandgren, E. P., Palmiter, R. D., & Brinster, R. L. (1995). Complete reconstitution of mouse liver with xenogeneic hepatocytes. *Proceedings of the National Academy of Sciences, 92*(11), 4942-4946.

Rouabah, H. A., Park, B. Y., Zaouk, R. B., Morgan, H., Madou, M. J., & Green, N. G. (2011). Design and fabrication of an ac-electro-osmosis micropump with 3D high-aspect-ratio electrodes using only SU-8. *Journal of Micromechanics and Microengineering, 21*(3), 035018.

Saucedo-Espinosa, M., & Lapizco-Encinas, B. (2015). Design of insulator-based dielectrophoretic devices: Effect of insulator posts characteristics. *Journal of Chromatography A, 1422*, 325-333.

University of Malaya

Saunders, R. E., Gough, J. E., & Derby, B. (2008). Delivery of human fibroblast cells by piezoelectric drop-on-demand inkjet printing. *Biomaterials, 29*(2), 193-203.

Schütte, J., Hagmeyer, B., Holzner, F., Kubon, M., Werner, S., Freudigmann, C., . . . Becker, H. (2011). "Artificial micro organs"—a microfluidic device for dielectrophoretic assembly of liver sinusoids. *Biomedical microdevices, 13*(3), 493-501.

Schwan, H. P., & Sher, L. D. (1969). Alternative-Current Field-Induced Forces and Their Biological Implications. *Journal of the Electrochemical Society, 116*(1), 22C-26C.

Sharma, C. S., Sharma, A., & Madou, M. (2010). Multiscale carbon structures fabricated by direct micropatterning of electrospun mats of SU-8 photoresist nanofibers. *Langmuir, 26*(4), 2218-2222.

Shih, M.-C., Tseng, S.-H., Weng, Y.-s., Chu, I.-M., & Liu, C.-H. (2013). A gel-free multi-well microfluidic device utilizing surface tension for cell culturing. *Sensors and Actuators B: Chemical, 177,* 295-307.

Shoichet, M. S., Li, R. H., White, M. L., & Winn, S. R. (1996). Stability of hydrogels used in cell encapsulation: An in vitro comparison of alginate and agarose. *Biotechnology and bioengineering, 50*(4), 374-381.

Singh, A., Jayaram, J., Madou, M., & Akbar, S. (2002). Pyrolysis of negative photoresists to fabricate carbon structures for microelectromechanical systems and electrochemical applications. *Journal of the Electrochemical Society, 149*(3), E78-E83.

Song, Y., Chen, C., & Wang, C. (2015). Graphene/enzyme-encrusted three-dimensional carbon micropillar arrays for mediatorless micro-biofuel cells. *Nanoscale, 7*(16), 7084-7090.

Srivastava, S. K., Gencoglu, A., & Minerick, A. R. (2011). DC insulator dielectrophoretic applications in microdevice technology: a review. *Analytical and bioanalytical chemistry, 399*(1), 301-321.

Stevens, K. R., Ungrin, M. D., Schwartz, R. E., Ng, S., Carvalho, B., Christine, K. S., . . . Bhatia, S. N. (2013). InVERT molding for scalable control of tissue microarchitecture. *Nat Commun, 4,* 1847. doi: 10.1038/ncomms2853

Stulík, K., Amatore, C., Holub, K., Marecek, V., & Kutner, W. (2000). Microelectrodes. Definitions, characterization, and applications (Technical report). *Pure and Applied Chemistry, 72*(8), 1483-1492.

Sung, H.-J., Meredith, C., Johnson, C., & Galis, Z. S. (2004). The effect of scaffold degradation rate on three-dimensional cell growth and angiogenesis. *Biomaterials, 25*(26), 5735-5742.

Tay, F. E., Yu, L., Pang, A. J., & Iliescu, C. (2007). Electrical and thermal characterization of a dielectrophoretic chip with 3D electrodes for cells manipulation. *Electrochimica acta, 52*(8), 2862-2868.

University of Malaya

Teixidor, G. T., Gorkin Iii, R., Tripathi, P., Bisht, G., Kulkarni, M., Maiti, T., . . . Park, B. (2008). Carbon microelectromechanical systems as a substratum for cell growth. *Biomedical Materials, 3*(3), 034116.

Teixidor, G. T., Zaouk, R. B., Park, B. Y., & Madou, M. J. (2008). Fabrication and characterization of three-dimensional carbon electrodes for lithium-ion batteries. *Journal of Power Sources, 183*(2), 730-740.

Than, N. N., & Newsome, P. N. (2015). A concise review of non-alcoholic fatty liver disease. *Atherosclerosis, 239*(1), 192-202.

Thiha, A., Ibrahim, F., Muniandy, S., & Madou, M. J. (2019). Microplasma direct writing for site-selective surface functionalization of carbon microelectrodes. *Microsystems & nanoengineering, 5*(1), 1-12.

Toh, Y.-C., Lim, T. C., Tai, D., Xiao, G., van Noort, D., & Yu, H. (2009). A microfluidic 3D hepatocyte chip for drug toxicity testing. *Lab on a Chip, 9*(14), 2026-2035.

Voldman, J. (2006). Electrical forces for microscale cell manipulation. *Annu. Rev. Biomed. Eng., 8*, 425-454.

Voldman, J., Gray, M. L., Toner, M., & Schmidt, M. A. (2002). A microfabrication-based dynamic array cytometer. *Analytical Chemistry, 74*(16), 3984-3990.

Wang, C., Jia, G., Taherabadi, L. H., & Madou, M. J. (2005). A novel method for the fabrication of high-aspect ratio C-MEMS structures. *Journal of microelectromechanical systems, 14*(2), 348-358.

Wang, L., Flanagan, L., & Lee, A. P. (2007). Side-wall vertical electrodes for lateral field microfluidic applications. *Journal of microelectromechanical systems, 16*(2), 454-461.

Wang, X., Yang, J., & Gascoyne, P. R. (1999). Role of peroxide in AC electrical field exposure effects on Friend murine erythroleukemia cells during dielectrophoretic manipulations. *Biochimica et Biophysica Acta (BBA)-General Subjects, 1426*(1), 53-68.

Wang, Y., Ameer, G. A., Sheppard, B. J., & Langer, R. (2002). A tough biodegradable elastomer. *Nature biotechnology, 20*(6), 602.

Weiskirchen, R., & Tacke, F. (2014). Cellular and molecular functions of hepatic stellate cells in inflammatory responses and liver immunology. *Hepatobiliary surgery and nutrition, 3*(6), 344.

Wright, R. S., Anderson, J. W., & Bridges, S. R. (1990). Propionate inhibits hepatocyte lipid synthesis. *Proceedings of the Society for Experimental Biology and Medicine, 195*(1), 26-29.

Yafouz, B., Kadri, N., & Ibrahim, F. (2012). *A numerical analysis of electric field strength over planar microarray dot electrode for dielectrophoretic lab-on-chip device.* Paper presented at the Biomedical Engineering and Sciences (IECBES), 2012 IEEE EMBS Conference on.

University of Malaya

Yafouz, B., Kadri, N., & Ibrahim, F. (2013). Microarray dot electrodes utilizing dielectrophoresis for cell characterization. *Sensors, 13*(7), 9029-9046.

Yang, J., Chung, T. W., Nagaoka, M., Goto, M., Cho, C.-S., & Akaike, T. (2001). Hepatocyte-specific porous polymer-scaffolds of alginate/galactosylated chitosan sponge for liver-tissue engineering. *Biotechnology letters, 23*(17), 1385-1389.

Yang, R., & Wang, W. (2005). A numerical and experimental study on gap compensation and wavelength selection in UV-lithography of ultra-high aspect ratio SU-8 microstructures. *Sensors and Actuators B: Chemical, 110*(2), 279-288.

Yantzi, J., Yeow, J., & Abdallah, S. (2007). Multiphase electrodes for microbead control applications: integration of DEP and electrokinetics for bio-particle positioning. *Biosensors and Bioelectronics, 22*(11), 2539-2545.

Yao, J., Zhu, G., Zhao, T., & Takei, M. (2019). Microfluidic device embedding electrodes for dielectrophoretic manipulation of cells-A review. *Electrophoresis, 40*(8), 1166-1177.

Yu, Z., Xiang, G., Pan, L., Huang, L., Yu, Z., Xing, W., & Cheng, J. (2004). Negative dielectrophoretic force assisted construction of ordered neuronal networks on cell positioning bioelectronic chips. *Biomedical microdevices, 6*(4), 311-324.

Zhang, C., Khoshmanesh, K., Mitchell, A., & Kalantar-Zadeh, K. (2010). Dielectrophoresis for manipulation of micro/nano particles in microfluidic systems. *Analytical and bioanalytical chemistry, 396*(1), 401-420.

Zhang, J., Zhao, X., Liang, L., Li, J., Demirci, U., & Wang, S. (2018). A decade of progress in liver regenerative medicine. *Biomaterials, 157*, 161-176.

University of Malaya